

WI

FRACTURE BEHAVIOUR OF CERAMIC
CYLINDERS DUE TO THERMAL
STRESSES

by

NEGUSSIE ADEFRIS BELLHIU

3.Sc. Mechanical Engineering

SJHIV^{ptjcttV} OF NAIROBI

A thesis submitted in partial fulfilment
for the award of the Degree of Master of
Science in Engineering in the University
of Nairobi.

Mechanical Engineering Department

1986.

UNIVERSITY OF NAIROBI LIBRARY

0146890 9

This thesis is my original work and has not been presented for a degree in any other University.

A handwritten signature in black ink, appearing to read "Negussie Adefris". The script is cursive and somewhat stylized.

Negussie Adefris

This thesis has been submitted for examination with our approval as University supervisors.

Dr. J.K. Musuva

A handwritten signature in black ink, appearing to read "N.A. Jivraj". The script is cursive and somewhat stylized.

Dr. N.A. Jivraj

CCNTENTS

	<u>Page</u>
Contents	111
List of Tables	ix
List of Figures	x
List of Plates	xx
Acknowledgements	xvi
Abstract	xviii
Notations	xxi
	*
CHAPTER ONE: INTRODUCTION	1
1.1 Background and need for the present study	1
1.2 Prevailing conditions in domestic stoves	2
1.3 Hie present work	3
CHAPTER TWO: A REVIEW OF ASPECTS RELEVANT TO THERMAL FRACTURE OF CERAMICS	6
2.1 Introduction	6
2.2 The temperature distributions	7
2.2.1 The heat conduction problem	7
2.2.2 Initial and boundary conditions	8
2.2.3 Solution of heat conduction problem	9

	<u>Page</u>
2.3	The stress distribution 13
2.3.1	The general axi-symmetrical problem 14
2.3.2	The thick walled long cylinder 15
2.3.3	Transient thermal stress due to rapid temperature changes 16
2.3.4	Stresses due to heating or cooling at a constant rate 18
2.4	A review of aspects relevant to failure 19
2.4.1	Introduction 19
2.4.2	Thermal shock resistance 19
2.4.3	Influence of heat transfer conditions 25
2.4.4	Effect of specimen size 28
2.4.5	Thermal fatigue 28
2.4.6	Failure probability 30
 CHAPTER THREE: HEAT TRANSFER CHARACTERISTICS, AND TEMPERATURE AND STRESS DISTRIBUTION IN HOLLOW CYLINDERS 40	
3.1	Introduction 40
3.2	The stove model 41
3.3	The physical model 41
3.4	The mathematical model 43

	<u>Page</u>	
3.4.1	Heat transfer mechanisms	45
3.4.2	Properties of the ceramic model	47
3.5	The numerical solution	48
3.5.1	The temperature distribution	48
3.5.2	The stress distribution	49
3.5.3	The numerical output	50
3.6	Results and discussion	50
3.6.1	Effect of internal radius	52
3.6.2	Effect of external radius	53
3.6.3	Effect of thermal conductivity	53
3.6.4	Effect of density and specific heat	54
3.6.5	Effect of heat transfer coefficient	55
3.7	Conclusions	56
 CHAPTER FOUR: EXPERIMENTAL TEMPERATURE AND STRAIN ANALYSES		 75
4.1	Introduction	75
4.2	Experimental devices and data processing techniques	76
4.2.1	The test specimen	76
4.2.1.1	Specimen preparation	76
4.2.1.2	Properties of the specimen	76

	<u>Page</u>	
4.2.2	Experimental devices	77
4.2.2.1	The data logger	77
4.2.2.2	Digital thermometer	77
4.2.2.3	Digital strain indicator	77
4.2.3	The test layout	77
4.2.4	Data processing technique	78
4.3	Experimental procedure	79
	i	
4.3.1	Temperature measurement	80
4.3.2	Strain measurement	81
4.4	Results and discussion	82
4.4.1	Temperature measurement	82
4.4.2	Strain measurement	84
4.5	Conclusions	86
	 CHAPTER FIVE: THERMAL FRACTURE STUDIES	 100
5.1	Introduction	ICXJ
5.2	The test specimen and experimental devices	102
5.2.1	The specimen	102
5.2.1.1	Production of test specimens	102
5.2.1.2	The chemical composition	103
5.2.1.3	Strength of the specimens	104

	<u>Page</u>
5.2.1.4 Young's modulus and Poissons ratio	105
5.2.1.5 Specific heat capacity	105
5.2.1.6 Coefficient of thermal expansion	106
5.2.1.7 Thermal conductivity	106
5.2.2 Experimental devices	107
5.2.2.1 The specimen holder	107
5.2.2.2 The heating and cooling devices	107
5.2.2.3 The ultrasonic tester	108
5.2.2.4 Flexural strength	108
5.2.2.5 Crack detection	108
5.3 Experimental methods and data processing techniques	109
5.3.1 Experimental techniques	109
5.3.2 Thermal shock resistance	111
5.3.3 Thermal fatigue	111
5.4 Experimental procedure	113
5.4.1 Thermal shock resistance	114
5.4.2 Thermal fatigue	114
5.5 Results and discussions	115
5.5.1 Results	115
5.5.1.1 Thermal shock resistance	115
5.5.1.2 Thermal fatigue	117
5.5.2 Discussion	118
5.5.2.1 Thermal shock resistance	118
5.5.2.2 Thermal fatigue	122

	<u>Page</u>
5.6	Conclusions 124
	CHAPTER SIX: OVERALL CONCLUSIONS AND RECOMMENDATIONS 144
6.1	Conclusions 144
6.2	Recommendations 147
6.3	Suggestions for future work 149
	APPENDICES
A1.1	Finite difference equations for the cylinder model 152
A1.2	A program to calculate transient temperature and stress distribution across the wall of a hollow cylinder 158
A2.1	Trapezoidal method for approximating an integral 167
A2.2	Solution for the general axisymmetrical problem 169
A2.3	Transient thermal stresses in solid circular cylinders 173
A3	Concepts of statistical analysis 176
A3.1	Concept of ranking 176
A3.2	Concept of correlation analysis 177
A3.3	The Weibull distribution 178
	References 184

List of Tables

	<u>Page</u>
Table 2.1: Thermal stress at the surface and centre of different geometries subjected to thermal shock	34
Table 2.2: Temperature difference between surface and centre of various shapes cooled at a constant rate	36
Table 3.1: Physical properties of the ambient atmosphere 'at 250°C	57
Table 5.1: Chemical composition of specimens	128
Table 5.2: Strength of specimens	128
Table 5.3: Physical properties of specimens	129
Table 5.4a: Values of thermal conductivity for Nyeri clay	130
Table 5.4b: Values of thermal conductivity for Maragua clay	130
Table 5.5: Values of material properties n and m determined from T-SPT diagram, and strength data	131
Table 5.6: Speed of propagation of ultrasonic waves through Nyeri clay before and after thermal shocks	132

Table 5.7:	Speed of propagation of ultrasonic waves through Maragua clay before and after thermal shocks	132
Table 5.8:	Analysis of variance for the Nyeri clay	133
Table 5.9:	Analysis of variance for the Maragua clay	133
Table A3.1	Values of correlation coefficient	179
Table A3.2	Median ranks	180
Table A3.3	5 and 95 percent ranks	181

List of Figures

Figure 1.1	The traditional three stages woodstove	5
Figure 1.2	Improved two pot woodstove with chimney	5
Figure 2.1	'Energetic theory' approach for thermal shock resistance	37
Figure 2.2	Strength before and after thermal shock cracking for high and low strength materials	38
Figure 2.3	The loading arrangement for specimens subjected to four points flexure	39
Figure 3.1	The stove model	58
Figure 3.2(a)	The physical modeling situation	59
Figure 3.2(b)	The temperature distribution	59

	<u>Page</u>	
Figure 3.3	Temperature distribution across the wall of the cylinder as a function of time	60
Figure 3.4	Temperature of the inner and outer surfaces of the cylinder as a function of time	61
Figure 3.5	Circumferential stress distribution across the wall of the cylinder as a function of time	62
Figure 3.6	Circumferential stresses at the inner and outer surfaces of the cylinder as a function of time	63
Figure 3.7	Effect of inner radius on the temperature at the inner surface as a function of time	64
Figure 3.8	Effect of inner radius on the circumferential stress at the outer surface as a function of time	65
Figure 3.9	Effect of external radius on the temperature at the inner surface as a function of time	66
Figure 3.10	Effect of the external radius on the circumferential stress as a function of time	67

	<u>Page</u>	
Figure 3.11	Effect of thermal conductivity on the temperature at the inner surface as a function of time	68
Figure 3.12	Effect of thermal conductivity on the circumferential stress at the outer surface as a function of time	69
Figure 3.13	Effect of specific heat capacity of the model on the temperature at the inner surface as a function of time	70
Figure 3.14	Effect of density of the model on the circumferential stress at the outer surface as a function of time	71
Figure 3.15	Effect of the specific heat of the model on the circumferential stress at the outer surface as a function of time	72
Figure 3.16	Effect of the heat transfer coefficient, h , on the temperature of the inner and outer surfaces as a function of time	73
Figure 3.17	Effect of the heat transfer coefficient, h , on the circumferential stress at the outer surface	74
Figure 4.1	The test layout	88
Figure 4.2	Apparent strain curve	89

	Page	
Figure 4.3	Inner wall temperature as a function of time	90
Figure 4.4	Temperature rise of the inner surface as a function of time	91
Figure 4.5	Temperature at the external surface as a function of time	92
Figure 4.6	Temperature distribution across the wall of the cylinder	93
Figure 4.7	Temperature versus time at different points in the cylinder wall	94
Figure 4.8	Inner surface temperature at the edge of the cylinder as a function of time	95
Figure 4.9	Measured strain at the inner surface of the cylinder (320 W)	96
Figure 4.10	Measured strain at the inner surface of the cylinder (120 W)	97
Figure 5.1	Fracture strength of the Nyeri specimen after water quenching at different thermal shock severities	134
Figure 5.2	Speed of ultrasonic pressure waves versus thermal shock severity for the Nyeri specimen	135
Figure 5.3	Speed of ultrasonic pressure waves versus fracture strength for the Nyeri specimen	136

	<u>Page</u>	
Figure 5.4	Fracture strength of the Maragua specimen after water quenching at different thermal shock severities	137
Figure 5.5	Speed of ultrasonic pressure waves versus thermal shock severity for the Maragua specimen	138
Figure 5.6	Speed of ultrasonic pressure waves versus fracture strength for the Maragua specimen	139
Figure 5.7	Thermal fatigue life versus survival probability for the Nyeri specimen	140
Figure 5.8	Thermal fatigue life versus survival probability for the Maragua specimen	141
Figure 5.9	Fracture stress distribution of the Nyeri specimen	142
Figure 5.10	Fracture stress distribution of the Maragua specimen	143
Figure A2.1	The variation of non-dimensional surface circumferential stress in an infinite circular cylinder with non-dimensional time for varying Biot number	175
Figure A3.1	Weibull slope error at 90 percent confidence interval	182

	<u>Page</u>
Figure A3.2 Position of the Weibull mean	183

List of Plates

Plate 4.1 Test set-up for strain and temperature measurements	98
Plate 4.2 Test set-up for strain and temperature measurements [*]	99

ACKTO/LEDGBENTS

I express my appreciation to my supervisors Dr. J.K. Musuva and Dr. N.A. Jivraj who have given valuable guidance, advice and encouragement in the preparation of this thesis. Dr. D.R. Newman deserves special thanks and recognition for his valuable guidance and thorough criticisms of the research work.

I thank the Appropriate Technology Centre staff and the Fine Art Department staff at Kenyatta University who assisted me in getting some literature and equipment for the work. The Geology Department laboratory staff and the Mechanical Engineering Department workshop staff at the University of Nairobi deserve thanks for helping in all aspects.

I wish to express my gratitude to the Transport section of the University of Nairobi for their cooperation. Mr. S.J. Njue deserves special thanks for helping in the production of test specimens. Mr. T. Assefa and Ms. W. Forawi deserve special thanks for all the help and encouragement.

To Ms. F. Kollikho I express my appreciation for her unfailing cooperation and for the high standards of typing which she has maintained.

Finally, special mention should be given to the ANSTI secretariat for all the support and encouragement they provided for this work.

ABSTRACT

Recently developed domestic stoves are equipped with ceramic lining that surround the fire. During use these linings are exposed to thermal stresses arising due to the temperature gradients across the walls of the linings and restraint of expansion resulting from the presence of different phases with different coefficients of thermal expansion in a multiphase ceramic system. These stresses cause the ceramic lining to fracture after a considerably short service life.

A numerical model is designed in order to study the thermal and stress characteristics of the lining. The effects of geometric parameters, thermal conductivity, specific heat capacity, density and heat transfer conditions have been studied. Experimental temperature and strain analyses were employed on hollow cylinders produced from Nyeri clay to establish the validity of the numerical results.

Thermal fracture behaviour was investigated using the method of quenching of cylindrical specimens from a certain preselected higher temperature.

Some specimens were produced from clay and sand mixture from Maragua and others from clay from Nyeri.

Chemical composition of the specimens was determined and thermal and physical properties were measured and/or estimated.

Thermal shock behaviour was monitored by the use of low frequency (40 kHz) longitudinal ultrasonic waves and four points flexural loading. The minimum thermal shock severity required to initiate cracks and damage caused after cracking was determined.

Thermal fatigue behaviour was monitored by visually observing the formation and propagation of cracks on the specimen surfaces. It was possible to construct the 'thermal shock severity - probability - time¹ (T-SPT) diagram and hence use the result to predict the thermal fatigue life. Use of ultrasonic technique was extended so as to monitor thermal fatigue and decrease in the speed of propagation of ultrasonic waves with number of thermal cycles (shocks) was obtained.

It was found that after several thermal shocks the Nyeri clay suffered more damage (loss of strength) than the Maragua clay. The Maragua clay was found to have a longer fatigue life than the Nyeri clay. Use of ultrasonic wave to monitor' fatigue was found to be applicable to the Nyeri clay whereas there was an insignificant interaction effect

between the measured speed of ultrasonic pressure waves through the Maragua samples and the numbers of thermal shocks they were subjected to.

Based on these conclusions, a number of suggestions have been made as to the future work on this project.

NOTATIONS

Alphabetical

- A - material constant
- A' - material constant
- a - crack half length
- a_i - initial crack length
- a^{\wedge} - final crack length
- (Bi) - Biot number
- b - constant
- C, c - constants
- C_p - specific heat capacity
- E - Young's modulus
- e - thermal emissivity
- (Gr) - Grashoff number
- g -' acceleration due to gravity
- h - combined radiative and convective heat transfer coefficient
- h - convective heat transfer coefficient
- h^{\wedge} - radiative heat transfer coefficient
- K^{\wedge} - stress intensity factor
- k - thermal conductivity
- L - material constant
- M - number of cycles
- M' - number of cycles

m	- Weibull's modulus
$\Gamma\left(\frac{m+1}{m}\right)$	- Gamma function
N	- crack density per unit volume
(Nu)	- Nusselt number
n	- material constant
(Pr)	- Prandtl number
P_j	- failure probability
P	- survival probability
p	- constant ;
Q	- heat input
q	- heat input per unit area
R	- thermal shock parameter
R'	- thermal shock parameter
R''	- thermal shock parameter
R'''	- thermal shock parameter
R_d	- Boltzman constant
r	- radial coordinate
r^i	- internal radius
r_2	- external radius
s	- safety factor
S_t	- Stefan-Boltzmann constant
T	- temperature
T^1	- new temperature level
T_a	- initial temperature
ΔT	- temperature difference

critical temperature difference

time

time interval

activation energy

volume

pre-exponential factor

total energy

distance

axial coordinate

Greek alphabet

- α - linear coefficient of thermal expansion
 β - volume coefficient of thermal expansion
 γ - surface energy
 δ - non-dimensional heat transfer coefficient
 ϵ - strain
 θ - circumferential coordinate
 k - thermal diffusivity
 U - dynamic viscosity
 ν - Poisson's ratio
 ϕ - stress function
 ρ - density
 σ - stress
 σ_f - fracture stress
 σ_{flex} - flexural stress
 σ_0 - normalizing stress
 σ_R - rupture strength
 σ_t - tangential stress
 - tensile stress
 - threshold stress
 τ - shear stress
 ψ - stress function
 - rate of heating or cooling

- X - stress function
- non-dimensional stress
- ft - stress function

CHAPTER ONE

1. INTRODUCTION

I

1.1 BACKGROUND AND NEED FOR *THE* PRESENT STUDY

Almost 10C% of the rural Kenyan households use woodstoves while over 8C% of the urban households use charcoal stoves. In reoently developed dcrrestic charcoal and wood stoves there is an increasing tendency to use ceramic linings. Ceramic materials are often used to protect woodstove walls (usually mud) against high temperatures. Moreover, these linings can reduce stove body 'losses which in effect would mean increasing the efficiency of the stove if other losses (such as flue gas loss) could be controlled {1}. Low material cost, simple manufacturing methods, reasonable weight and excellent thermal stability are seme of the features that make these ceramics preferred materials for the construction of these stove linings {2}.

During use these ceramics are exposed to thermal stresses arising due to the terrperature gradients across the WSlls of the linings and restrain of expansion resulting frcm the presence of different phases with different coefficients of thermal expansion in a multiphase ceramic system. Due to unfavourable combination of values of thermal conductivity, Young's modulus, strength and coefficient of thermal expansion ceramics exhibit lav resistance to thermal

stress fracture. These conditions cause the ceramic linings to fracture after a considerably short service life. Hence, the need for this study.

1.2 PREVAILING CONDITIONS IN DOMESTIC STOVES

Stoves heat up quickly after lighting-up.

Domestic charcoal stoves attain a maximum internal temperature of 700°C. The inner surface temperature is usually 500-600°C while in a single-wall metal stoves the external surface temperature may reach up to 200-300°C. On removal of the spent charcoal the wall temperatures decrease very quickly. The single-wall metal charcoal stove with ceramic lining is depicted in Figure 3.1.

Some improved woodstoves have had their temperatures measured at Kenyatta University {3}. Within 3-10 minutes the temperatures near the first pot, and at the beginning of the tunnel joining the two pots (see Figure 1.2) reached 400-450°C. On taking out the combustible wood, these temperatures dropped to 100-200°C in 5-10 minutes. Figures 1.1 and 1.2 show the traditional and improved woodstoves respectively.

Thus rapid heating and cooling is common phenomena

in stoves. The cooling can be more severe when water (or any other liquid) spills on the stoves, causing dramatic changes in the heat transfer coefficients.

The other common phenomenon in domestic stoves is that they are normally used a number of times a day. Lighting-up and putting-out of fire involves repeated thermal shock commonly referred to as thermal fatigue.

The common phenomena in stoves can be summarized as:

- i) High temperature gradients across the wall and non-homogeneity of material and hence thermal stresses (temperature differences of 100–340°C were observed depending on stove designs {3})
- ii) Rapid heating and cooling and hence thermal shock
- iii) Repeated use of stove and hence thermal fatigue.

1.3 THE PRESENT WORK

The present study was conducted in order to understand what is happening in these ceramic linings. The main aspects covered and researched can be classified as follows:

- i) A review of thermal condition, thermal stresses, and thermal fracture phenomena relevant to ceramics is presented.

- ii) Investigation of temperature and stress conditions is done on models that closely simulate actual condition in stoves. A numerical as well as an experimental technique has been used in these studies •

- iii) Studies related to thermal shock resistance have been conducted.

- iv) Studies on the thermal fatigue of ceramics have been conducted .

- v) Based on the above studies a number of conclusions have been derived and recommendations and suggestions for future work have been made.

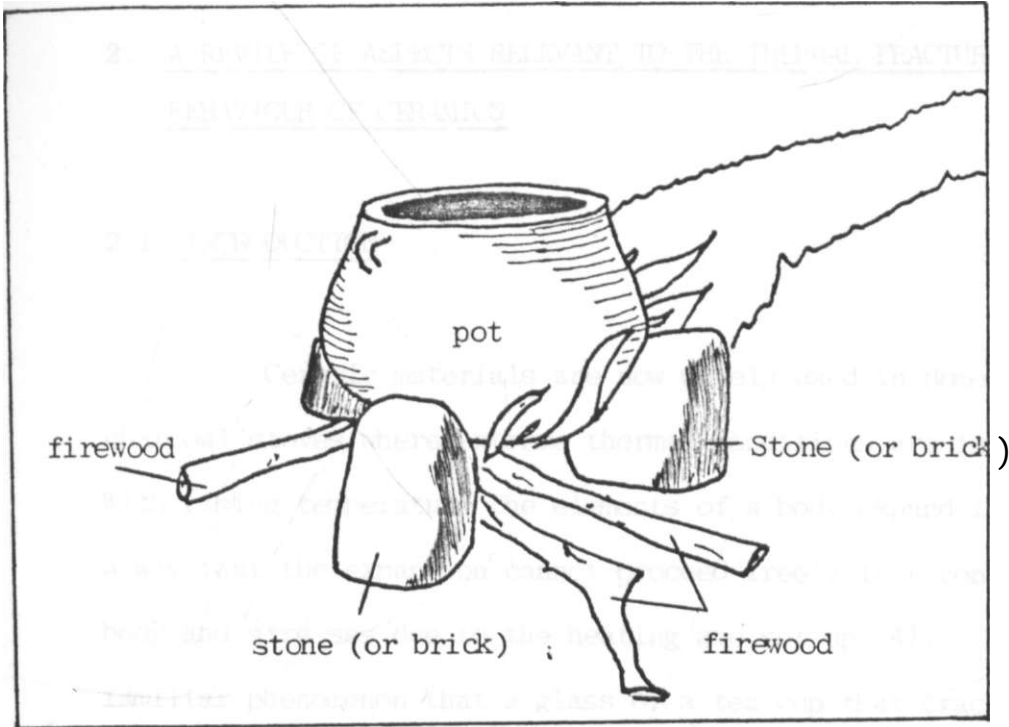


Figure 1.1: Hie traditional three stones (or bricks) woodstove

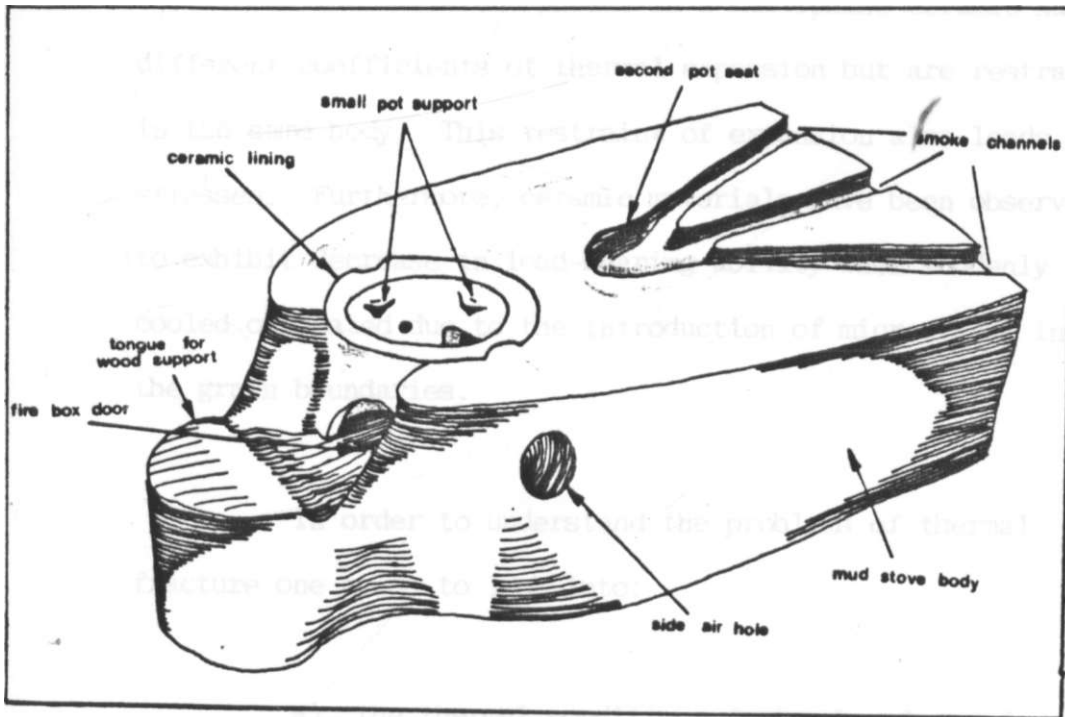


Figure 1.2: Iripoved two pot woodsstove

CHAPTER TWO

2. A REVIEW OF ASPECTS RELEVANT, TO THE THERMAL FRACTURE
BEHAVIOUR OF CERAMICS
I

2.1 INTRODUCTION

Ceramic materials are now widely used in domestic charcoal stoves where extreme thermal conditions are inherent. With rising temperature the elements of a body expand in such a way that the expansion cannot proceed freely in a continuous body and stresses due to the heating are set up {4}. The familiar phenomenon that a glass or a tea cup that cracks when suddenly heated or cooled is due to these stresses {5}. The individual crystals in an anisotropic polycrystalline ceramic or the different phases in a multiphase ceramic have different coefficients of thermal expansion but are restrained in the same body. This restraint of expansion also leads to stresses. Furthermore, ceramic materials have been observed to exhibit decrease in load-bearing ability when suddenly cooled or heated due to the introduction of microcracks in the grain boundaries.

In order to understand the problems of thermal fracture one needs to look into:

- a) the thermal conditions during heating and cooling of bodies,
- b) the stress conditions during heating and cooling, and

- c) the thermal fracture behaviour of ceramic bodies.

In this chapter a review of the methods of solution for the thermal conditions and aspects relevant to thermal stress, thermal fracture and thermal fatigue are presented.

2.2 THE TEMPERATURE DISTRIBUTION

2.2.1 The heat conduction problem

The physical problem of thermal conduction can be described by the Fourier heat conduction equation {6}, which is normally derived based on energy balance, as follows:

$$k \nabla^2 T + \dot{Q} = \rho C_p \frac{\partial T}{\partial t} \quad \dots(2.1)$$

where the quantity

$$k = k/\rho C \quad \dots(2.2)$$

and k , ρ , C , \dot{Q} , T , t and α are thermal conductivity, density, specific heat capacity, internal heat generation, temperature, time and thermal diffusivity respectively.

The quantity $\nabla^2 T$ in cylindrical coordinates is as follows:

r, θ and z being the radial, hoop and axial directions respectively. In the absence of heat generation, and when the initial and boundary conditions are independent of the coordinates θ and z, the temperature will be a function of r and t only and Equation (2.1) reduced to:

$$\frac{1}{k} \frac{\partial T}{\partial t} = \frac{\partial^2 T}{\partial r^2} + \frac{1}{r} \frac{\partial T}{\partial r} \quad (2)$$

2.2.2 Initial and boundary conditions

For the heat conduction problem to be described fully it is necessary to specify the initial and boundary conditions. The initial condition describes the initial temperature of the solid, which is usually constant. The boundary conditions are mathematical expressions of the condition at the bounding surfaces of the body which could be:

- i) prescribed surface temperature,
- ii) prescribed heat input,
- iii) perfectly insulating surface, or
- iv) heat loss by any or combination of the heat loss mechanisms (conduction, convection and radiation).

2.2.3 Solution of heat conduction problem

Various methods are available to tackle the heat conduction problem. The choice of any method depends on the boundary conditions, the dependence of properties on temperature, the accuracy required, the means of computation, etc. The major methods are:

- (a) Separation of variables
- (b) Laplace transformation
- (c) Conformal mapping
- (d) Integral technique
- (e) Electrical analogy
- (f) Numerical methods
- (g) Approximate analytical procedures, and techniques derived by extending the above procedures.

(a) Separation of variables

This method is conveniently applicable only when the thermal properties are constant and when the solid is bounded by a surface of a convenient coordinate system. For short times the infinite series obtained by this procedure converges very slowly. Jaeger {7} has applied this method for the case of infinite circular cylinders subjected to elevated surface temperature on the cylindrical surface side.

(b) Laplace transform

This procedure is applicable to any heat conduction problem which leads to a linear boundary-value problem, if the coefficients of the unknown temperature functions are only space dependent, and the non-homogeneous terms being both time and space functions. The solution ensures good convergence for both long and short time expressions. However, the inversion of the transformed solution is sometimes quite difficult: at times it can only be performed by numerical integration of definite integrals.

(c) Conformal mapping

This method is applicable only for the solution of two dimensional, steady-state problems with constant thermal conductivity. It has proved {7} to be a powerful solution for problems of wedges, angles, etc. This procedure involves the finding of an analytic function which transforms the original boundary condition into a simpler one in the complex plane {8}, solving for the temperature distribution in the complex plane and transforming the temperature distribution back into the x-y plane.

(d) Integral technique

The application of the integral technique is simpler

for cases when the thermal properties are assumed constant. It is a useful and quick method when the main interest is to examine the temperature of the surface of a solid. Prasad and Rursman {1} have used the method to determine the thermal behaviour of a rectangular cavity heated from the inside.

(e) Electrical analogy

When space derivatives are approximated and the time derivatives retained a formulation well suited for electrical analog computation is obtained. This analogy has proved very valuable {9} in the analysis of many types of complex transient heat flow problems.

(f) Numerical methods

The effect of temperature dependent thermal properties or non-linear boundary condition make it difficult for the analytical techniques to be used. Thus in these circumstances it is frequently necessary to employ numerical methods such as finite differences, finite elements or boundary element methods {10}. Numerical methods require the use of high speed computers and are memory intensive.

(g) Approximate analytical procedure

Several methods have been developed {0.1,12,13} for

obtaining approximate solutions in the analytical form that do not have the drawbacks of successive calculation steps as in the case of numerical methods. Such treatment related to heat conduction have been extensively studied by Biot [13].

Besides the above procedures several other techniques have been derived by extending the previous solutions. Some of such methods are:

- i) superposition technique and
- ii) product solution

i) Superposition technique

This method will give good results if it is required to determine, say, change of boundary conditions after certain time duration. More complex cases may be treated (14), by this method.

ii) Product Solution

Many important solutions to initial value problems can be obtained as a product of simpler ones.

In the present study 'Numerical method' has been adopted to investigate thermal conditions in domestic stove linings. The procedure was found easy to adopt to the real

problem where the thermal properties and heat transfer coefficients were functions of temperature. In addition the method could provide results rather quickly (with the help of a computer) when there is a need to investigate a large number of parameters.

2.3 THE STRESS DISTRIBUTION

One of the main causes of stress in a ceramic body is non-uniform heating, which will introduce non-uniform expansion. Thus stresses due to the heating are set up. For a perfectly elastic rod restrained in one direction the stress, a , is given by:

$$a = E\alpha(T - T_a) \quad \dots(2.5(a))$$

where E , α , T and T_a are Young's modulus, coefficient of thermal expansion, new temperature level and initial temperature respectively. For the case of an infinite slab the stress will include the Poisson's ratio, u , as given by:

$$a = E\alpha(T - T_a)/(1-u) \quad \dots(2.5(b))$$

The fracture of glass {5} when suddenly heated or cooled is attributed to such stresses.

2.3.1 The general axis-symmetrical problem

By making use of stress functions, Hoyle [15] has shown that the thermal stresses in an axis-symmetrical solid can be given by the following equations in the cylindrical coordinate system:

The radial stress

$$\sigma_r = \frac{1}{r^2} \left(\frac{1}{3} \frac{\partial^2 \phi}{\partial r^2} + \frac{1}{3} \frac{\partial^2 \psi}{\partial z^2} - \frac{1}{1-\nu} \frac{\partial \phi}{\partial r} \right) \quad \dots(2.6)$$

The circumferential stress

$$\sigma_\theta = \frac{1}{r^2} \left(\frac{1}{3} \frac{\partial^2 \phi}{\partial r^2} - \frac{1}{3} \frac{\partial^2 \psi}{\partial z^2} - \frac{1}{1-\nu} \frac{\partial \phi}{\partial r} \right)$$

The axial stress

$$\sigma_z = \frac{1}{r} \frac{\partial^2 \psi}{\partial z^2} \quad \dots(2.8)$$

and the shear stress

where ϕ and ψ are two stress functions governed by the following equations:

$$\nabla^2 \phi = \frac{1}{r} \frac{\partial^2 \phi}{\partial r^2} + \frac{\partial^2 \phi}{\partial z^2} + \frac{r E \alpha}{1-\nu} \frac{\partial \phi}{\partial r} = \frac{3T}{3r} \quad \dots(2.10)$$

and

$$8r^2 - r - 9r - 3z^2 = 0 \quad \dots(2.11)$$

These stress functions have been derived from other two stress functions ϕ and ψ so as to avoid relaxation problems at the boundaries:

$$\phi = \frac{r}{3r} \dots (2.12)$$

and:

$$1 - \nu \frac{8r}{3r} \dots(2.13)$$

where ϕ is an arbitrary function of r and z such that:

$$\tau_{rz} = \frac{32}{3} \frac{\partial \phi}{\partial r} \frac{\partial \psi}{\partial z}, \text{ and } \dots = \dots \text{ The operator } V^2 \text{ is defined by}$$

Equation (2.3).

2.3.2 The thick walled long cylinder

When the temperature distribution is only a function of the radial distance and the cylindrical surface is free of traction in hollow circular cylinders, the radial, the circumferential and the axial stresses are respectively as follows [4]:

$$\sigma_r = \frac{aE}{1-\nu} \left(\frac{1}{r^2} \frac{d^2 \phi}{dr^2} - \frac{1}{r} \frac{d\phi}{dr} \right) - \frac{r}{n} \frac{d\psi}{dr} \quad \dots(2.14)$$

$$e^{-\alpha z} = \frac{r_2 + r_1}{r_2 - r_1} \left(\frac{1 - \nu_1}{1 - \nu_2} \right)^{1/2} \left[\int_{r_1}^r \frac{T_r dr}{r} + \int_{r_1}^{r_2} \frac{T_r dr}{r} \right] \quad \dots (2.15)$$

$$\alpha z = \frac{1}{1 - \nu} \left(\frac{r_2^2 - r_1^2}{r_2^2 - r_1^2} \right)^{1/2} \left[\int_{r_1}^r \frac{T_r dr}{r} + \int_{r_1}^{r_2} \frac{T_r dr}{r} \right] \quad \dots (2.16)$$

where r , n and r_2 are arbitrary radius, internal radius and external radius respectively.

The solid cylinder case is shown {4,14} to be a special case of the above where r_1 is set to zero and l'Hopital's rule {16} is applied for the indeterminate expressions at $r = 0$.

The difficulty in using these equations is that the temperature distribution in the cylinder has to be known as a function of r in order to solve them, which is seldom available for practical transient temperature cases. Buist {17} has shown that after solving the diffusion equation for temperature distribution using numerical technique, a simple least squares curve fit to a polynomial which provides an expression that can easily be integrated can be obtained.

2.3.3 Transient thermal stresses due to rapid temperature change

In the ideal case the relationship for thermal stress during rapid heating or cooling is given by:

$$\sigma = E\alpha AT / (1-\nu) \quad \dots(2.17)$$

Generalizing this expression for any geometry:

$$\sigma = E\alpha AT \cdot f(\nu) \quad \dots(2.18)$$

where $f(\nu)$ is a function of Poisson's ratio. Kingery [5] has summarized these relationships and are presented in Table 2.1.

In the most general case:

$$\sigma = W_D \frac{E\alpha AT}{1-\nu} \quad \dots(2.19)$$

where W_D is a dimensionless parameter, with values between 0 and 1, and is known as "non-dimensional stress" or "coefficient of reduction of stress" and is generally a function of a non-dimensional heat transfer coefficient, β , defined by:

$$\beta = 10 \cdot \frac{h}{k} \quad \dots(2.20)$$

where r , h and k are the radius of the cylinder, the convective heat transfer coefficient and the thermal conductivity respectively.

It has been proposed by Buessem [18] that for the case of infinite cylinder:

$$W_D = (2.0 + 4.3/\beta - 0.5 \exp(-16/\beta))^{-1} \quad \dots(2.21)$$

for the case of cooling, and

$$i_p = (2.0 + 4.3/5)^{-1} \quad \dots(2.22)$$

for the case of heating.

Singh et. al. {19} proposed the value of i_p as:

$$i_p = (1.451 + 4.95/5)^{-1} \quad \dots(2.23)$$

and this was modified by Glandus {20} as:

$$i_p = (1.451 + 4.95/6 - 0.45 \exp(-16/6))^{-1} \quad \dots(2.24)$$

2.3.4 Stresses due to heating or cooling at a constant rate

When a body is cooled or heated at constant rate (w K/sec) a parabolic temperature distribution is set up.

For a half thickness of a slab (plate), r_m , and thermal diffusivity $k = k/\rho C^{\wedge}$, the following stresses are developed

$$\text{on the surface } \sigma_g = - \frac{r_m^2}{1-\nu} \frac{dT}{3k/\rho C_p} = - \frac{AT}{1-\nu} \quad \dots(2.25)$$

$$\text{and in the centre } \sigma_c = - \frac{r_m^2}{1-\nu} \frac{dT}{6k/\rho C_p} = - \frac{g^{\circ}t_{AT}}{1-\nu} \quad \dots(2.26)$$

Expressions for the temperature difference between surface and centre of various geometries are given in Table 2-2 a⁵J per Kingery {21}. The temperature difference, AT , is in terms of (J) , R_m and K in such cases,

2.4 A REVIEW OF ASPECTS RELEVANT TO FAILURE

2.4.1 Introduction

Although problems of thermal cracking of ceramics are as old as the industry itself, not a great deal has been published regarding the subject until the last forty years {22}. For reliable engineering design and optimum material selection it is imperative that the thermal fracture behaviour of commercial ceramics be understood.

Gradients of thermal expansion can lead to micro crack formation on phase boundaries or grain boundaries {23}. Such cracks can greatly reduce the strength of the material.

2.4.2 Thermal shock resistance

Stresses of the nature described in Section 2.3.3, under conditions of rapid temperature change will cause weakening or fracture. The resistance to this phenomena is called thermal shock resistance.

The "thermoelastic theory" (concerned with the initiation of new cracks when thermal stresses exceed a certain limit) defines the thermal shock parameter R {21} as:

$$R = a_f(1-\nu)/Ea. \quad (2.27)$$

where σ^* , ν , E and a are fracture stress (quoted as "strength beyond which crack developed" by Glandus {20}), Poisson's ratio, Young's modulus and coefficient of thermal expansion respectively. When the shock is severe R represents the maximum temperature gradient ΔT_c the body can withstand without failure. This parameter is multiplied by a shape factor, according to Table 2.1, depending on the shape of the solid under consideration and represents the corresponding temperature gradient to cause fracture.

For the less severe condition of thermal shock ΔT_c is generally greater than R and is given by the relationship {20}:

$$\Delta T_c = R/W^{-1} \quad \dots(2.28)$$

where W was previously defined as the coefficient of reduction of stress.

For the conditions when the rate of heating and cooling is low (with values of Biot number less than 2.0 {18}) a factor $R' = kR$, where k is the thermal conductivity, has been found useful for consideration as a thermal shock parameter {5, 18, 20}. The critical temperature ΔT_c is then given by:

$$\Delta T_c = \frac{R'C}{r_0 h} \quad \dots(2.29)$$

where r_0 , h and C are the radius, the heat transfer coefficient and a constant respectively. The value of the constant C is given as 4.3 by Glenny and Royston {18}, 3.2 by Kingery {21} and 4.95 by Glandus {20} depending on the experimental results each author or authors obtained.

Hasselman {24} proposed another theory that describes crack propagation (popularly known as the 'energetic theory' (20,23), and this examines thermal shock fracture in the absence of external body forces. It takes into account a mechanical solid model uniformly cooled at a temperature difference ΔT , and rigidly restrained to induce a state of triaxial stress {14} σ given by:

$$\sigma = \frac{E \Delta T}{1-2\nu} \dots(2.30)$$

It assumes {20^25} the material to be totally brittle and that it contains N Griffith flaws {26} per unit volume. The cracks are assumed to be circular, uniformly distributed and that they simultaneously propagate in the radial direction.

The total energy $W^$ per unit volume released during fracture is composed of the fracture energy and the elastic energy $\frac{1}{2} \sigma \epsilon a^2$ (which is basically the product of the two surfaces' area created during cracking, and the surface energy γ). This total energy is given by:

$$\frac{w}{t} = \frac{3 (\Delta T)^2 E}{1-2\nu} \left(1 + \frac{1.6 (1-\nu^2)}{9(1-2\nu)} \right) + \frac{\gamma a^2}{2Ea(1-\nu^2)} \quad \dots(2.31)$$

where E, ν, a and γ are Young's modulus of uncracked specimen, Poisson's ratio, crack length and surface energy of the material respectively.

According to Hasselman [24, 25] the stability criterion was given by the following inequality:

$$\frac{\partial W}{\partial a} < 0 \quad \dots(2.32)$$

Thus the critical temperature difference required for crack instability is given by:

$$\Delta T_c = \frac{\gamma}{a} \sqrt{\frac{1-\nu^2}{9(1-2\nu)}} \left(1 + \frac{1.6(1-\nu^2)}{9(1-2\nu)} \right) \sqrt{\frac{3}{2Ea(1-\nu^2)}} \quad \dots(2.33)$$

Figure 2.1 illustrates this result by presenting a qualitative variation of ΔT_c as a function of crack length. It appears that ΔT_c passes through a minima that separates a zone of stability from a zone of instability. For short cracks the critical temperature difference is given by:

$$\sigma_{AT_c} = \frac{2-2\nu}{a} \sqrt{\frac{2E(1-\nu^2)a}{\dots}} \dots(2.34)$$

This corresponds to the left portion of the curve in Figure 2.1. σ_{AT_c} here does not depend on the crack density. For long cracks σ_{AT_c} is a linear function of N as shewn by the equation

$$\sigma_{AT_c} = \left(\frac{4-2\nu}{2E(1-\nu^2)} \sigma_{AT_c}^2 \right)^{1/2} \dots(2.35)$$

The spreading of initial cracks is accompanied by the release of elastic energy that is greater than the gain of surface energy. This excess energy is transformed into the propagation energy [20,25]. When the crack length reaches a length defined by Equation (2.34), it still possesses kinetic energy and continues to propagate until the potential energy released equals the total surface fracture energy. By equating the initial and final conditions of Equation (2.31), the final crack length for short cracks is given by.

$$a_f = \sqrt{\frac{8(1-\nu^2)a_1 N}{\dots}} \dots(2.36)$$

According to Griffith [27] for plane strain condition the fracture stress is given by:

$$a = \left(\frac{LJ}{2a(1-\nu^2)} \right)^{1/2} \dots(2.37)$$

Thus giving the final crack length in terms of fracture stress:

$$\frac{f_1}{a_f} = \left(\frac{3(1-2\nu)ct}{4tNY E} \right)^{1/2} \quad \dots(2.38)$$

The most extensively used parameters in this theory are R'' and $R' \cdot \cdot'$ where

$$R'' = EY / a_r^2(1-2\nu) \quad \dots(2.39)$$

and

$$R' \cdot \cdot' = R'' / Y \quad \dots(2.40)$$

However, the quantitative use of both 'thermoelastic' and 'energetic' theories has been found {23} to be difficult for reasons ranging from estimation of certain parameters to the actual definition of certain quantities (such as the fracture strength, coefficient of reduction of stress, ip, etc.). but are useful for qualitative purposes such as:

- i) pointing out parameters relating to cracking (the critical temperature difference),
- ii) pointing out parameters related to damage (decrease in strength), and
- iii) Comparison between two materials for the purposes of optimizing the 'cracking resistance'

AT_c and the 'damage resistance' (loss of strength) as shown in Figure 2.2.

2.4.3 Influence of heat transfer conditions

Behaviour of thermal fracture in brittle materials varies with different heat transfer conditions. Some of these are outlined below.

a) Constant heat transfer coefficient

This condition is the one previously discussed in Section 2.4.2. Three parameters R , R' and R'''' may be required.

b) Constant temperature gradient

A fixed temperature differential can be produced in a cylinder carrying a hot fluid from inside and cooled from outside as in the case of tubes. Under this condition thermal conductivity has no influence. The limiting temperature difference if cracking is to be avoided is given {28}:

$$AT = C.R' \underline{\hspace{10em}} (2.41)$$

where

$$C = \frac{2 \cdot n(r_2/r_1)}{\left\{ 1 - \frac{r_1^2}{r_2^2 - r_1^2} \ln(r_2/r_1) + \frac{1 - v^2}{2} \left(\frac{r_2}{r_1} \right)^2 \right\}} \quad (2.42)$$

r_2 and r being external and internal radii respectively.

c) Constant heat flow

In this case the material must conduct all the heat supplied as in the case of a heating element surrounded by a ceramic tube. The maximum heat flow, q , which can be conducted without failure is given by:

$$q = C'R \quad \dots(2.43)$$

where

$$C' = \frac{2\pi n}{\ln(r_2/r_1)} \quad \dots(2.44)$$

and c is given by Equation (2.42).

d) Constant rate of change of temperature in the heat transfer medium

Kingery (21) suggests this could be the case when a solid is heated in a furnace, where the temperature gradient

will depend on the temperature of the furnace. The maximum rate of temperature change to avoid cracking is proportional to $\frac{k\alpha_f(1-\nu)}{\rho C_f E a}$ where ρ and C_f are density and specific heat capacity of the body respectively.

e) Convective heating or cooling

The heat transfer coefficient varies with temperature and it becomes an important factor in such a case. The maximum temperature difference for failure to be avoided [29]. for the case of a sphere is:

$$T_{\max} = \frac{5}{E \cdot a} (i + \frac{1}{Bi}) \quad \dots(2.45)$$

where (Bi) is Biot number.

f) Radiative heating or cooling

During radiative heating or cooling thermal emissivity becomes an important material property. The maximum temperature of a black radiating surface to avoid fracture as given by Hasselman [30] (for the case of small spheres) is:

$$T_{\max} = \left(\frac{5\alpha_f(1-\nu)k}{S^r \cdot a E e} \right) \quad \dots(2.46)$$

where S_t and e are the Stefan Boltzmann constant and the thermal emissivity respectively.

2.4.4 Effect of specimen size

Cardall and Ging {29} investigated effect of specimen size in high strength alumina spheres and confirmed that the limiting temperature difference to cause cracking is proportional to the reciprocal of the size of the specimens. Glenny and Royston {18} used commercial grade alumina and showed the strength decreases with increasing size of specimens.

2.4.5 Thermal fatigue

Ceramics exhibit decrease in strength under conditions of thermal fatigue or repeated thermal shock {31}. Hasselman et. al. {31} described the slow crack growth rate of ceramics by the equation:

$$\frac{da}{dt} = v_0 \exp(b^* - U) / R_0 T \quad \dots(2.47)$$

where b_0 , t , K_1 , U , R_0 and T are a constant, time stress intensity factor, activation energy, Boltzmann constant and the absolute temperature respectively, and v_0 is a pre-exponential factor and proposed a computer simulation technique for the life time prediction, in which the extension

of the most critical flaw was calculated from its initial size a^0 to its final size a^f . The stress and stress intensity factors were calculated for a given time interval increment Δt of the transient stress pulse. Velocity and crack depth at the next time step were estimated by the use of Equation (2.47) and its integral respectively. By the use of computational iterative procedure to a prescribed convergence criterion (at which the stress intensity factor approaches the critical intensity factor), Hasselman et. al. [31] came up with a procedure that counts thermal cycles to failure.

Kamiya and Kainigaito [32] proposed an analysis of thermal fatigue analogous to the analysis developed for the static fatigue. In their analysis they described the slow crack growth rate of ceramics [33] by

$$\frac{da}{dt} = A K_I^n \quad \dots(2.48a)$$

where K_I , A and n are stress intensity factor and material constants [34] respectively. Alternatively they described [32] the crack growth rate by

$$\frac{da}{dt} = A' \exp(-L/RT) K_T^n \quad \dots(2.48b)$$

where R , T , L and A' are gas constant, temperature and material constants respectively. The stress intensity factor K_I , is given by [27]:

$$K^{\wedge} = Y a a^{\wedge} \dots(2.$$

where Y, a and a are a geometric factor, applied stress and crack length respectively.

Using Equations (2.48) and (2.49) and the Weibul statistics {27} discussed in the next section Kamiya and Kamigaito {32, 33} arrived at the relationship

$$M' AT \dots(2.50)$$

where M and M' are nuirfoers of cycles of thermal fatigue corresponding to AT and AT' thermal shock severity respectively at a common value of survival probability and n is the material constant as defined earlier.

2.4.6 Failure probability

Material strength variability is an inherent feature in brittle materials. In the study of brittle conppnents a statistical treatment, from which the probability of failure can be assessed is required. Epstain {35} proposed a statistical theory of fracture called 'the weakest link concept', which suggests that the brittle fracture strength is determined by the single irost dangerous flaw. For a material having N flaws (links) if $F^{\wedge}o$ is the probability of failure at stress o the probability of failure for the N links is then given by:

$$F_n(o) = 1 - (1 - F_{JC0})^{1*} \quad \dots(2.51)$$

Using the theory of limits (16) $F^{\wedge}(a)$ can be approximated by:

$$F_N(0) = 1 - \exp(- NF_x(o)) \quad \dots(2.52)$$

for the whole N chain links, the links being proportional to the volume of the material. For an elemental volume, dv, Weibull proposed an empirical formulation of f(a) such that:

$$\int_v f(a)dv = - NF_x(a) \quad \dots(2.53)$$

and defined f(a) as:

$$f(a) = \left(\frac{a-a_0}{a_0} \right)^m \quad \text{for } a > a_u \quad \dots(2.54)$$

$$f(a) = 0 \quad \text{for } a < a_u \quad \dots(2.55)$$

where a_0 , a_q , a and m are threshold stress, normalizing stress, applied stress and Weibull modulus respectively.

The probability of failure will be:

$$P_f = 1 - \exp\left(- \int_v \left(\frac{a-a_0}{a_0} \right)^m dv\right) \quad \dots(2.56)$$

Alternatively the probability of survival P_s will be:

$$P_s = \exp\left(- \int_v \left(\frac{a-a_0}{a_0} \right)^m dv\right) \quad \dots(2.57)$$

For the case of uniaxial stress, the probability of survival is:

$$p_s = \exp\left(-V \left(\frac{\sigma - \sigma_0}{\sigma_0}\right)^m\right) \quad \dots(2.58)$$

where V is the stressed volume. According to failure probability the mean strength is defined as [27]:

$$\bar{\sigma} = \int_0^{\infty} \sigma dP_x = \int_0^{\infty} \sigma P d\sigma \quad \dots(2.59)$$

For the case of uniaxial strain, the probability can be integrated to give:

$$V \int_0^{\infty} \sigma^m dP_x$$

where $\Gamma\left(\frac{m+1}{m}\right)$ is the gamma function,

The ratio of the mean strength of a four point loaded beam (see Figure 2.3) to a uniaxially loaded one is given by:

$$\frac{\bar{\sigma}_{Flex}}{\bar{\sigma}_p} = \frac{2Y(m+1)^2}{(2+(m+1)(Y-2))} \quad \dots(2.61)$$

The selection of working stress of brittle components is done by defining a safety factor which is the ratio of the mean strength to the strength at a given probability. Thus, s , the safety factor is then given by:

$$s = \frac{\bar{\sigma}}{\sigma(P_s)}^{1/m} \quad \dots(2.62)$$

The Weibull statistical theory has been extensively used in relation to thermal failure. Manson and Smith [36] applied the theory to predict the strength of discs subjected to thermal shock. Stanley and Wprp?etson [37] extended the analysis for multiaxial loading conditions and proposed a method for applying the analysis on a cylinder subjected to thermal and pressure loading.

Shape	Surface	Centre
Infinite slab	$\sigma_x = 0$ $\sigma_y = \sigma_z = \frac{t^2}{1-\nu} (T_a - T_s)$	$\sigma_x = 0$ $\sigma_y = \sigma_z = \frac{Ea}{1-\nu} (T_a - T_c)$
Thin plate	$\sigma_y = \sigma_z = 0$ $\sigma_x = aE(T_a - T_s)$	$\sigma_y = \sigma_z = 0$ $\sigma_x = E(T_a - T_c)$
Thin disk	$\sigma_r = 0$ $\sigma_t = \frac{(1-\nu)Ea}{1-2\nu} (T_a - T_s)$	$\sigma_r = \frac{(1-\nu)Ea}{2(1-2\nu)} (T_a - T_c)$ $\sigma_t = \frac{(1+\nu)Ea}{2(1-2\nu)} (T_a - T_c)$
Long solid cylinder	$\sigma_r = 0$ $\sigma_z = \frac{Ea}{1-\nu} (T_a - T_s)$	$\sigma_r = \frac{Ea}{2(1-\nu)} (T_a - T_c)$ $\sigma_z = \frac{Ea}{2(1-\nu)} (T_a - T_c)$
Long hollow cylinder	$\sigma_r = 0$ $\sigma_z = \frac{Ea}{1-\nu} (T_a - T_s)$	$\sigma_r = 0$ $\sigma_z = \frac{Ea}{1-\nu} (T_a - T_c)$
Solid sphere	$\sigma_r = 0$ $\sigma_t = \frac{2Ea}{1-\nu} (T_a - T_s)$	$\sigma_r = \frac{2Ea}{3(1-\nu)} (T_a - T_c)$ $\sigma_t = \frac{4Ea}{3(1-\nu)} (T_a - T_c)$
Hollow sphere	$\sigma_r = 0$ $\sigma_t = \frac{Ea}{1-\nu} (T_a - T_s)$	$\sigma_r = 0$ $\sigma_t = \frac{Ea}{1-\nu} (T_a - T_c)$

Table 2.1: Thermal stress at the surface and centre of different geometries subjected to thermal shock.

2

E = Modulus of elasticity (N/m)

a = Coefficient of thermal expansion (K^{-1})

ν = Poisson's ratio

T_{ct} = Initial temperature (K)

T_s = Surface temperature (K)

T_c = Core temperature (K)

moBi

UHTV1'

Shape r_m in metres	Temperature difference (K)
Infinite plate (half thickness = r_m)	$0.50 \frac{K}{\sqrt{\rho r^2}}$
Infinite cylinder (radius = r_m) ;	$0.25 \frac{K}{\sqrt{\rho r^2}}$
Cylinder diameter = length (radius = r_m)	$0.201 \frac{K}{\sqrt{\rho r^2}}$
Cube (half thickness = r_m)	$0.221 \frac{K}{\sqrt{\rho r^2}}$

Table 2.2: Temperature difference between surface and centre of various shapes cooled at a constant rate

$\phi^r = dT/dt$ (K/sec).

k = thermal diffusivity (m^2/s)

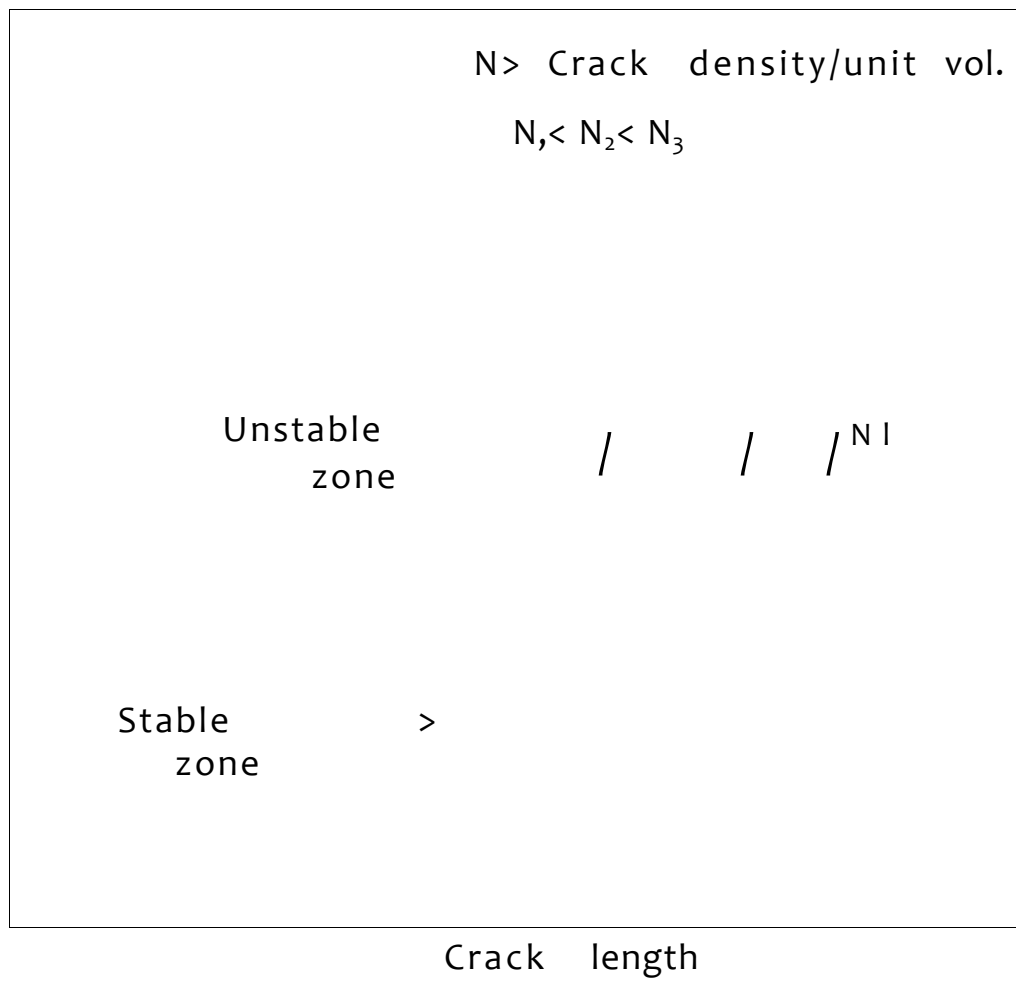


Figure 2.1: 'Energetic theory' approach for thermal shock resistance

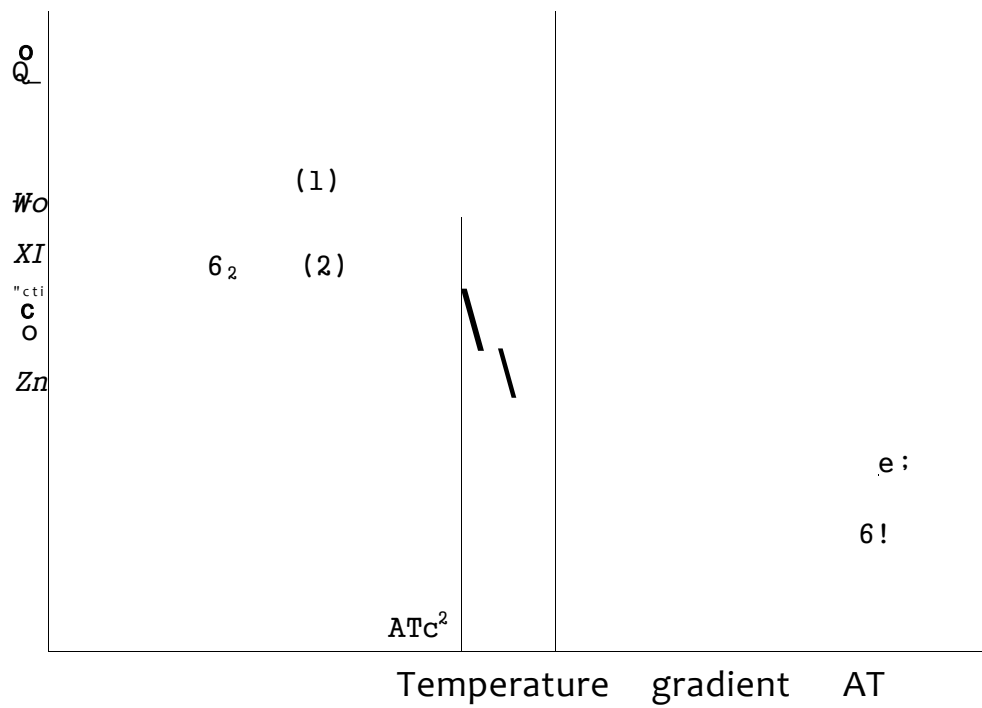


Figure 2.2: Strength before and after cracking for high strength (1) and low strength (2) materials versus thermal shock severity

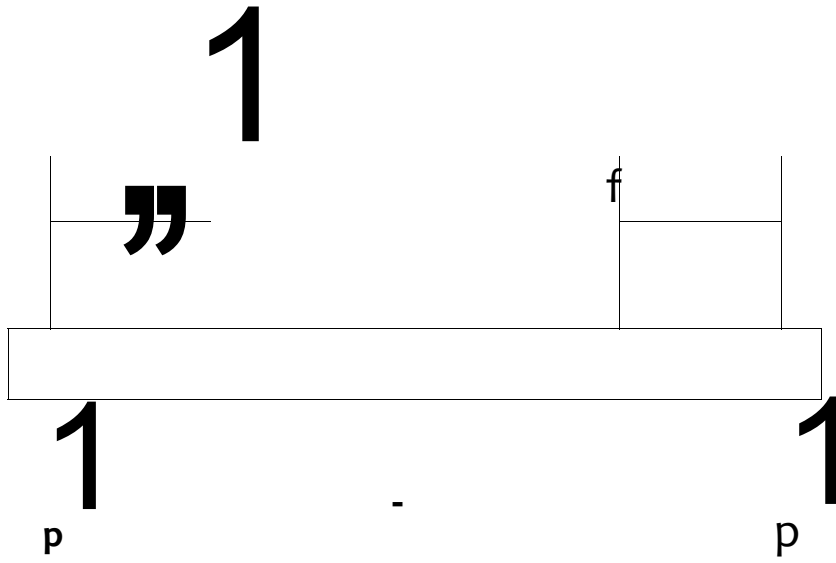


Figure 2.3: The loading arrangement for specimens subjected to four points flexure

CHAPTER THREE

3. HEAT TRANSFER CHARACTERISTICS, AND TEMPERATURE MP STRESS DISTRIBUTIONS IN HOLIPⁿ7 CYLINDERS

3.1 INTRODUCTION

Thermal stresses arise when the temperature of a solid is not uniform or when the solid is composed of different materials with different coefficients of thermal expansion.

%

Fundamental equations governing temperature, stresses and deformation in a solid suggest that the three quantities are interrelated. However, for most practical problems the effect of stresses and deformation upon temperature is quite small and can be neglected [14]. This procedure allows the determination of the temperature distribution to become the first, and independent step of thermal stress analysis, the second step being the determination of stresses and deformation due to the temperature distribution.

In this chapter, among other analyses the formulation of a mathematical boundary value problem for the determination of the temperature and stress distribution in ceramic cylinders is discussed. Such cylinders closely simulate the actual wall conditions found in domestic stoves (popularly known as jikos'in Kenya), thus obtaining results that can be used to improve the ceramic lining found in 'jikos'.

Heat within the ceramic lining is transferred solely by conduction. However transfer of heat to and from the surfaces takes place by other modes of heat transfer. Choice of these boundary conditions on the cylinder surfaces have been made so that there will be no serious deviation introduced from the actual conditions found in the stoves.

3.2 THE STOVE MODEL

Figure 3.1 shows the prototype of a stove model considered in this study. It basically consists of a slightly tapered cylindrical ceramic lining surrounding the fuel, in this case charcoal. The wall of the lining and the pot on top of the stove receives heat from the charcoal by convection and radiation. Only 15.4%–27.9% of the heat liberated has been reported to be used up as useful heat and 31.1%–42.4% as stove body losses [1]. The purpose of this investigation is to study the distribution of temperature and hence stress due to such heat transfer.

3.3 THE PHYSICAL MODEL

Modelling of heat transfer from heat sources such as wood and charcoal is rather complex and requires knowledge of the heat liberated from the heat source as a function of time and is presently under study [1]. For the purpose of the

present study the heat input will be considered as a constant heat source which is symmetrically placed in the centre of the lining. Hereafter heat input is referred to that portion of the heat lost through the ceramic liner in the stove model.

The conical lining, since the cone angle is very small, will be represented by a hollow cylinder with an internal radius r_1 and an external radius r_2 . In addition end effects are ignored so that the heat supplied by the source will totally be transmitted to the cylinder and end heat losses are neglected. With these assumptions the problem reduces to one of a one dimensional transient heat conduction in a cylinder with constant heat supply from the inside. The physical situation is depicted in Figure 3.2(a).

The surface at $r=r_2$ which is initially at a temperature T_a as the rest of the cylinder, is exposed to the heat source suddenly at time $t = 0$, and thereafter heat is transferred to the inner wall mainly by radiation. Although heat transfer by natural convection takes place between the heating element and the air occupying the space between the heating element and the inner surface, and later between the same air and the inner surface the effect will be neglected due to two reasons:

- i) the temperature differences between the heating

element and the fluid inside the cylinder, and the fluid and the inner surface of the cylinder normally is not large, and

it) the surface area of the inner surface is over eight times that of the heating element. According to Newton's equation {38} the rate of heat transfer by convection between a surface and a fluid is directly proportional to the heat transfer surface area. Thus natural convective heat transfer between the heating element and the air within the cylinder, and then between the same air within the cylinder and the inner surface of the cylinder can be negligible.

The temperature distribution across the wall of the cylinder varies with time and is shown qualitatively in Figure 3.2(b).

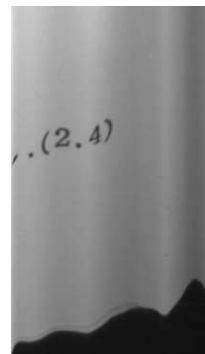
3.4 THE MATHEMATICAL MODEL

The physical model of Section 3.3 can be described mathematically by the following equations:

In the cylinder wall

$$\frac{c_p \rho}{k} \frac{\partial T}{\partial t} = \frac{\partial^2 T}{\partial r^2} + \frac{1}{r} \frac{\partial T}{\partial r}$$

At the inner surface



$$Q = h_r A_i (T_e - T(r_i, t)) \quad \dots(3.1(a))$$

$$h_r (V_i)^{3-1} = \dots$$

which can be combined as:

$$Q = -k A_i \frac{\partial T}{\partial r} \Big|_{r_i} \quad \dots(3.2)$$

and at the outer surface:

$$h(T(r_o, t) - T_{\infty}) = -k \frac{\partial T}{\partial r} \Big|_{r_o} \quad \dots(3.3)$$

where T is temperature, t time, r radius, r_i internal radius, r_o external radius, A_i internal surface area, h_r radiative heat transfer coefficient, Q heat input, Cp specific heat capacity, p density, k thermal conductivity, T[∞] the ambient temperature and T the temperature of the surface of the heating element.

The boundary condition at the outer surface of the cylinder is not that of a perfectly insulated material and there is heat loss at that end both due to convection and radiation. The heat transfer coefficient h is here defined as:

$$h = h_c + h_r \quad \dots(3.4)$$

where h and h_r are the natural convective and radiative heat transfer coefficients respectively.

3.4.1 Heat transfer mechanisms

(a) Convection

The major heat loss mechanisms at the outside surface are assumed to be by convection and radiation both during heating up and cooling of the cylinder. At the inside surface cooling takes place mainly due to convective heat transfer.

Local convective heat transfer coefficients are correlated using the following dimensionless parameters [37]–

$$(Nu) = C.(Gr)^p(Pr)^p \quad (3.5)$$

$$(Nu) = hL/k_f \quad (3.6)$$

$$(Gr) = \rho_f^2 g S_f L^3 \Delta T / \mu_f^2 \quad (3.7)$$

$$(Pr) = \mu_f C_{p_f} / k_f \quad (3.8)$$

where (Nu) is the Nusselt number, (Gr) Grashoff number and (Pr) Prandtl number. The properties h_f , ρ_f , β_f , and C_{p_f} are convective heat transfer coefficients of characteristic length L , density, volume expansion coefficient, the dynamic viscosity and specific heat capacity of the fluid respectively,

g and AT are acceleration due to gravity and the temperature difference between the fluid and the convective surface respectively. C and p are constants that depend on the flow conditions. For the case of vertical cylinders in the laminar flow range C and p are 0.59 and 0.25 respectively. All properties are determined at an average temperature of the wall and the ambient atmosphere and are presented in Table 3.1. Alternatively simplified equations have been presented for the heat transfer coefficient for the natural convection from various surfaces to air at atmospheric pressure { 39, 40 }.

For vertical cylinder they are:

$$h = 1.42 (AT/L)^{0.25} \quad (3.9)$$

for the case of laminar flow, and

$$h = 0.95 (AT)^{1/3} \quad (3.10)$$

for the case of turbulent flow. Where h is the heat transfer coefficient in W/m^2K , AT , temperature difference between the wall and the ambient atmosphere in degrees centigrade and L vertical dimension in metres.

For the model assumed, the flow was all in the laminar range with a very small boundary layer, and Equation (3.9) was

applied.

(b) Radiation

Energy exchange by radiation is the predominant heat flow mechanism at the outside surface at high temperatures, because the heat flow depends on the fourth power of the absolute temperature. To include radiation in the thermal network involving convection it was found convenient to define thermal radiative conductance, h_r , as {38}:

$$h_r = Q/A(T_1 - T_2) = F_{1-2} \left(S_L \frac{1}{T_w^2} - \right) \quad (3.11)$$

where F_{1-2} , S_L , A , T_w and T_2 are radiation body shape factor, Stefan-Boltzmann constant, area upon which F_{2-2} is based, wall temperature and a reference temperature respectively. For a small gray body of area A_1 inside a large enclosure of area A_2 ($A_1 \ll A_2$) F_{1-2} takes the value of the thermal emissivity e {38} which approximately has the value 0.70 for Fire clay. Heat transfer from the heating element to the inner surface is assumed to take place by radiation.

3.4.2 Properties of the ceramic model

Thermal properties of ceramics such as thermal conductivity, specific heat capacity, etc. vary greatly with temperature. However due to unavailability of values of the

properties of the ceramics under consideration as a function of temperature, constant properties are assumed. If a relationship of the form $f(T)$ could be correlated for the properties it would be possible to incorporate it in the thermal equations of the mathematical model. Further work on the properties of these ceramics as a function of temperature should be done in the future.

3.5 THE NUMERICAL SOLUTION

3.5.1 The temperature distribution

Equations (3.2), (3.3) and the right hand side of Equation (2.4) were solved by Central Difference Numerical Approximation Technique. Since the problem is to find the temperature at the next time step the time derivative was regarded as the slope of the temperature with respect to time and Forward Difference Approximation was used in the left hand side of Equation (2.4). The derivation of the finite difference equations is presented in Appendix A.1.1. A computer program that assumes that initially all the temperatures are at room temperature has been written to simulate this condition. The program presented in Appendix A.1.2 was designed to calculate the temperature distribution at small time increment, Δt , within which the temperature was assumed to be constant. The distribution obtained was used to calculate

the temperature distribution at the next time step $t+\Delta t$.

3.5.2 The stress distribution

At each time step the temperature distribution is substituted in Equations (2.14), (2.15) and (2.16), and this resulted in an integral expression for the radial, circumferential and axial stresses as a function of radius. In order to overcome the mathematical complexity of the resulting expression, a computer program (presented in Appendix A.1.2) which numerically integrates the expression was developed. The program was trapezoidal integration technique shown in Appendix A.2.1., thus giving the resulting stress expressions quickly.

The stress expressions can also be obtained by the use of the general axi-symmetrical equations given in Section 2.3.1 of the previous chapter. These equations can be solved by Finite Difference Techniques by using a method of forced convergence by human observation of parameters. The current computing facilities do not allow this and moreover it takes very large C.P.U. time to force arrays of two stress functions to convergence, thus this method is not applied in this work. A summary of the technique is presented in Appendix A.2.2.

3.5.3 The numerical output

The following three major sets of results are obtained from the solution of the numerical expressions:

(a) The temperature distribution across the wall of the cylinder: This result shows the temperature gradient and the rate of change of temperature with time. The highest temperature gradient usually occurs at the inside surface of the cylinder.

%

(b) The stress distribution across the wall of the model: This gives the magnitude and senses of stresses expected at the surfaces as a function of time. The maximum tensile stress always occurs at the outside surface for a model subjected to a laminar heat transfer conditions.

(c) The time required to reach steady state: This result is of great use from the point of view for the study of fracture. However, it will indicate the relative importance of stored heat in the wall and heat loss from the outer surface.

3.6 RESULTS AND DISCUSSION

A comparative discussion on the study of the temperature and stress distribution is presented in this section.

Figure 3.3 shows the temperature distribution across the wall of the cylinder as a function of time. The maximum temperature occurs at the inside surface. Figure 3.4 shows the temperature at the external and inner surfaces as a function of time. The heating rate of the inner wall is the highest during the first twenty minutes and decreases until steady state is reached. The cooling portion of the curve also indicates that the cooling rate is highest during the first few minutes. Figure 3.5 shows the circumferential stress distribution across the wall of the cylinder. The maximum stress is compressive and is found at the inner surface. The external surface is subjected to tensile stresses. Since ceramics have compressive strength that is four to eight times their tensile strength there will be emphasis on the study of the tensile stress at the external surface of the cylinder in this work. The radial stress (not shown) was compressive and about 10-12% of the maximum compressive stress. The stress distribution as a function of time is shown in Figure 3.6. The rate of change of stress is the highest during cooling which can be seen at 200 minutes in Figure 3.6.

The rest of the section will show what changes can be expected by changing the geometric parameters as well as changing certain physical properties of the material.

3.6.1 Effect of internal radius

For the same heat load the effect of internal radius on the temperature of the internal radius is negligible in the early transient region (up to 70 minutes after start-up). Figure 3.7 shows that the temperature at the inner surface increases sharply with a decrease in internal radius 70 minutes after start-up. The external wall temperature grows faster for higher internal radii (small wall thickness) and hence introducing lower thermal gradient. For the same heat supply the stress at the external surface is higher for smaller internal radii and so is the compressive stress at the inner surface. Steady state is achieved quickly for smaller wall thickness. The effect of the internal radius on the stress at the external surface is shown in Figure 3.8.

The effect of internal radius described above is quite different from the conditions found in real situations. Here the effect of internal radius is studied on the basis that there is a constant heat supply. However, in real situations the heat supply depends on the amount of charcoal burning inside the stove lining. With an increase in the inner radius the amount of charcoal that can be accommodated inside the cylinder is increased and so is the heat supply. At higher energy input one would expect to get similar response as when increasing the inner radius, as the heat supply per unit area is increased then.

3.6.2 Effect of external radius

Figure 3.9 shows that the temperature of the inner surface is lower in the transient range for larger external radii. Steady state is achieved faster for models with small external radii- However the temperature of the external surface increases rapidly for lower radii and very gradually for the cases of large external radii, thus introducing an increasing temperature gradient across the wall with an increase in external dimensions.

External tensile stresses are lowered with increasing radius in the transient state at the expense of very high compressive stresses at the inner surface. The inner wall stress rises the slowest for models with large external radii while models with thinner walls respond fast. Figure 3.10 shows the effect of the external radius on the tensile stress at the outer surface

3.6.3 Effect of thermal conductivity

It is a trivial deduction that the temperature gradient across a wall is high for materials with low values of thermal conductivity. This can be observed by inspecting the Fourier equation of heat conduction {7}:

$$q = -k \frac{dT}{dx} \quad (3.12)$$

where q , k , T and x are heat input per unit area, thermal conductivity, temperature and a coordinate axis respectively. Figure 3.11 presents the effect of thermal conductivity on temperature as a function of time. Change in thermal conductivity has a major effect on the inner surface temperature and very little on the outer surface. This could be attributed to the dependence of heat flow through the outer wall on the convective and radiative heat transfer coefficients at the outer surface.

*

Figure 3.12 shows the effect of thermal conductivity on the tensile stresses at the outer surface. It is shown that, there, stresses increase with decrease in thermal conductivity.

Decrease in thermal conductivity has the effect of increasing the compressive stress at the inner surface. However since most ceramics have a very high compressive strength compared to their tensile strengths this could be less detrimental to the material strength.

3.6.4 Effect of density and specific heat

Density and specific heat of the model in question appear at the same side of the Fourier heat conduction equation:

$$\frac{c_p \rho}{k} \frac{\partial T}{\partial t} = \frac{\partial^2 T}{\partial r^2} + \frac{1}{r} \frac{\partial T}{\partial r} \quad \dots (2.4)$$

This suggests that the effect of both parameters on temperature and stress is similar. Figure 3.13 presents the effect of specific heat on the temperature of the inner surface as a function of time. The major change occurred between 40 and 120 minutes after start-up. At 80 minutes after lighting, changing the specific heat from 800 to 1100 J/kg°C changes the inner surface temperature from 475° to 415°C. For the same change in specific heat the temperature gap is smaller in the early transient state and the steady state. Figures 3.14 and 3.15 show the effect of density and specific heat on the stress at the inner surface. These parameters have very little effect on the thermal stress distribution.

3.6.5 Effect of heat transfer coefficient

There is considerable uncertainty involved in treating the heat transfer coefficient as a variable because of the variation of the properties of air with temperature. Moreover in real situations stoves are also used in the open where the speed of wind could be substantial. Thus it is useful to investigate temperature and stress conditions when the coefficient of heat transfer is changed. Figure 3.16 shows the effect of the heat transfer coefficient of the temperature of the inner and outer surfaces as a function of time.

Increasing the heat transfer coefficient by a factor of two lowered both the inner and outer surface temperatures. The outer surface responded faster than the inner mainly because most of the heat loss was at that end. Figure 3.17 shows the effect of the heat transfer coefficient on the tensile stress at the outer surface. Stresses increased with increase in the heat transfer coefficient. The major increase in stress occurred in the transient state.

3.7 CONCLUSIONS

The highly idealized model presented has proved its usefulness by providing quickly and simply the relative changes that could be expected by changing the geometric parameters as well as the changing of the material of construction. The main weakness of the model lies in the treating of the problem as that of an ideal isotropic material and assuming a constant rate of heat supply at any instant which may not be the case in real stove situations.

Further discussions on the subject are presented in Section 4.5 of the next chapter.

Physical Properties of air		
Density	(ρ)	= 0.6783 kg/m ³
Volume expansion coefficient	(β)	= 0.0032 /K
Specific heat	(C_p)	= 1046.8 J/kgK
Dynamic viscosity	(μ)	= 0.000027 N/m ² s
Thermal conductivity	(k)	= 0.042 W/nK

Table 3.1 : Physical properties of the ambient atmosphere at 250°C.

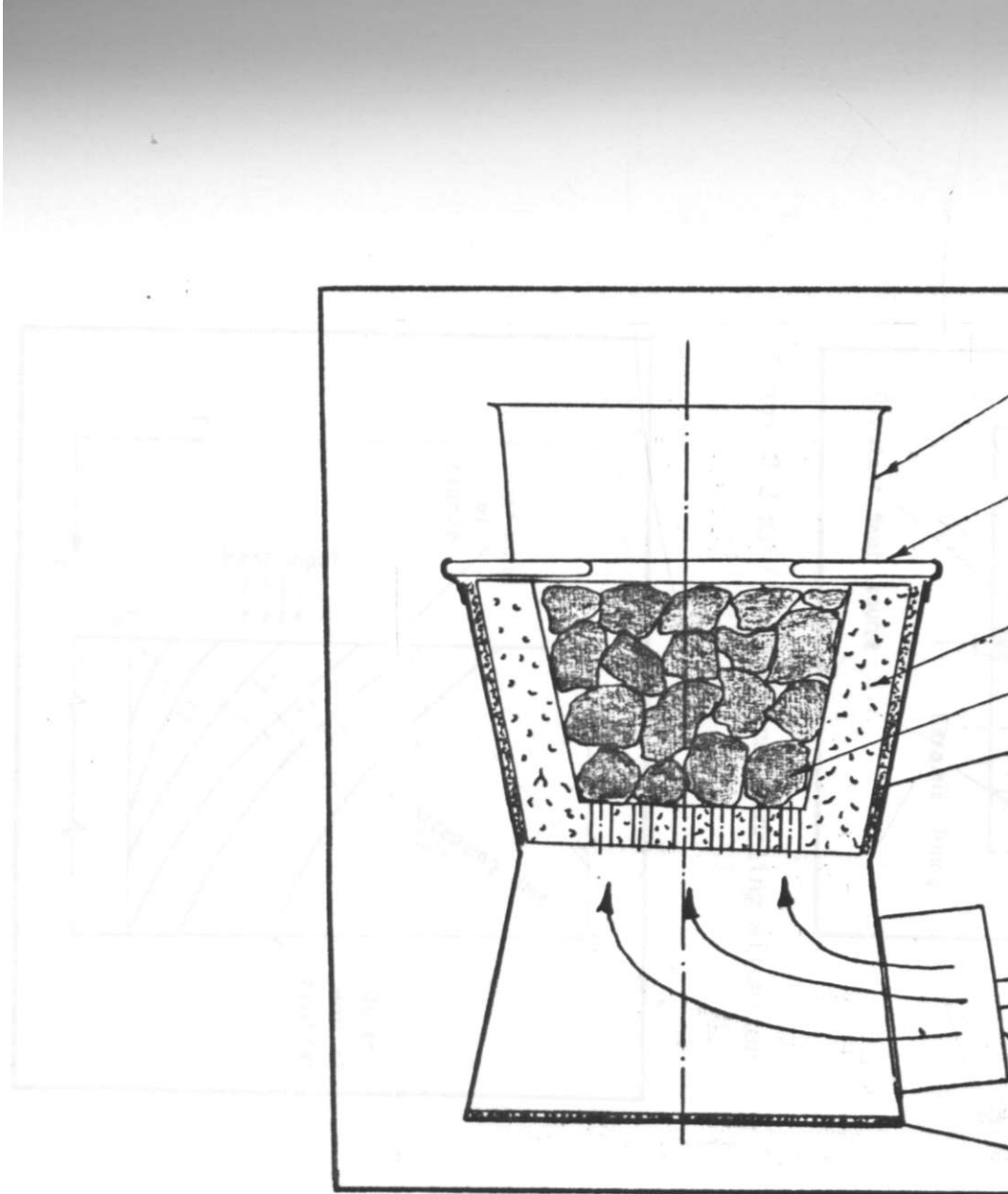


Figure 3.1: Hie stove model

/Pot

^pot Rest


^Ceramic Liner

Charcoal Bed

∞

Insulation
(drawn not to seal*)

}

 Air Inlet Port

• Insulation

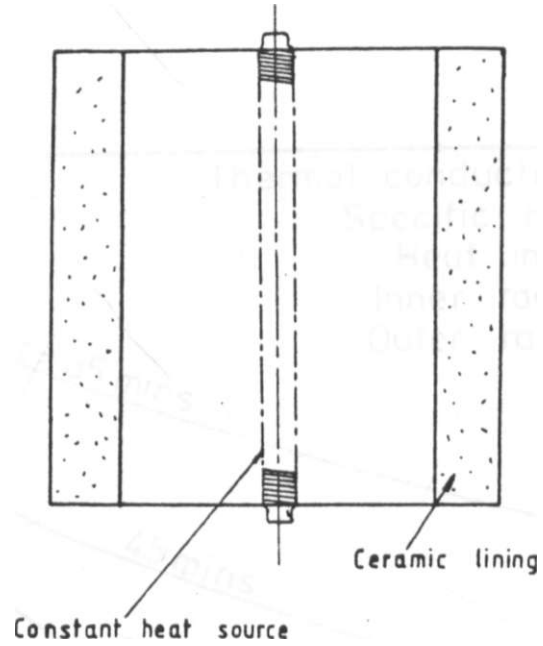


Figure 3.2(a): The physical modeling situation

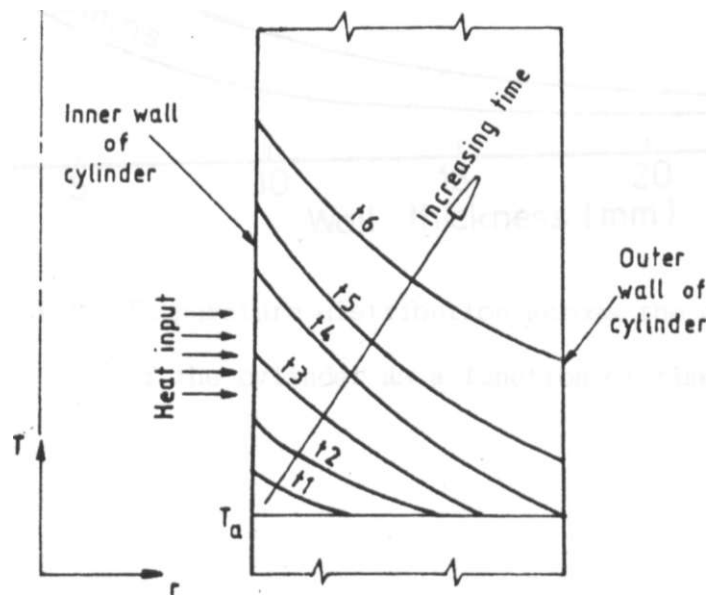


Figure 3.2(b): The temperature distribution

Thermal conductivity 0.52 W/mK
Specific heat 970 J/kgK
Heat input 750 W
Inner radius 72 mm
Outer radius 97 mm

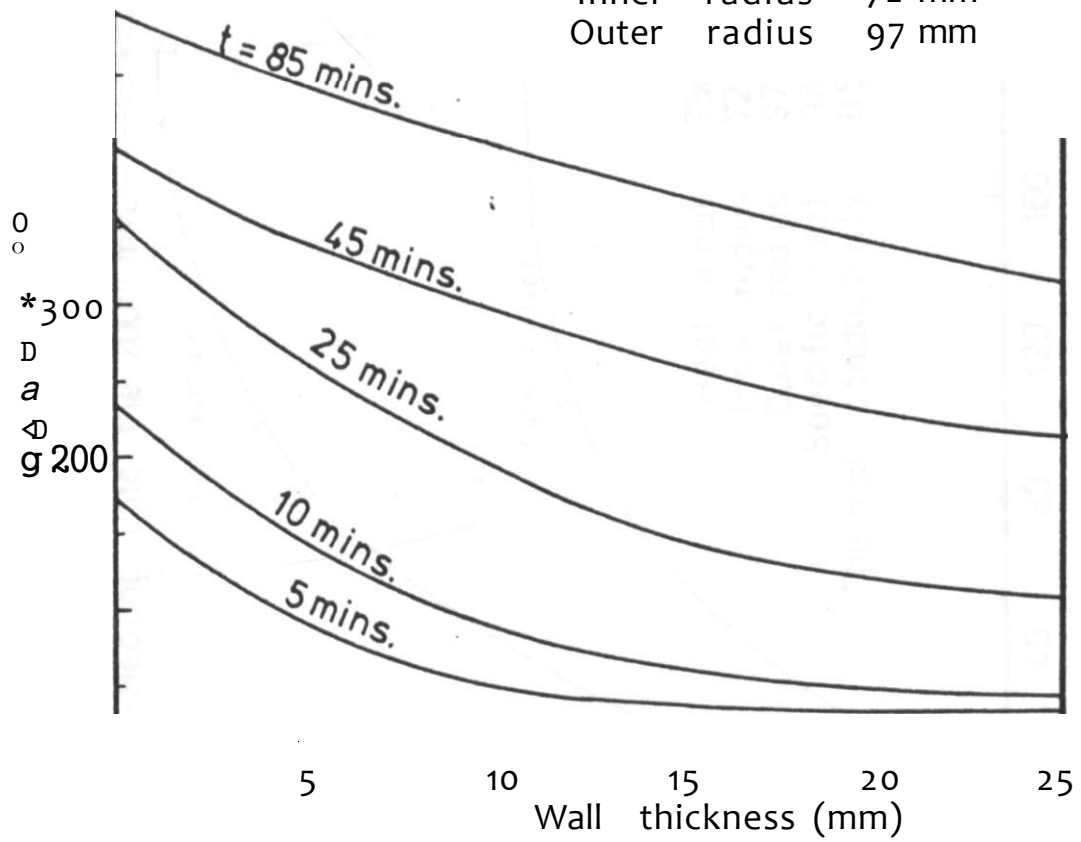


Figure 3.3: Temperature distribution across the wall of the cylinder as a function of time

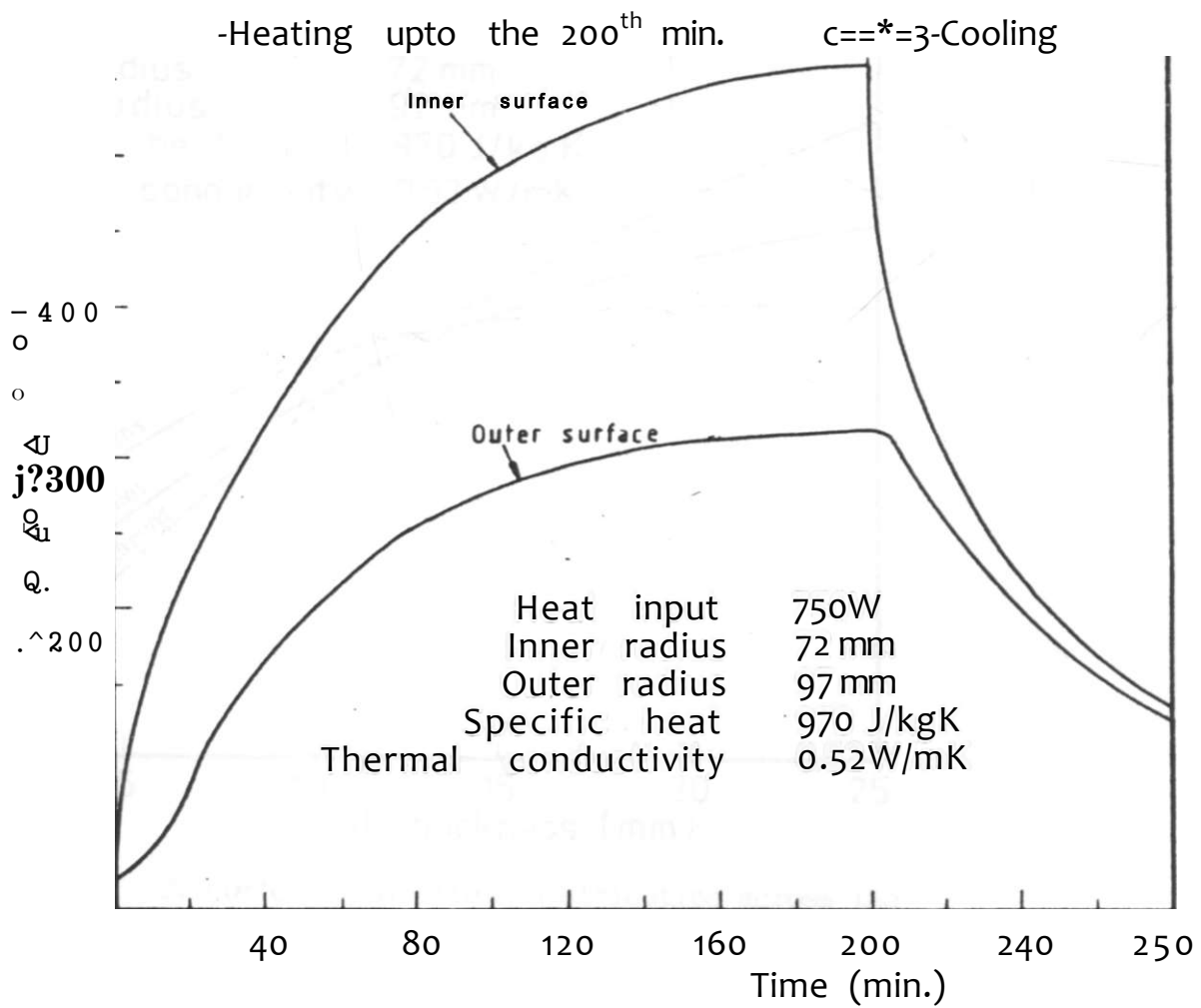
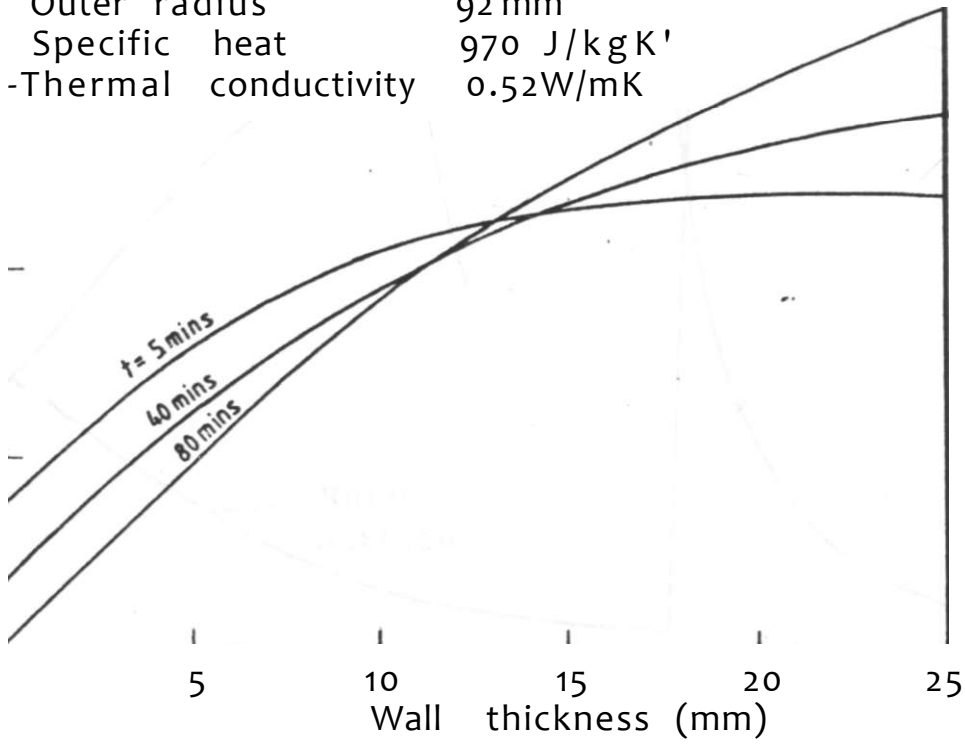


Figure 3.4: Temperature of the inner and outer surfaces of the cylinder function of time

Heat input 750 W
 Inner radius 72 mm
 Outer radius 92 mm
 Specific heat 970 J/kgK'
 -Thermal conductivity 0.52W/mK



a
to

Figure 3.5: Circumferential stress distribution across the wall of the cylinder as a function of time

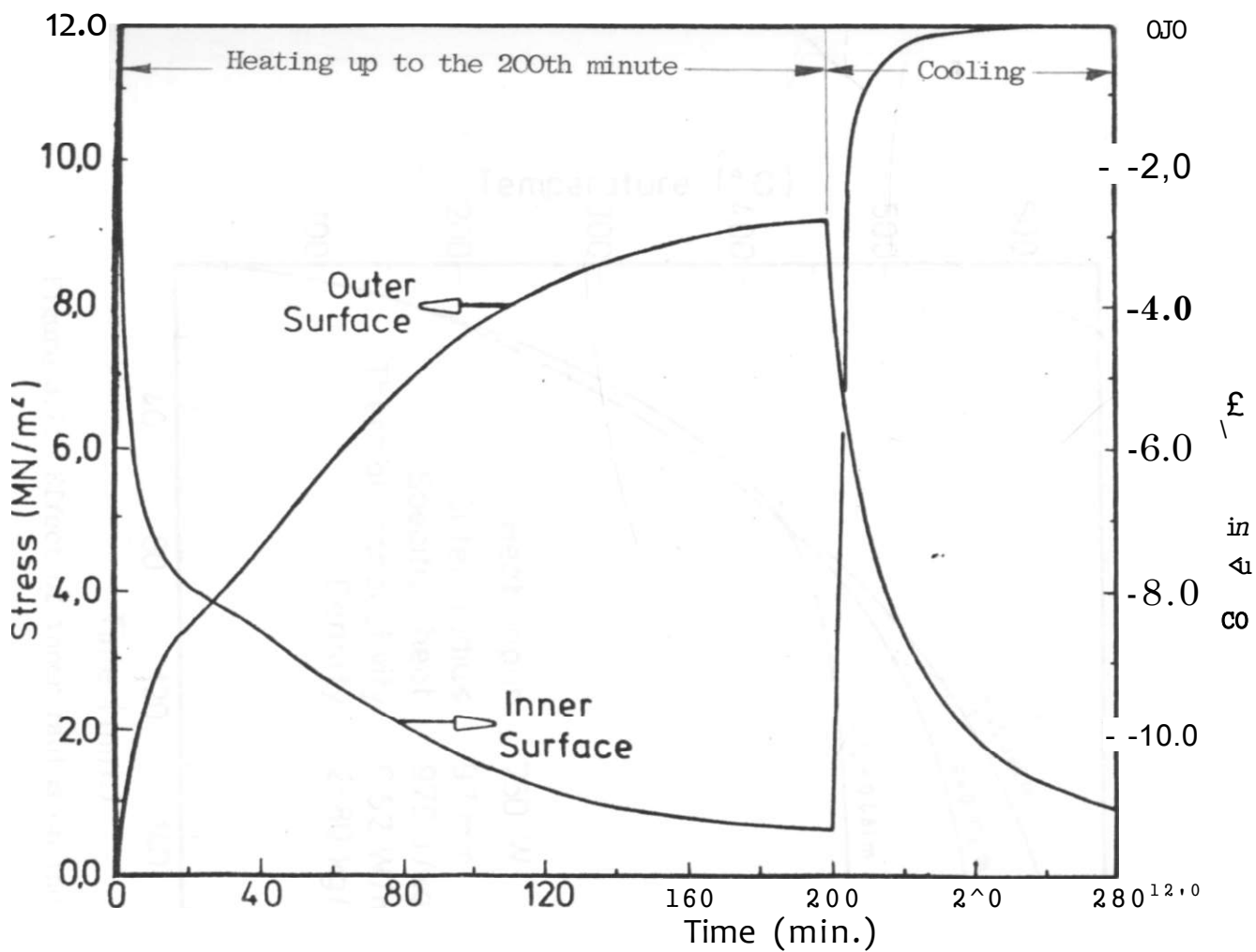


Figure 3.6: Circumferential stresses at the inner and outer surfaces of the cylinder as a function of time.

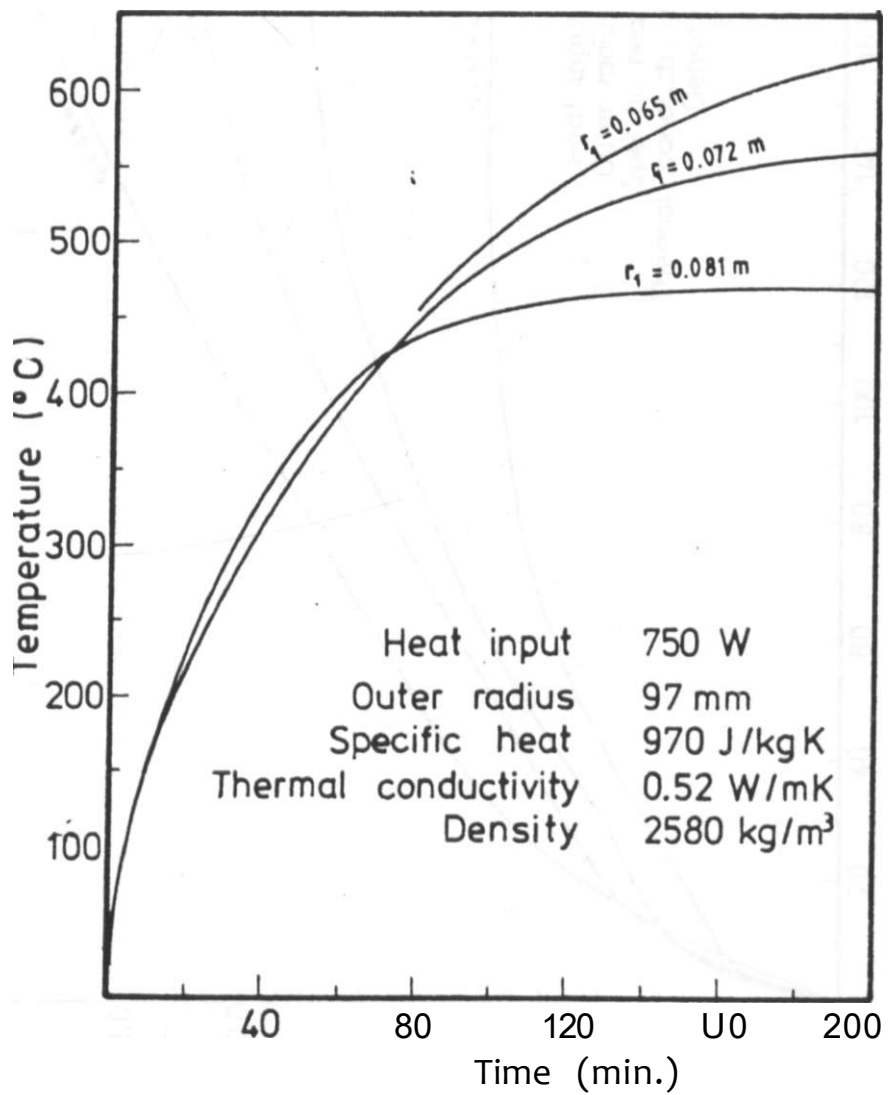


Figure 3.7: Effect of inner radius on the temperature at the inner surface as function of time.

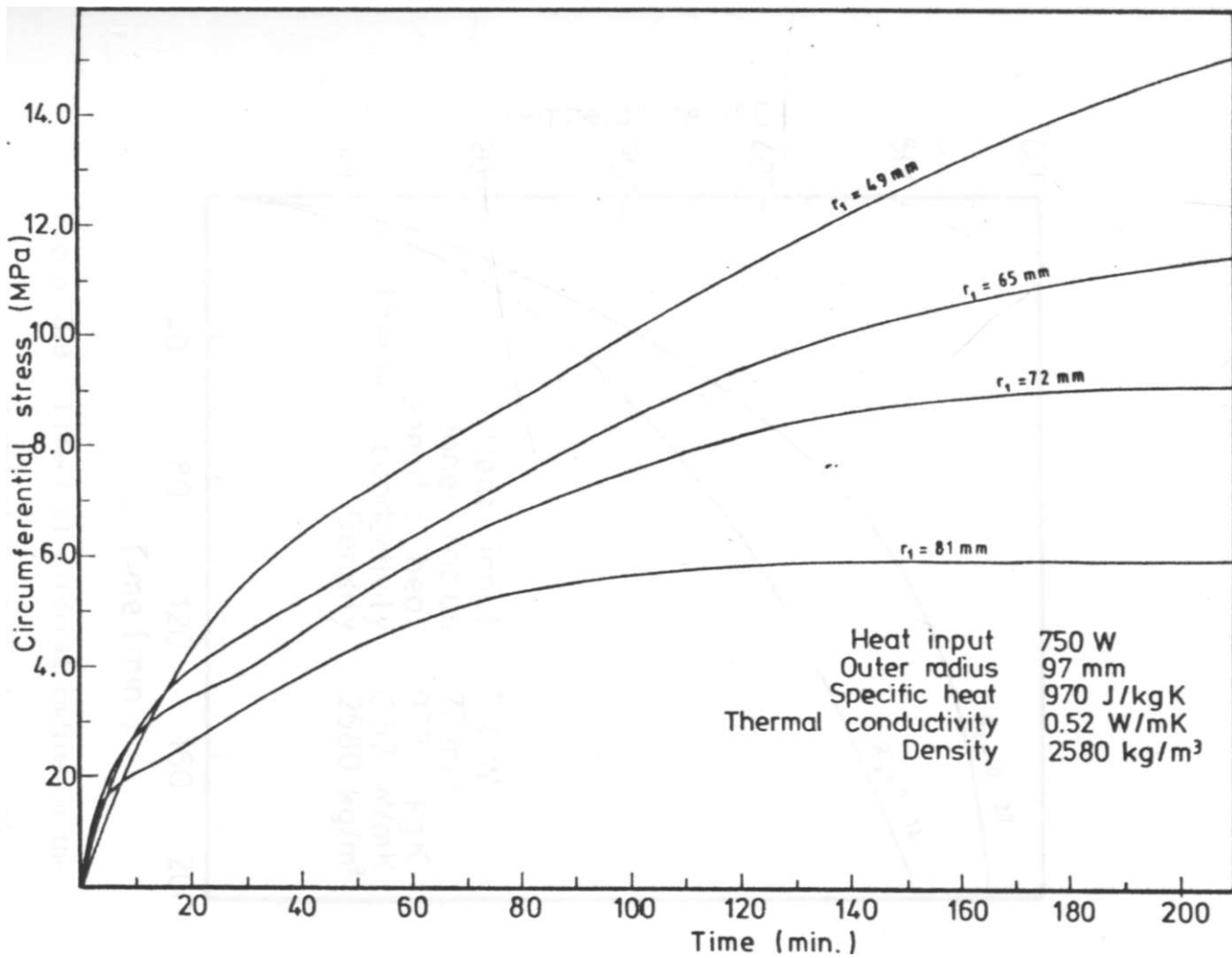


Figure 3.8: Effect of internal radius on the circumferential stress at the outer surface as a function of time

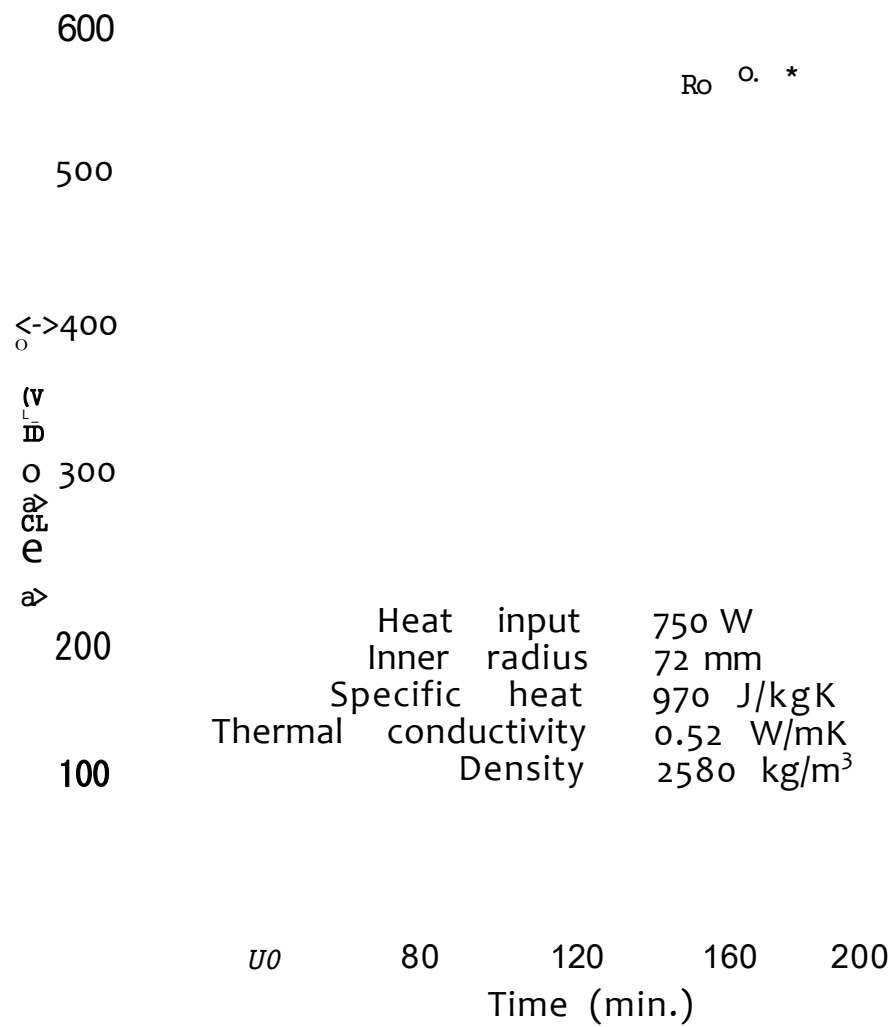


Figure 3.9: Effect of external radius on the temperature at the inner surface as function of time

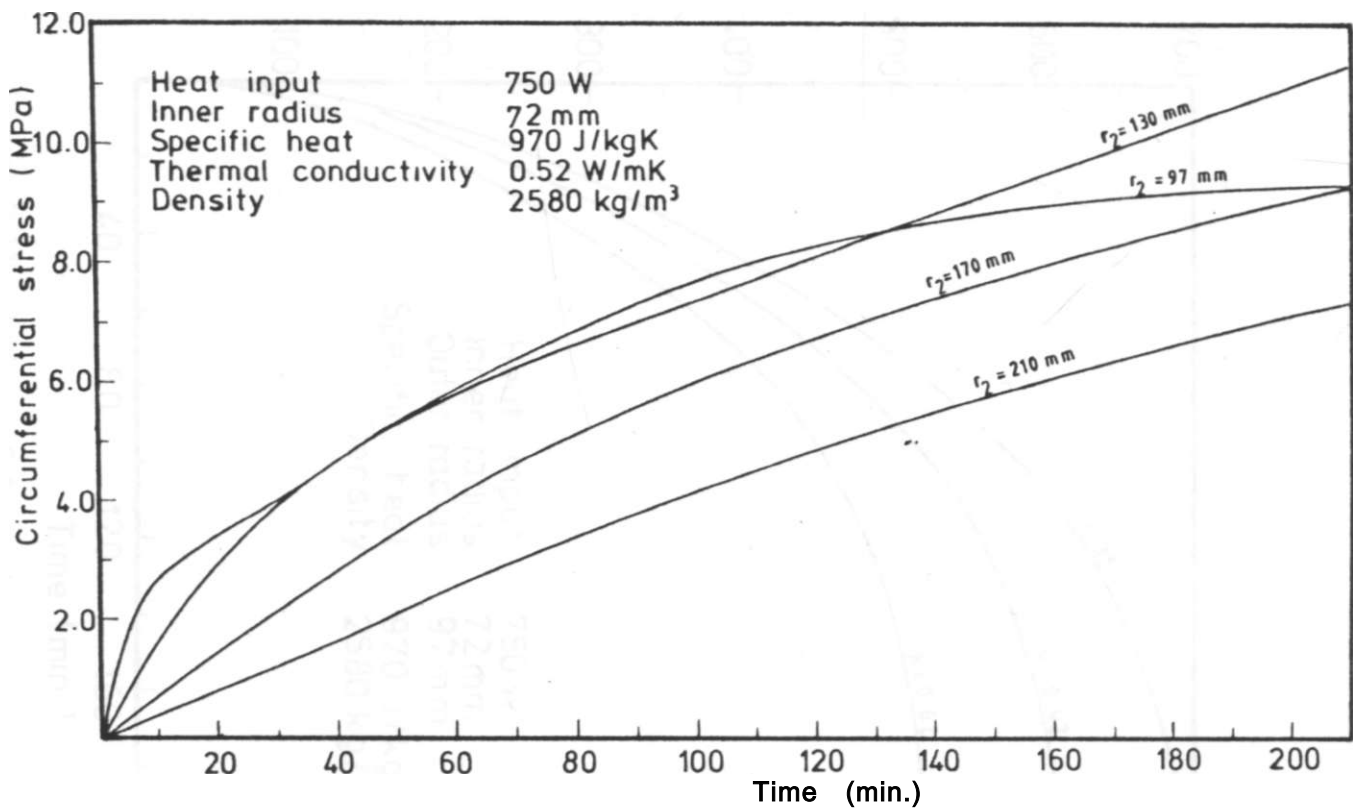


Figure 3.10: Effect of the external radius on the circumferential stress at the outer surface as a function of time

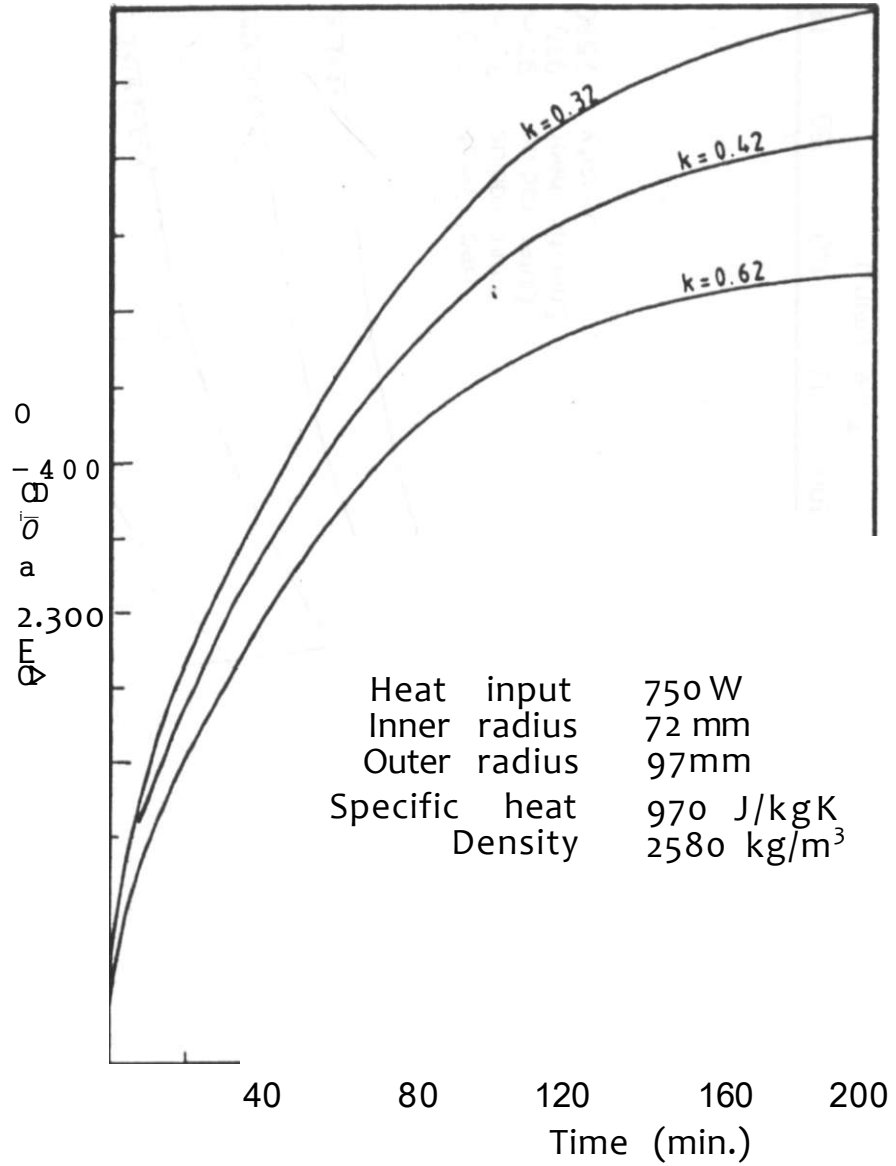


Figure 3.11: Effect of thermal conductivity on the temperature at the inner surface as a function of time

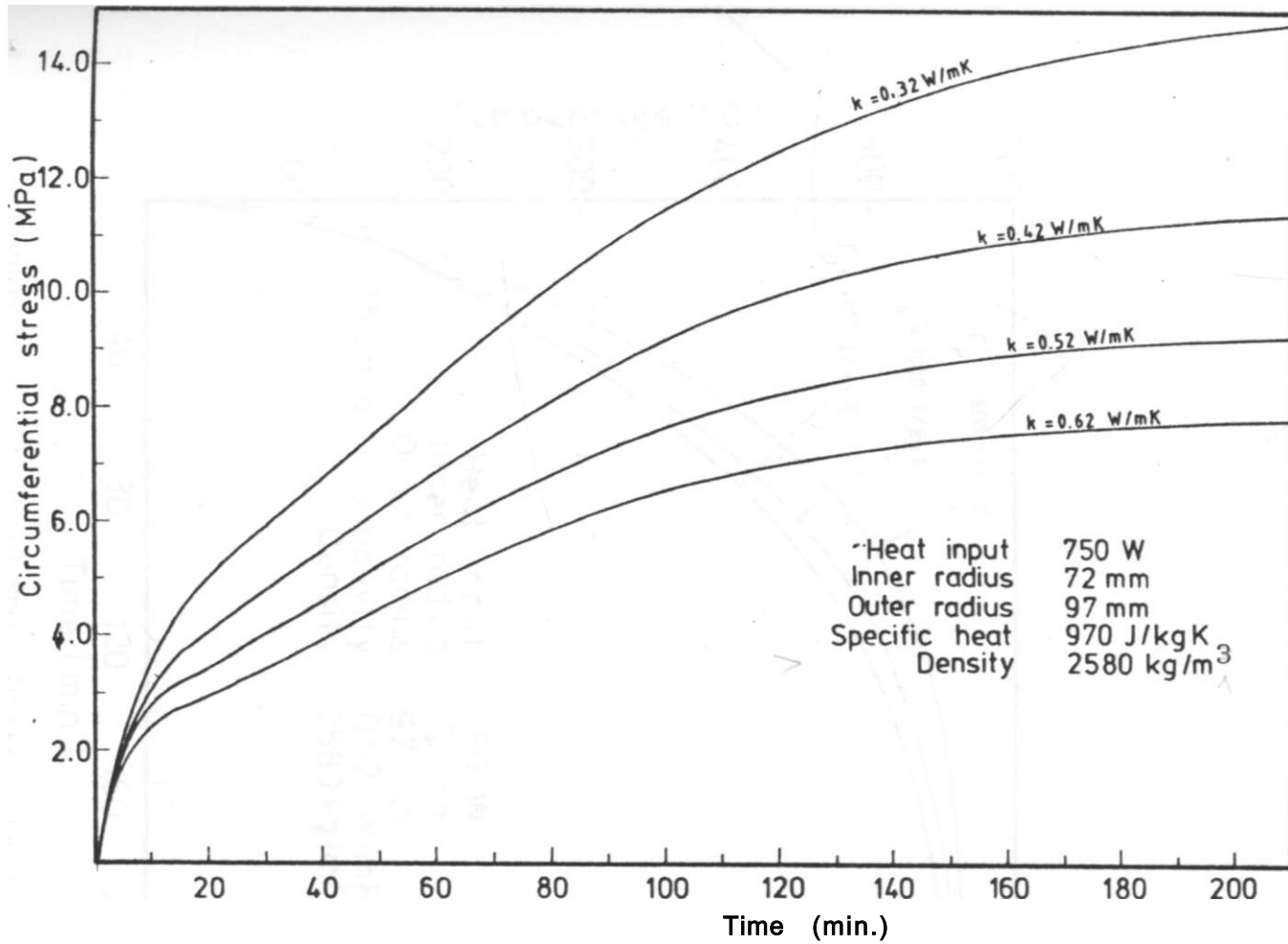
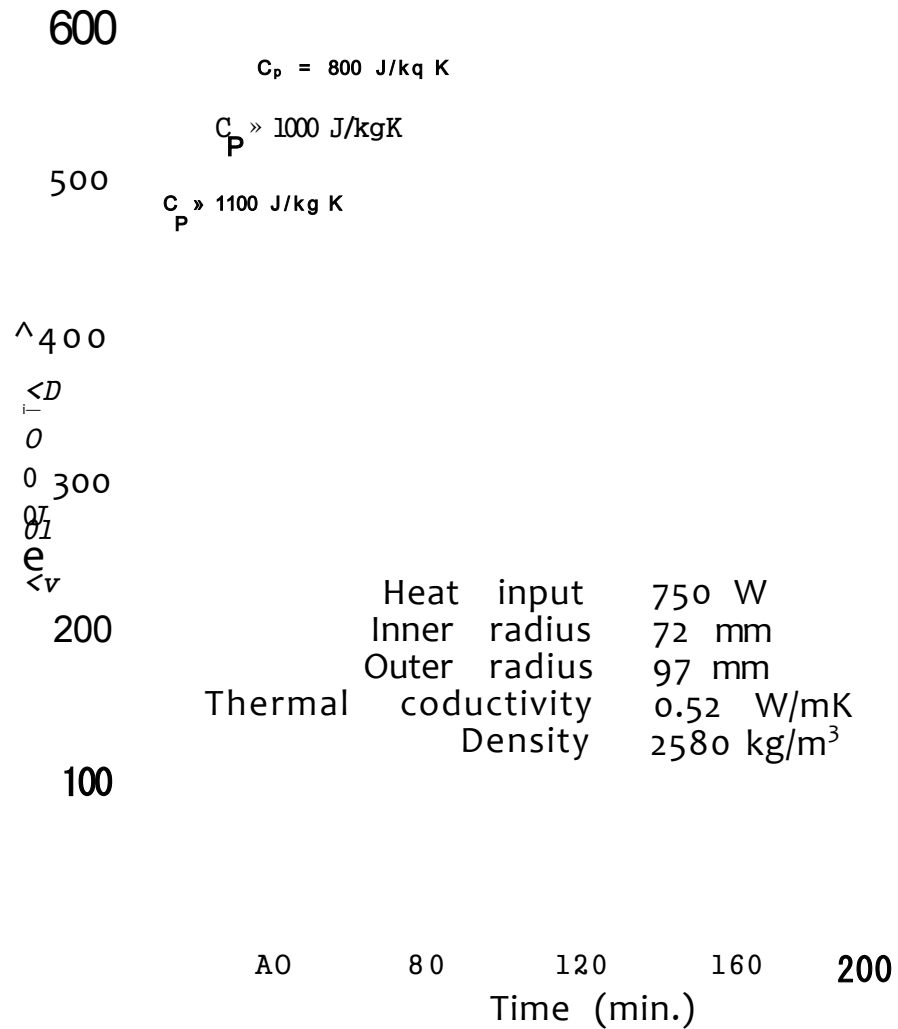


Figure 3.12: Effect of the thermal conductivity of the model on the circumferential stress at the outer surface as a function of time



. Figure 3.13: Effect of specific heat capacity of model on the temperature at the inner surface as a function of time

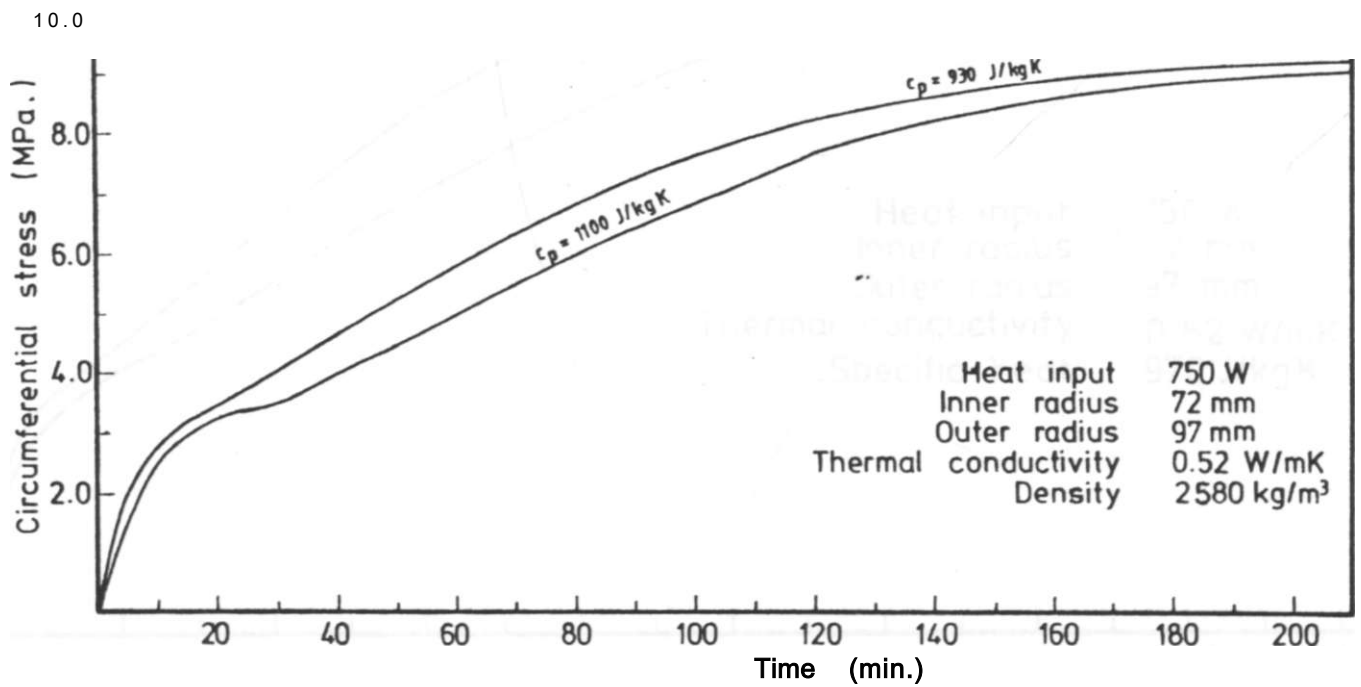


Figure 3.15: Effect of the specific heat capacity of the model on the circumferential stress at the outer surface as a function of time

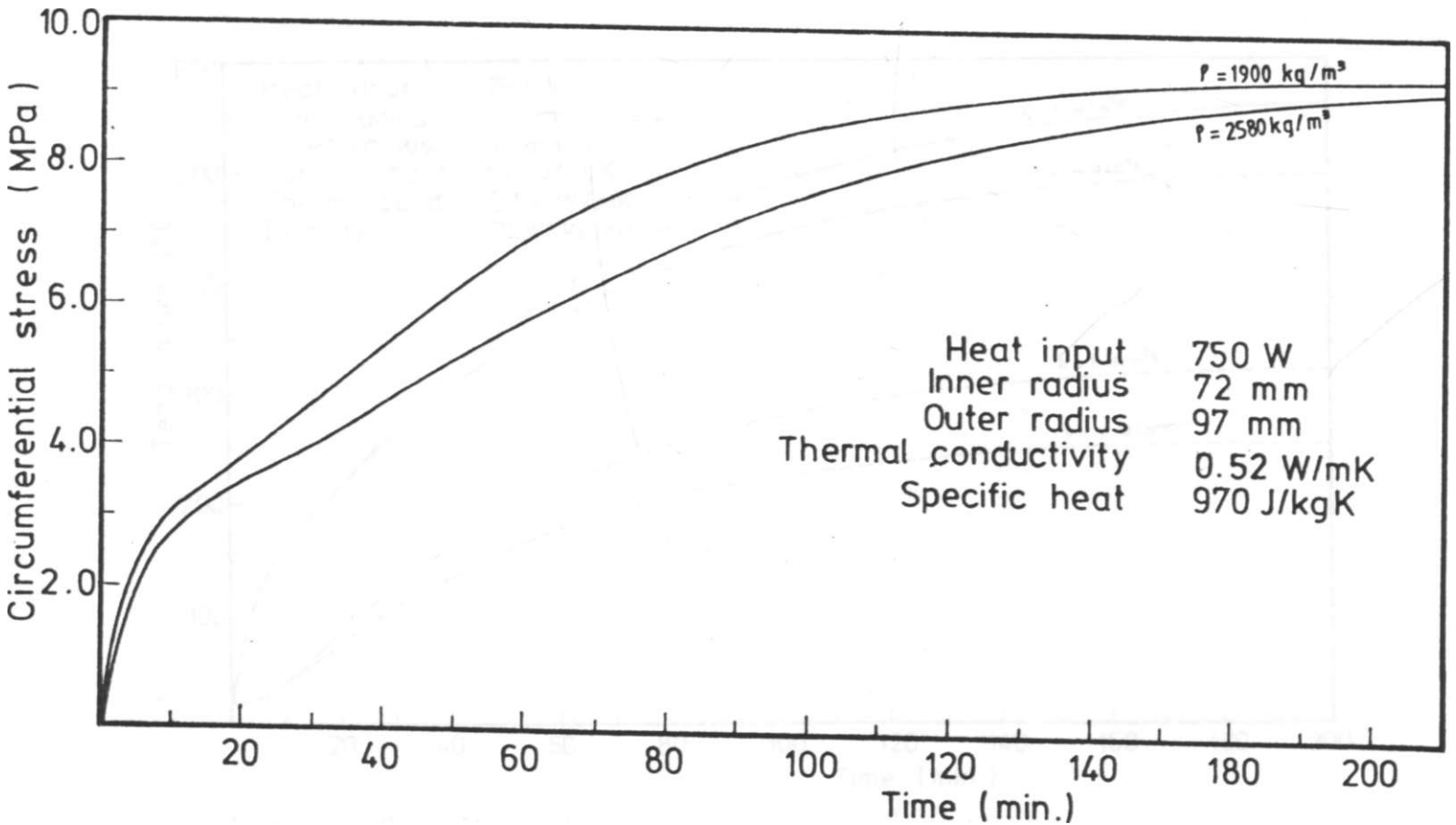


Figure 3.14: Effect of density of the model on the circumferential stress at the outer surface as a function of time

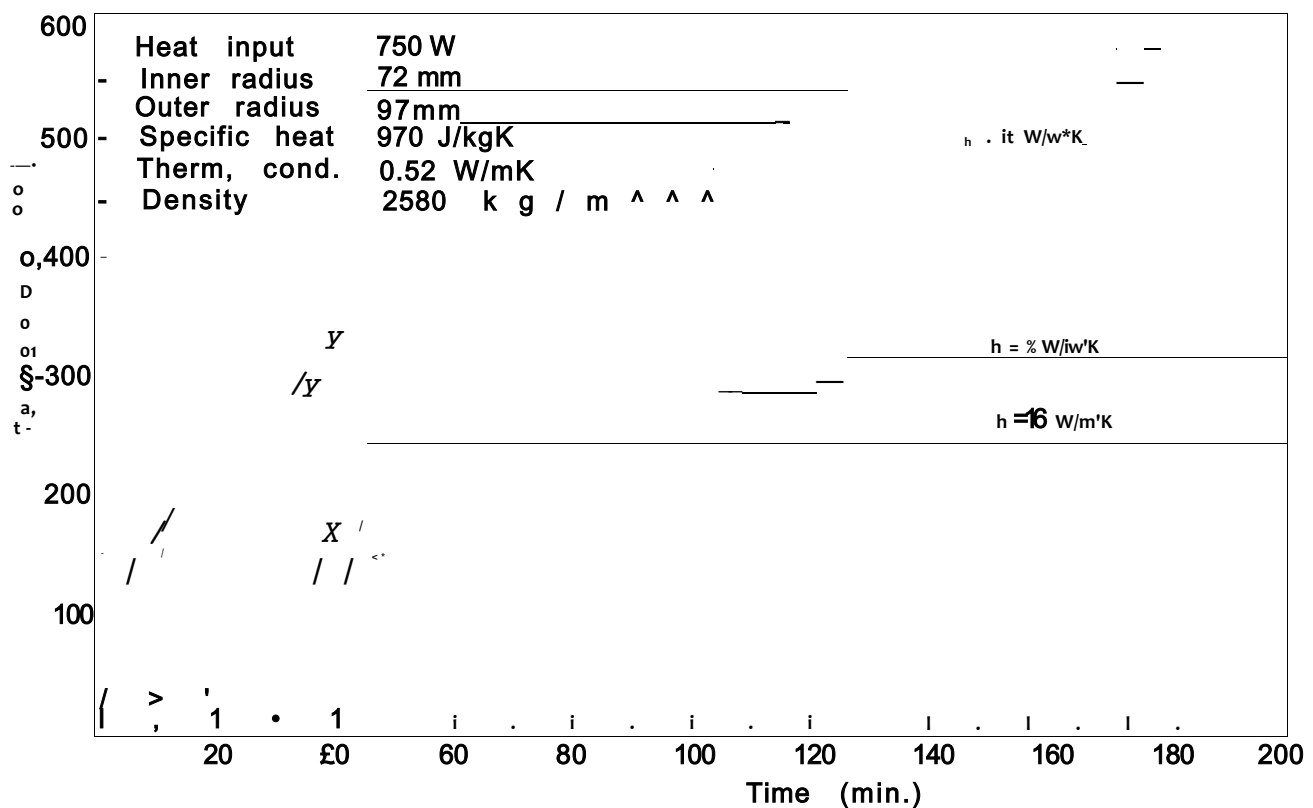


Figure 3.16: Effect of the heat transfer coefficient, h , on the temperatures of the inner and outer surfaces as a function of time

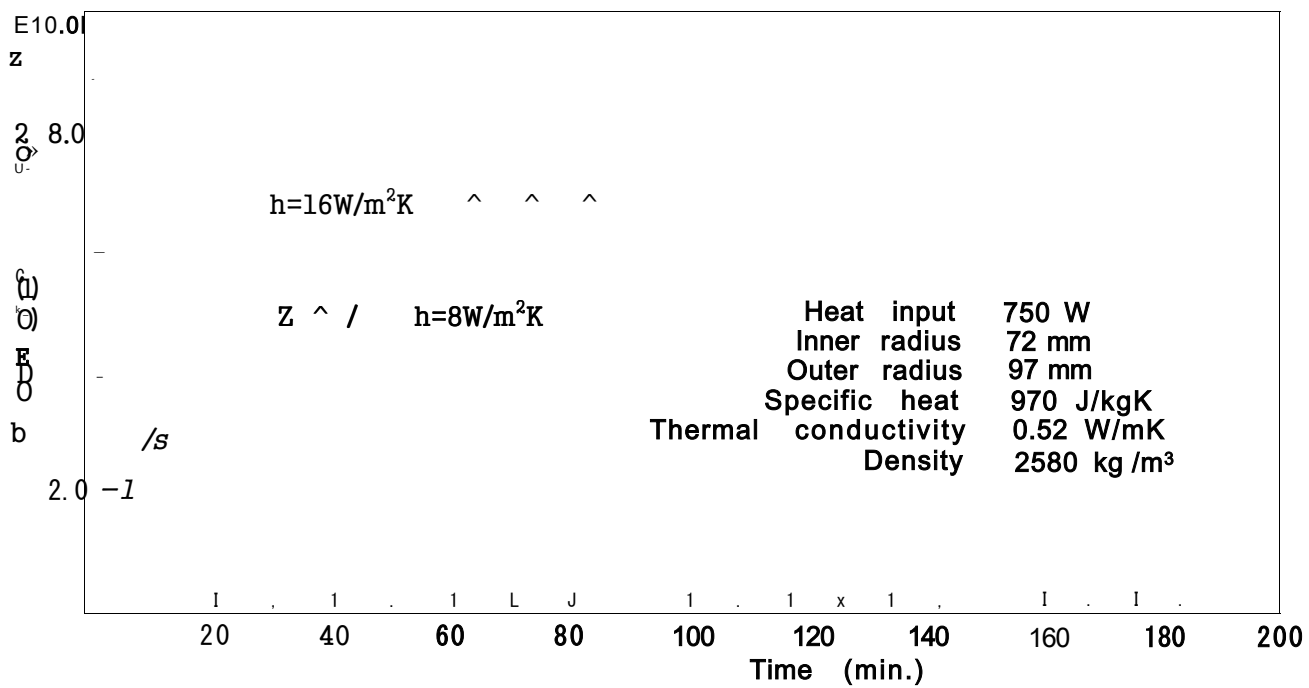


Figure 3.17: Effect of the heat transfer coefficient, h , on the circumferential stress at the outer surface

CHAPTER K)UR

4. EXPERIMENTAL TEMPERATURE AND STRAIN ANALYSES

4.1 INTRODUCTION

The problem considered in Chapter 3 consists of the determination of stresses under prescribed temperature distribution. The formulation employed rested on the assumptions that:

- i) the temperature can be determined independent of the deformation of a body,
- ii) the deformations are small, and
- iii) the material behaves elastically at all times.

However, when it comes to practical situations some assumptions may be invalid and could lead to very different results. Thus experimental investigation is an important tool to confirm the analytical work.

In this chapter the experimental work carried out to investigate temperature and stress distribution is described. Comparisons are then made with the numerical modelling predictions.

4.2 EXPERIMENTAL DEVICES AND DATA PROCESSING TECHNIQUES

4.2.1 The test specimen

4.2.1.1 Specimen preparation

Hollow cylindrical specimens with an external diameter of 194 nm and an internal diameter of 144 nm were moulded from the clay material from Nyeri, which was sieved, soaked in water, allowed to dry until a mouldable (plastic) consistency was obtained and finally wedged to remove air pockets trapped in the mixture. The cylinders were then fired in 8 hours to 1100°C in an electric kiln at the Fine Art Department of Kenyatta University in Nairobi. After firing the length of the specimen was 260 mm.

4.2.1.2 Properties of the specimen

A detailed description of the properties of the Nyeri specimen is given in Chapter 5. The chemical composition analysis of the fired material was done at the Department of Mines and Geology of the Ministry of Energy and Natural Resources. The results obtained are presented in Table 5.1.

4.2.2 Experimental devices

4.2.2.1 The data logger

Temperature measurement and recording was done by the use of Schlun-foerger Solatron data logger, Model 3430. The 30-channel logger could record temperature rise at various locations on the sample at 15 seconds intervals. Temperature recording was done within the range of ± 0.1 C.

4.2.2.2 Digital thermometer

During strain measurement the external and internal surface temperatures were measured by Fluke 2100A digital thermometer within the range of $\pm 0.1^{\circ}\text{C}$.

4.2.2.3 Digital strain indicator

Measurement and recording of strain was done by Vishay Ellis 20 strain indicator, Vishay Ellis 25 recorder and Vishay Ellis 21 scanner. Strain recording was done within the range of ± 1 microstrain.

4.2.3 The test layout

The test set-up is shown in Figure 4.1 and Plates 4.1 and 4.2. It consists of a 1 KW heating element intermittently heating the cylindrical specimen which is covered by an asbestos lid (that can be removed during cooling)

from the inside. A variable transformer was used to control the power output by regulating the voltage applied. An ammeter and a voltmeter were also included in the circuit (see Figure 4.1). Strains at the inside and outside surfaces of the cylinder were monitored using electrical resistance strain gauges connected to a strain indicator. The temperature distribution across the wall was measured using unshielded thermocouples that monitored the temperatures of the specimen using either a data logger or a digital thermometer.

4.2.4 Data processing technique

Due to the high apparent strain involved in measuring strain at high temperatures the apparent strain curve shown in Figure 4.2 was obtained by binding the strain gauge on the same material as the cylinder and measuring the output with static temperature increment as recommended by the strain gauge manufacturers (personal communication).

The circumferential and axial strains were obtained by basically reading the strain on the indicator and subtracting the apparent strain at the measured temperature.

The theoretical strains were calculated from the stress results using the well known formulae:

$$e_{\theta} = \frac{1}{r} \left(v \frac{\partial v}{\partial r} + v^2 \right) + \alpha (T - T_0) \quad \dots (4-1)$$

$$e_z = \frac{\partial v}{\partial z} + \alpha (T - T_0) \quad \dots (4-2)$$

where e_{θ} and e_z are the circumferential and axial strains respectively. Since there is no pressure nor body force, the radial stress σ_r is zero for this case.

i

The temperature variation in the transient state was observed to give a large scatter when analyzing data at every time interval separately. Thus a procedure of plotting strain versus temperature from the strain-time and temperature-time data, fitting a curve to the strain-temperature data and subtracting the apparent strain at the temperature was adopted. From that it was possible to draw a strain-time curve with very little scatter. This data processing procedure was found to be consistent, and gave the expected strain-time curve. Mai arri J?cob {41} obtained similarly shaped strain-time curve for glass subjected to thermal stress.

4.3 EXPERIMENTAL PROCEDURE

This section covers experimental details not covered in the previous sections.

4.3.1 Temperature measurement

In one of the cylindrical specimens' wall, described in Section 4.2.1.1, six holes, each of 2.5 mm diameter, that go half way along the length were drilled (before the specimen dried) at distances of 7, 8.5, 12, 15, 17 and 20 mm from the inner surface respectively. The spacing was chosen so as to get enough temperature measuring points to estimate the temperature distribution across the wall of the cylinder. Unshielded Iron-constantan thermocouple wires were inserted in these holes. The measuring junction of the thermocouple wires were spot welded. The inside and outside temperatures were monitored using similar thermocouples fixed to the specimen surfaces by high temperature adhesive. The thermocouples were connected to a data logger.

The specimen was heated to steady state condition at 150V, 320W and 912W loads and was allowed to cool from the acquired steady state temperatures. Temperature readings were recorded by the data logger every 1 minute for the first 10 minutes and every 5 minutes up to steady state conditions. The same schedule was followed for the cooling, temperature readings. The same measurements were repeated for the investigation of temperature conditions towards the edge of the cylinder by adjusting the inserted thermocouple wires and the ones fixed on the surfaces to a distance of 25 mm below the edge of the cylinder.

4.3.2 Strain measurement

High temperature strain gauges were bound on the surface of a cylinder using foundry adhesive (corfix), one in the axial and another in the circumferential direction. This was done at four points, at the centres of the inner and outer surfaces and 25 mm below the edge of the cylinder, both at the inside and outside surfaces. The strain gauges were connected to a terminal box which in turn was connected to a digital strain indicator, scanner and digital printer assembly. Four unshielded Iron-constantan thermocouples with conductor diameter of 0.8 mm and bare measuring junction (for rapid temperature response) bound on the surface at the four points monitored the temperature of the surface. The thermocouples were connected to a digital thermometer. Readings of temperature and strain were taken at 320W load every one minute for the first ten minutes and thereafter every five minutes for the next fifty minutes. The same procedure was repeated at 150W load. These heat loads and heating duration were selected so that the temperature limit set by the strain gauge properties was not exceeded.

4.4 RESULTS AND DISCUSSION

4.4.1 Temperature measurement

Figure 4.3 presents the measured temperature rise and cooling of the cylinder inner surface as a function of time. For comparison purposes the numerical results for the same power input of 912W is shown on the same Figure. The temperature of the inner wall in the experimental model is higher compared to the numerical model during the first 70 minutes of heating and is lower from then onwards. This discrepancy could be attributed to the fact that thermal conductivity and other properties vary with temperature. Figure 4.4 is a replica of Figure 4.3 along with segments of the numerical model run at different values of thermal conductivity and confirms the fact that the gap in the discrepancy would narrow if the theoretical model utilizes values of thermal conductivity as a function of temperature (for instance $k = a + bT + cT^2 + dT^3 + \dots$). It is observed that the thermal conductivity of this material increases with temperature (see next Chapter – Section 5.2.1.7). Presently there is some work on thermal conductivity for some ceramic materials as a function of temperature being done at the Physics Department of the University of Nairobi. The cooling part of the curve in Figure 4.3 matches very closely with the

numerical results suggesting the dependence of temperature on radiative and convective heat transfer coefficients during cooling.

The temperature rise of the external surface is shown in Figure 4.5. The output of the thermocouple fixed at the outer surface was much lower than the results obtained from the computer work. This could be attributed to the effects of natural convection at the measuring junction of the thermocouple. The temperature distribution across the wall of the cylinder as a function of time shown in Figure 4.6 also confirmed these observations by indicating a sudden drop of temperature at the external surface. However, extrapolated values from Figure 4.6 for the external wall temperature were found to agree well with the numerical results. Figure 4.7 shows the temperature rise of different points in the cylinder wall versus time.

The edge effects on the temperature distribution is shown in Figure 4.8 where readings of temperature were taken 25 mm from the edge of the cylinder. The general behaviour of the temperature distribution is similar to the ones observed at the centre. However, it can be seen that at the edges steady state is achieved at a temperature of 470°C compared to the steady state value of 530°C at the centre due to the heat loss through the asbestos cover. The discrepancy suggests that development and intensive mathematical treatment of the stove model is required in the future.

There are various factors that can affect the measurement of temperature. These could be:

- i) junction error,
- ii) circuit error,
- iii) radiation error, and
- iv) convection error.

However, the exact values of the quantity measured nor the exact error associated with the measurement can be ascertained {42}- Thus an uncertainty margin of $\pm 1.5^{\circ}\text{C}$ based on the manufacturers data can be used as the possible error during temperature measurement. In this work all temperature measurements will have an error margin of $\pm 2.0^{\circ}\text{C}$ to indicate more confidence in the estimate of the measurement.

4.4.2 Strain measurement

Figures 4.9 and 4.10 present the rate of straining of the inner surface of the cylinder for the cases of loading at 320W and 150W power inputs respectively. Both results shew the expected strain behaviour for transient conditions. The scatter in both Figures is due to the problem involved in strain measurement in the transient state. The strain output can not always follow the transient temperature variation as described by the strain gauge manufacturer (personal communication). Mai rrc1 Jrco^v {41} have usee high temperature strain gauges whose output were monitored by a 2-pen recorder at maximum temperatures of 130°C . This method

can be adopted to measure strains and fracture behaviour in stoves in the future.

Both axial and circumferential strains measured were higher than the strains that were numerically calculated. This could be attributed either to low coefficient of thermal expansion or to high modulus of elasticity (or both) estimated in the numerical model.

%

The measured axial strain values are lower than the circumferential strain values whereas 'the long cylinder' theory suggests that axial and circumferential strains are equal at the surface [14]. This observation may suggest two possibilities:

- (i) the experimental model deviates from the assumed highly idealized 'long cylinder' problem in which case the general axi-symmetrical solution [15] presented in Section 2.3.1 will give better estimation and
- (ii) the material tested could have been an anisotropic material. It might have had anisotropy in both mechanical and thermal properties. Both Figures 4.9 and 4.10 suggest that the specimen could have exhibited

higher Young's modulus and/or higher coefficient of thermal expansion in the circumferential direction. In such cases a procedure for calculating stresses developed by Stanley and Margetson {37) should be of great help.

4.5 CONCLUSIONS

%

The study presented here verifies the usefulness of the numerical model of Chapter 3. The results obtained in the numerical solution can be used in predicting thermal and stress conditions provided that the physical and thermal properties of the material of construction of the stove linings are known. The following conclusions can be drawn:

(a) Increase in external radius transforms the whole thermal and stress cycles in the transient state, decreasing the tensile stresses at the outer surface at the expense of increased internal compressive stress.

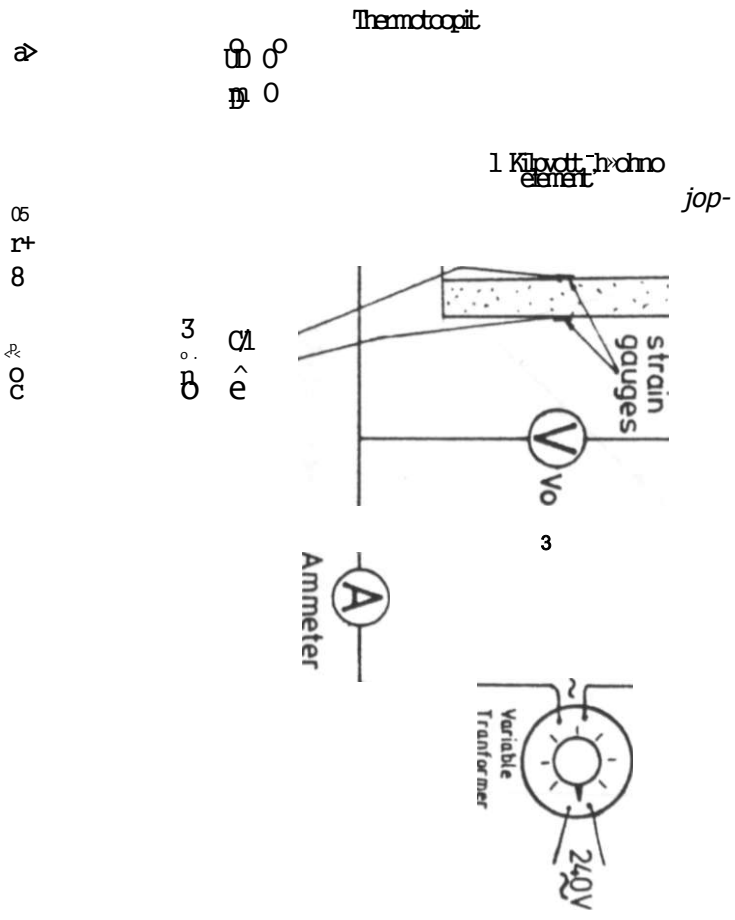
4

(b) Very good insulators are bound to have their external surface subjected to high tensile

stresses without affecting the internal compressive stresses a great deal.

- (c) Change in heat capacity per unit volume ($P-C_p$) does not affect the temperature and stress distribution much, but tends to affect the time to reach steady state.

- (d) For cases of high heat transfer coefficient h_i at the external surface the inner compressive stress is not affected much. However, the tensile stresses at the outer surface are observed to be high in the transient state.



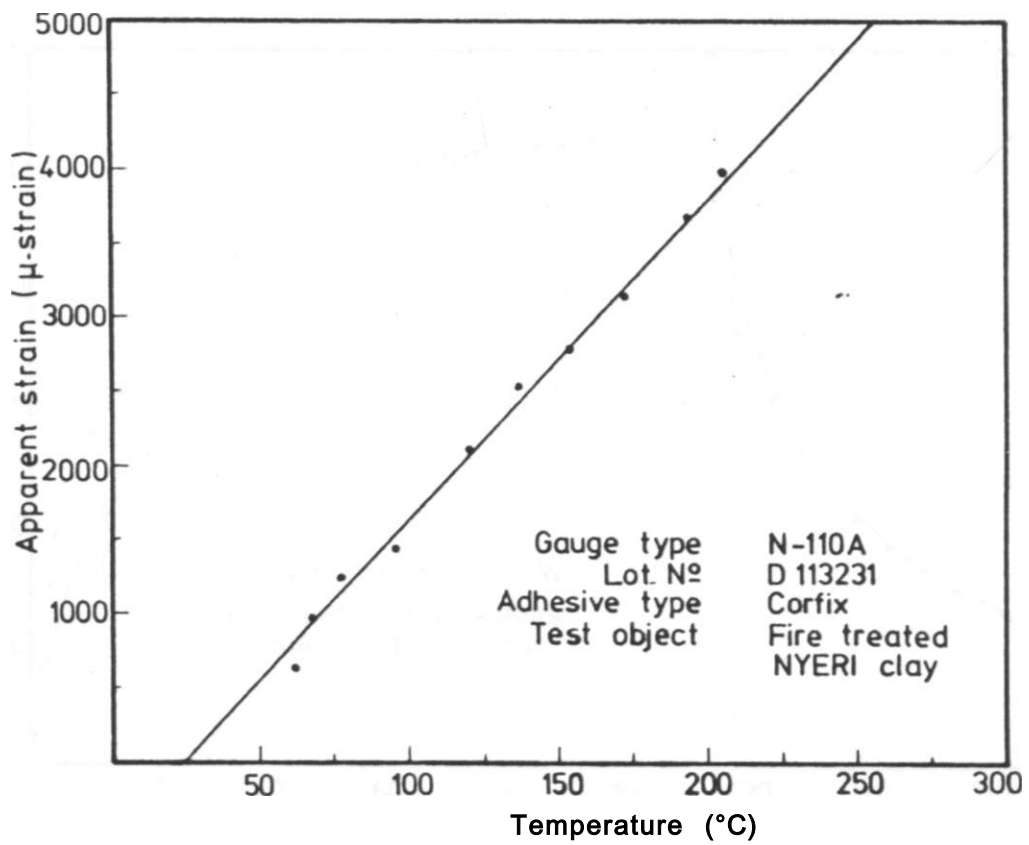


Figure 4^-. Apparent strain curve

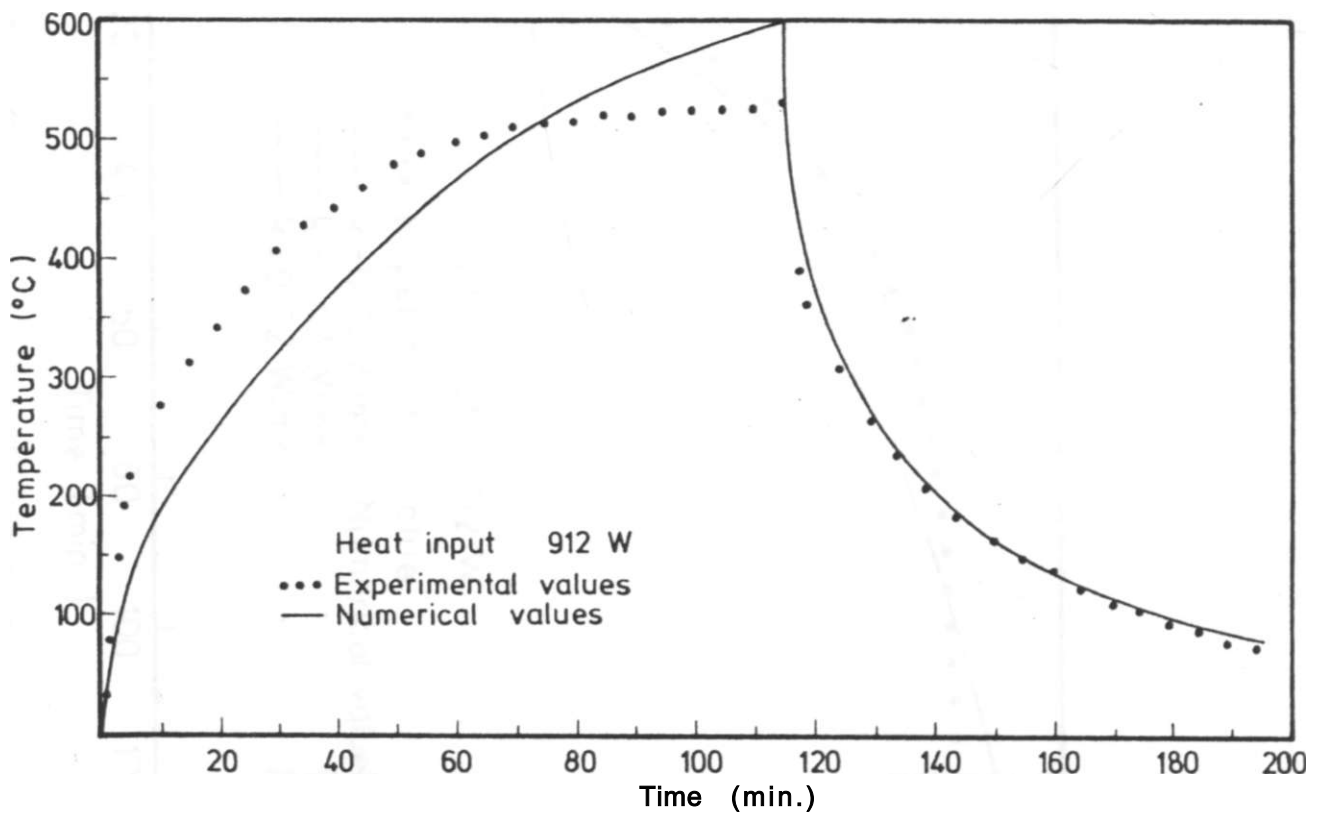


Figure 4.3: Inner wall temperature as a function of time

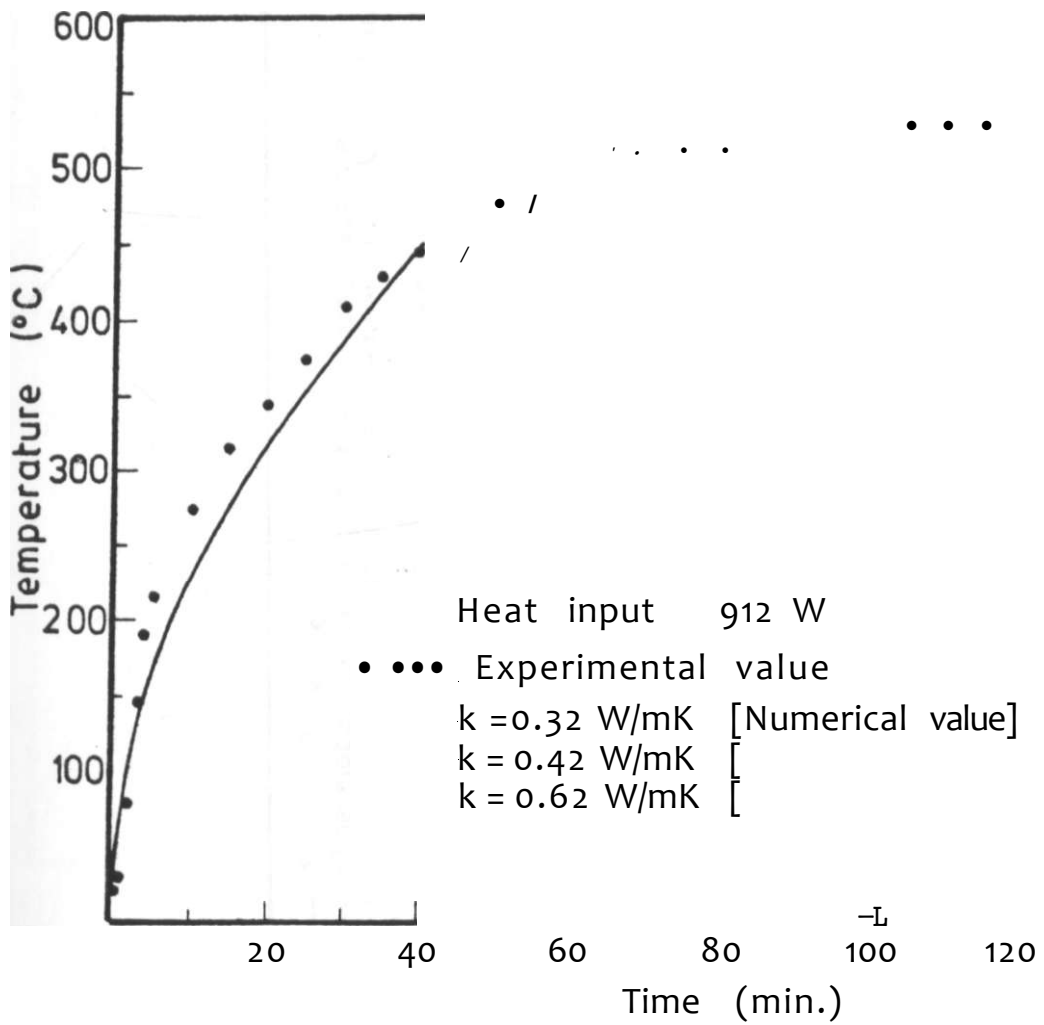


Figure 4.4: Temperature rise of the inner surface as a function of time

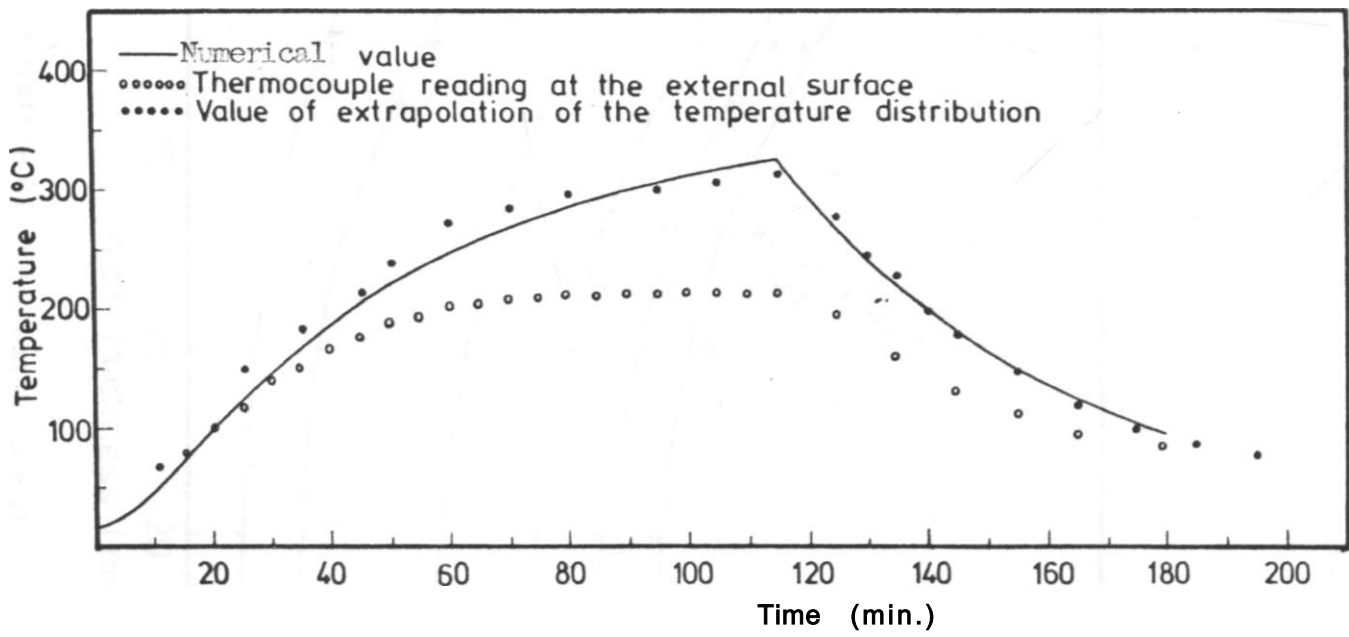


Figure 4.5: Temperature at the external surface as a function of time

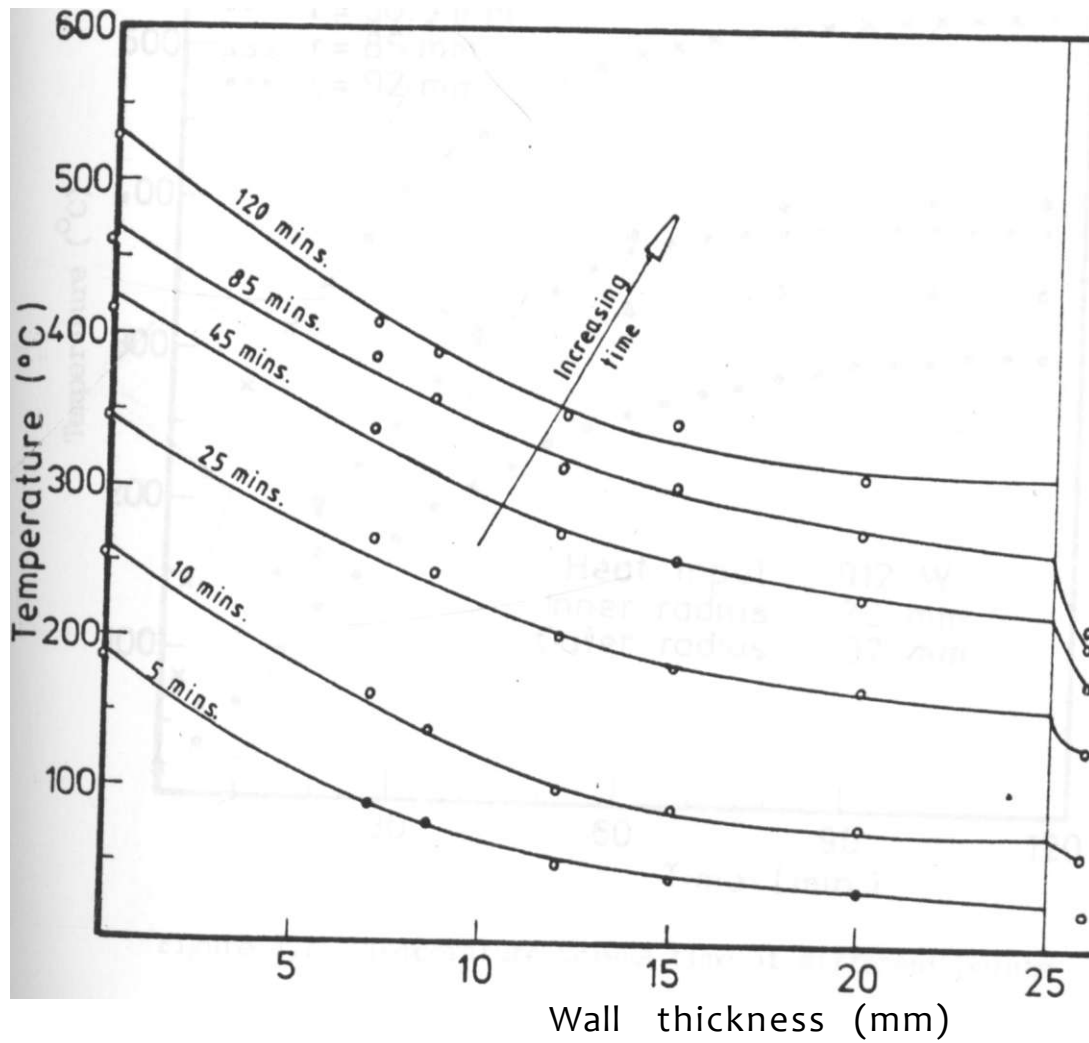


Figure 4.6: Temperature distribution across the wall of the cylinder

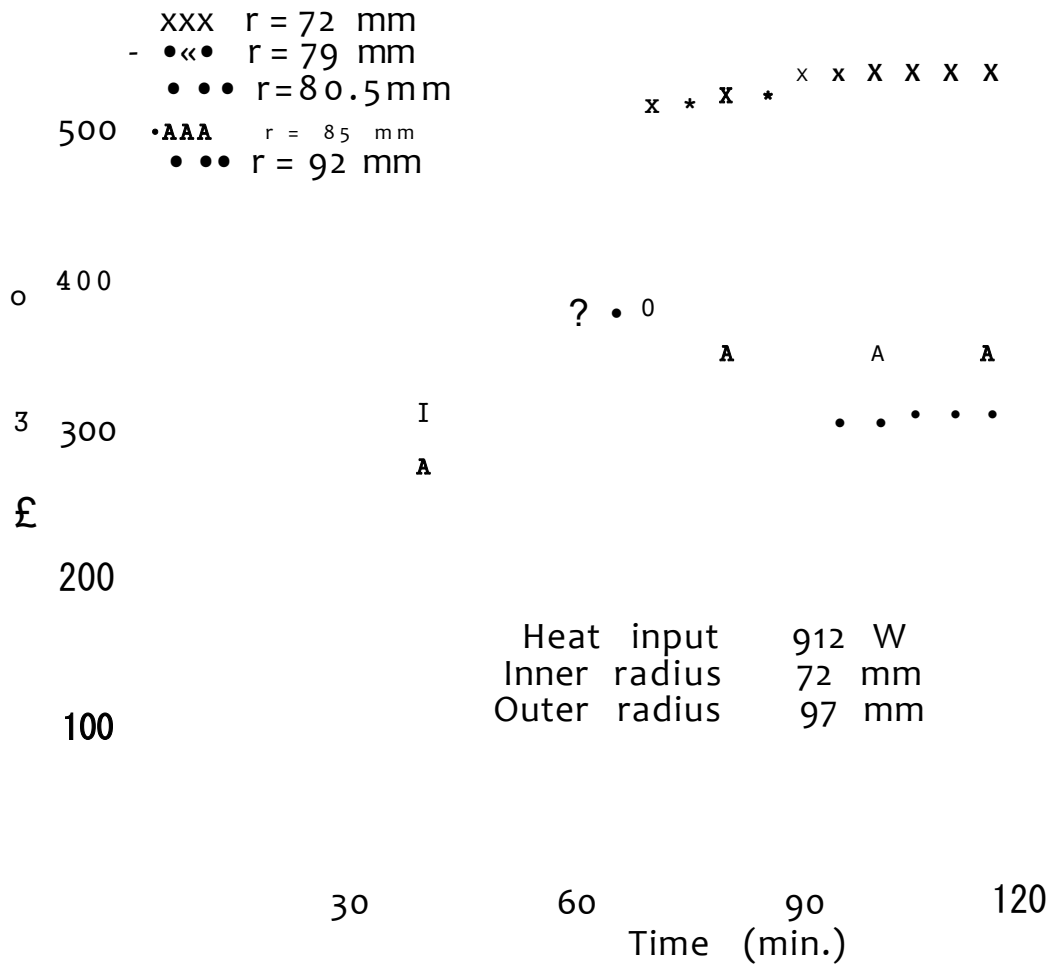


Figure 4.7: Temperature versus time at different points in the cylinder wall

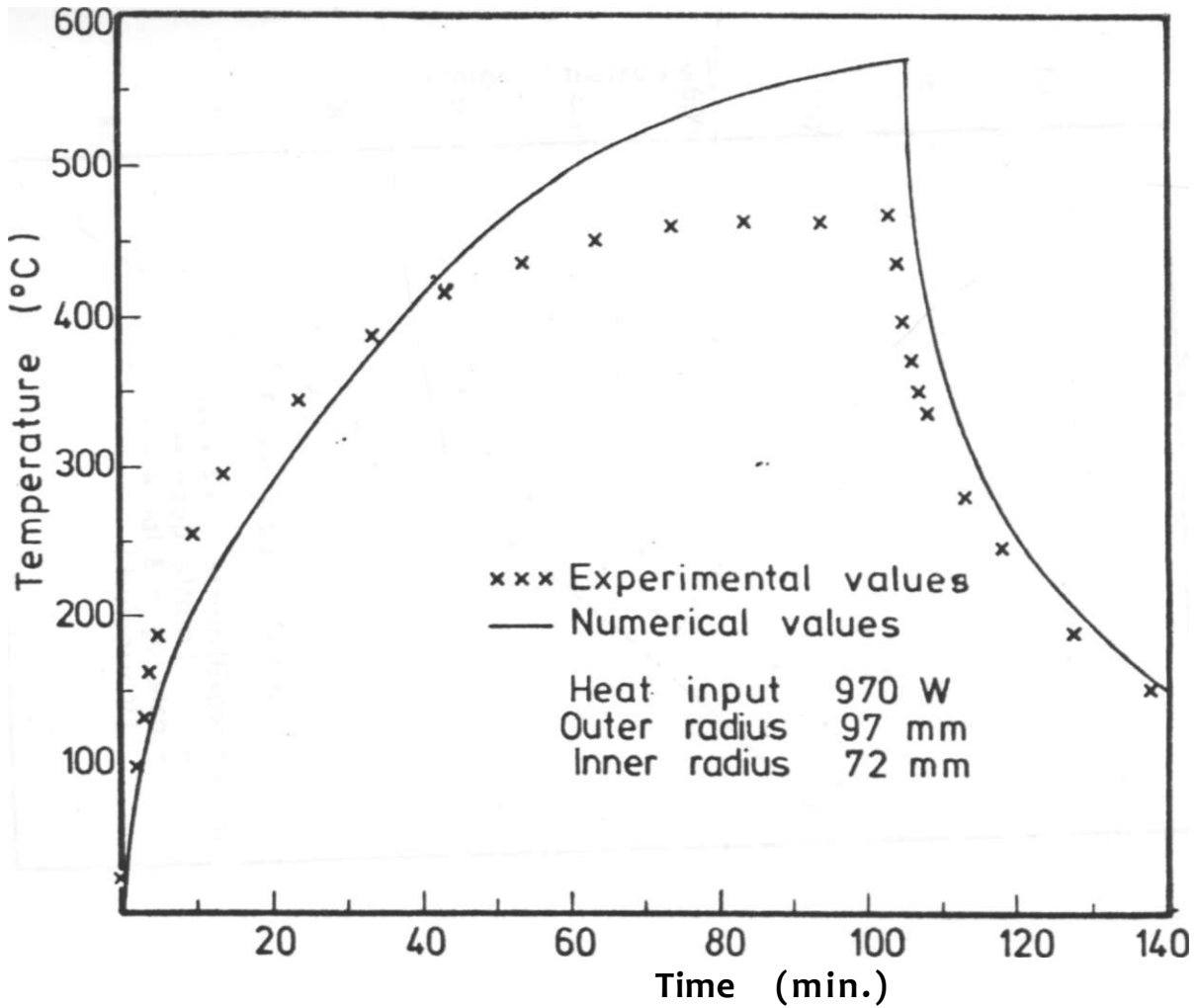


Figure 4.8: Inner surface temperature at the edge of the cylinder a function of time

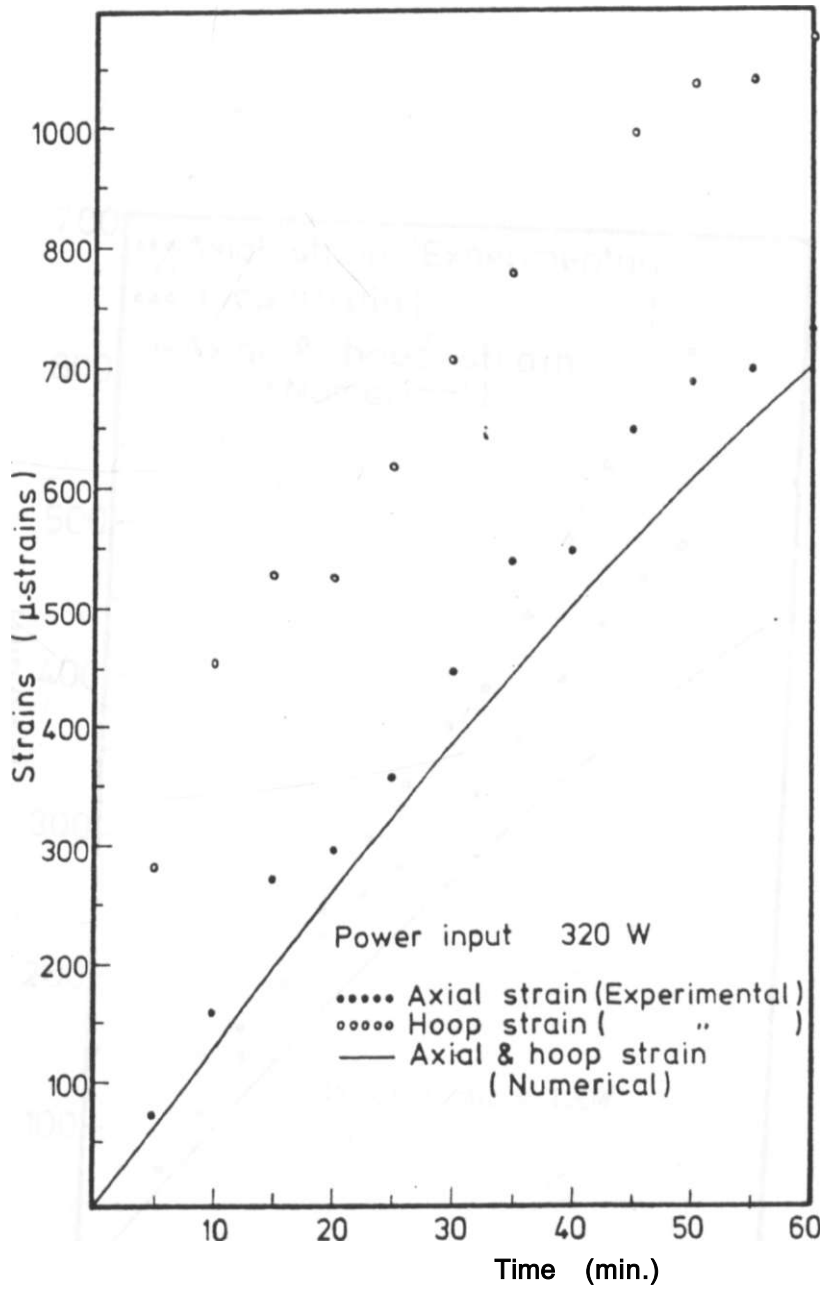


Figure 4.9: Measured strain at the inner surface of the cylinder

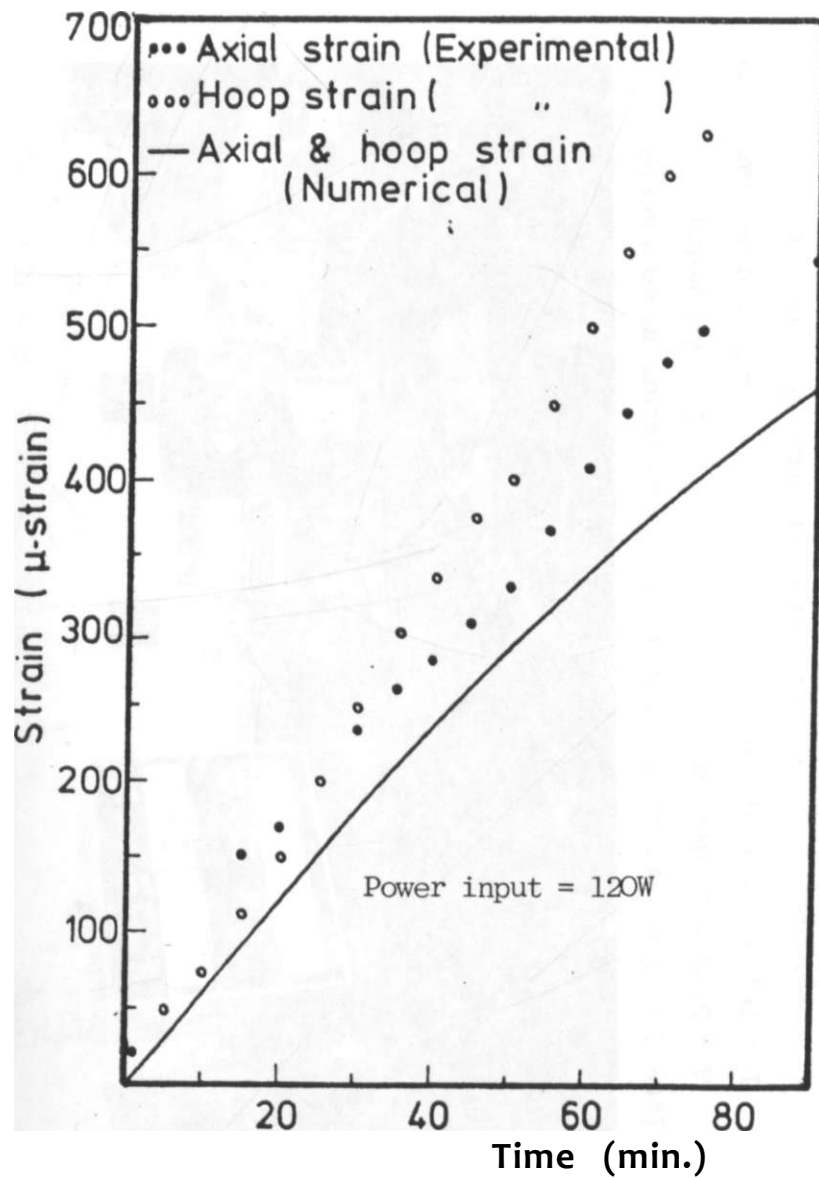


Figure 4.10: Measured strain at the inner surface of the cylinder



Plate 4.1 Test set-up for strain and teirperature measurements

A - Strain indicator

E - Voltmeter

B - Digital thermometer

F - Variable transformer

C - Terminal box (strain gauge circuit)

G - Specimen

D - Anmeter

I - Stand with heating elements

CHAPTER FIVE

5. THERMAL FRACTURE STUDIES

5.1 INTRODUCTION

A major factor determining the relevance of ceramics for use in domestic stoves (jikos) is their usefulness at high temperatures. Due to unfavourable continuation of values of thermal conductivity, coefficient of expansion, Young's modulus and strength many ceramics exhibit low resistance to thermal fracture [32]. For reliable design with ceramics a detailed understanding of the fracture phenomenon is required.

The most common phenomenon in domestic stoves (as described in earlier chapters) is rapid heating and cooling. This implies that good thermal shock resistance is necessary. Thermal shock resistance has basically two features:

- (i) The minimum shock severity to initiate cracks.
- (ii) The amount of damage done on the specimen during the shock (damage is the decrease in strength experienced by ceramics during thermal shocking).

The latter is an important factor in domestic stoves while one might ignore the former as there is no

catastrophic failure involved in stoves. However, this minimum shock could be used as a design parameter and proper knowledge of this data is imperative.

The other common phenomenon in domestic stoves is that they are normally used a number of times a day. 'Lighting-up' and 'putting-out' of fire involves repeated thermal shock, commonly referred to as thermal fatigue. Understanding of the fatigue behaviour of ceramics and the ability to predict thermal fatigue resistance and life is a matter of great importance to producers and users of stoves.

This chapter deals with studies on thermal shock resistances of local stove lining materials. Studies on the prediction of thermal fatigue life of the ceramics under consideration is presented. The materials used in the experiment are described and values of thermal and physical properties are presented. Some of the values of the properties are either assumed or estimated due to unavailability of relevant instruments.

5.2 THE TEST SPECIMEN AND EXPERIMENTAL DEVICES

5.2.1 The specimen

5.2.1.1 Production of test specimens

A sample of clay was collected from Nyeri and other samples of clay and sand were collected from Maragua. The sample from Nyeri was a similar material used for pottery and ceramic work at the Fine Art Department in Kenyatta University. The material from Maragua is used to produce clay work by the local people there. The Appropriate Technology Advisory Committee uses the same material for the production of domestic stoves' (jikos') linings in Nairobi.

The clay material from Nyeri was soaked in a large amount of water and allowed to pass through a sieve of 150 microns apertures in order to remove organic material. It was then allowed to dry until the mixture achieved a mouldable ('plastic') consistency.

The material from Maragua was soaked in water and was left for 24 hours so that water may completely penetrate each and every lump of clay. An equal portion (by weight) of the sand to the clay was sieved through a sieve of 850 Microns apertures. It was then thoroughly mixed with the

clay water mixture and then allowed to reach a 'plastic' consistency by letting water to evaporate from the mixture at room temperature.

Each mixture was charged in a pugmill and extruded through a metal die of 25 mm diameter fixed to the mill by the use of a proper grip. The extruded material was received on an oil lubricated plate in lengths of about 1300 mm. This was then chopped into 8 to 9 pieces each of length 130 mm each. Deformed pieces and pieces with defects were removed from the set. A total of 200 pieces of each specimen were produced in this manner. The specimens were fired at 1100°C in an electrical resistance kiln at the Fine Art Department in Kenyatta University. The specimen from Nyeri maintained a diameter of 23.5 mm and those from Maragua 22.5 mm. The edges of all specimens were machined using a diamond tool and polished.

The specimen from Nyeri will be referred to as Nyeri clay and that from Maragua as Maragua clay throughout the rest of this work.

5-2.1.2 The chemical composition

The quantitative analysis of the specimens was done at the Department of Mines and Geology within the Ministry of

Environment and Natural Resources. The chemical composition of the compounds by weight was determined. The results are presented in Table 5.1.

5.2.1.3 Strength of the specimens

For thermal stress application the greater similarity of stress distributions in bending tests to that occurring due to temperature gradient and the relatively greater freedom from stress concentration and alignment effects make bending tests a preferable method of strength measurement [21]. The bending strength was determined by four point loading in which the span was 101.6 mm and the distance between the two inner loads was 63.5 mm. The test was done on eighteen samples of each specimen and with the help of Weibull distribution the strength at 0.5 survival probability was taken as the strength of the material. The uniaxial tensile strength was determined by the use of the Weibull parameter m and the following equation for the ratio of the bending strength to strength at uniaxial tension [27]:

$$\frac{\sigma_{Flex}}{\sigma_T} = \left[\frac{2Y(m+1)^2}{(2+(m-1)(Y-2))} \right]^{1/m} \quad \dots (2.61)$$

Values of the Weibull modulus, m, Flexural Strength and Tensile strength are presented in Table 5.2.

5.2.1.4 Young's modulus and Poisson's ratio

Using an ultrasonic tester the velocity of propagation of pressure waves through the specimen was determined. A typical value of 0.25 {5} was assumed for the Poisson's ratio and the Modulus of elasticity E was determined from the following equation {43}:

$$E = \frac{\rho V^2 (1-\nu)}{1-\nu} \dots(5.1)$$

where ρ is the density, V the velocity of pressure waves and ν Poisson's ratio. Values of the modulus of elasticity are presented in Table 5.3.

5.2.1.5 Specific heat capacity

The specific heat capacities for the materials were estimated using simple calorimetric test. Preweighed samples of each clay were heated to a certain preselected high temperature and suddenly dropped in a known mass of water at 20°C. The content was stirred until the temperature being monitored by a thermometer reached a maximum value and started declining. Heat capacities of the specimens were

calculated by using simple energy balance equations. The heat capacities of each sample is presented in Table 5.3.

5.2.1.6 Coefficient of thermal expansion

Due to unavailability of the proper instruments for the measurement of coefficient of thermal expansion of the

-6

specimens, a typical value of $6 \times 10^{-6} /K$ (expansion coefficient for insulating brick) (44) was assumed for both the Nyeri and the Maragua clay. »

5.2.1.7 Thermal conductivity

Hollow circular cylinders of outer diameter 40.5 mm and inner diameter of 20.5 mm and length of 130 mm were produced from the Maragua sample for the determination of the thermal conductivity. Cylinders described in Chapter 4 were used to estimate the thermal conductivity of the Nyeri clay. The cylinders were heated by a 1000 W rated (57.6 ohm) electrical heating element from the inside and measurements of the heat input, internal surface temperature and external surface temperature were noted at steady state.

Under steady state condition the mean conductivity, k_m , over the range of temperatures T_1 and T_2 is given by the relation (7):

$$27ny/(T_1 - T_2) = Q \ln(r_2/r_1) \quad \dots(5.2)$$

where Q is a constant heat supply/ $a^{\wedge} \wedge \wedge r_2$
internal and external radii respectively.

Values of the thermal conductivity for different temperature ranges are shown in Table 5.4.

*

5.2.2 Experimental devices

5.2.2.1 The specimen holder

Specimen holders that accommodate 9 specimens at a time were produced at the Mechanical Engineering Department workshop in the University of Nairobi. Distance between two specimens, when placed in the holder, was 16 mm.

5-2.2.2 The heating and cooling device

A thermostatically controlled furnace of type Dryad Leicester, M100 model (English made) with a maximum operating temperature of 1200°C was used to heat specimens to the required temperature. The temperature of the furnace was monitored using a pyrometer.

Cooling was done by dropping the heated specimens into a container with a facility for running cooling water.

5.2.2.3 The ultrasonic tester

Extent of damage after thermal shock was monitored by the use of an ultrasonic tester of 40 kHz frequency at the Kenya Bureau of Standards. The digital tester with a transmitter and a receiver probe displayed pulse transit time directly.

5.2.2.4 Flexural strength

Four point bending device (with a total span of 101.6 mm and a span of 63.5 mm between the two central loading points attached to a Hounsfield Tensometer described in Section 5.2.1.3) was used to measure the flexural strength of specimens after thermal loading.

5.2.2.5 Crack detection

Because of the high porosity and defects of the ceramics being tested neither die-penetrant nor X-ray could be used to detect cracks. Use of a magnifying glass of magnification x2 and at times a microscope of magnification x6 was found to be the most suitable method.

5.3 EXPERIMENTAL METHODS AND DATA PROCESSING TECHNIQUES

One of the popular thermal fracture test methods, due to its simplicity, consists of quenching cylindrically shaped specimens from a preselected high temperature into a fluid medium at a lower temperature. This leads to a state of compression at the core of the cylindrical specimen and tension on the surface.

The actual thermal condition found in domestic stoves is less severe than the laboratory tests. In fact the purpose of the laboratory thermal shock is not to simulate the real condition, but to determine values of different parameters and be able to reproduce them in an effort to estimate performance in actual service. Moreover the use of parameters obtained in the laboratory for design purposes should produce better performance in the actual stove conditions which are less severe.

5.3.1 Experimental Techniques

-

Several experimental techniques have been developed in the past. Some methods are non-destructive which are helpful in studying the effect of thermal fatigue or repeated thermal shock, whereas others are measurement of rupture strength using destructive methods. Some of these methods are:

- (i) Measurement of the variation in the resistance to rupture (rupture strength) using three points loading on beams or bars, or biaxial flexure of a disc {20}.

- (ii) Measurement of the variation in impact strength in cylindrical bars using sensitive impact tester {2,3}.

- (iii) Observing the growth of cracks using die-penetrant {32}, microscopy {18} or visual inspection {31}.

- (iv) Measurement of the variation of acoustic attenuation and speed of propagation of ultrasonic waves in short cylinders {20}.

- (v) Measurement of the variation in frequency of resonance and damping capacity in cylinders or discs {20}.

5.3.2 Thermal shock resistance

For the study of thermal shock resistance, measurement of resistance to rupture by bending and measurement of the variation of the speed of ultrasonic waves was used.

The bending test was modified slightly by employing four point loading instead of three. A computer program for a quadratic least square fit was developed to fit the curve so that the values of the critical temperature, AT_c and the degree of damage, Aa / o_q (change in rupture strength/original rupture strength) could be estimated with reasonable accuracy.

5.3.3 Thermal fatigue

A method developed by Kamiya and Kamigaito {33} discussed in Chapter 2, was used to estimate the thermal fatigue life at a given thermal shock severity. The method basically uses visual inspection for the detection of crack. Occurance of a crack of a certain length was the criteria for failure.

Survival probability was estimated by the following equation {27}:

$$P(i) = i - (1=2:\&) \quad ..(5.3)$$

J

where i was the number of specimens that failed and J the total number of specimens. The same equation (5.3) discarding the data with extreme values [45], was used to determine Weibull parameters using mechanical testing methods for comparison purposes.

The Weibull modulus, m , was estimated by applying the well known probability analysis given by equation (2.58) in Chapter 2:

$$P_s = \exp\left(-V\left(\frac{a-a_0}{a_0}\right)^m\right) \quad \dots(2.58)$$

to the flexure data. By taking natural logarithm twice the above Equation (2.54) modifies to the form:

$$\ln(-\ln(P_g)) = \ln\left(\frac{a-a_0}{a_0}\right)^m + m \ln(a-a_0) \quad \dots(5.4)$$

so that a plot of $\ln(-\ln(P(i)))$ versus $\ln a$ should give a straight line with slope m .

The material constant, n , was estimated from the dependence of flexural stress on the stress rate using the equation [34, 46]:

$$\frac{\sigma}{\sigma'} = \left(\frac{\dot{\sigma}}{\dot{\sigma}'}\right)^{\frac{1}{n}} \quad \dots(5.5)$$

where σ and σ^1 are the flexural stresses at crosshead speeds of v and v^1 respectively.

5.4 EXPERIMENTAL PROCEDURE

The number of specimens to be shocked were charged in a specimen holder that could accommodate up to nine specimens and were heated to the required preselected temperature in an electrical resistance furnace whose temperature was thermostatically controlled within $\pm 5^\circ\text{C}$. Temperature of the furnace was monitored by the use of Platinum / 13% Platinum-Rodium sheathed thermocouple. The heating time varied depending upon the temperature that had to be attained; for instance heating to 500°C took 40 to 45 minutes. The specimens in their holder were manually transferred from the furnace into a water bath, the time of transfer being less than two seconds, and hence the change in specimen temperature could be neglected. The temperature of water was between 18 and 20°C . The temperature difference ΔT was generally taken as the difference between the temperature of the hot zone (furnace) and that of water by ignoring the intermediate minor shock during the transfer of the specimens from the furnace to the water bath as described above. Variation of the surface stress of a solid circular cylinder when subjected to different heat transfer

conditions is presented in Appendix A.2.3. The Biot number, (Pi), for the present sample in air at ambient atmosphere condition is approximately 0.2 while when cooling in water it is around 100. Hence the stress generated as a result of taking the specimen out of the furnace into the ambient atmosphere is only 3-5% of that generated during quenching of specimens in water and thus can be ignored.

5.4.1 Thermal shock resistance

The specimen holder was charged with four of each specimen at a time and shocked from different temperatures between 150 and 750°C in 50°C intervals. After drying the specimen at first the pulse transit time of ultrasonic pressure waves was recorded using an ultrasonic tester and then they were tested for rupture strength using the four point loading method described earlier.

5.4.2 Thermal fatigue

For the thermal fatigue test nine specimens were charged in a holder and were shocked at temperature differences of 530°C and 470°C. The specimens were dried in an oven and put back into the furnace for the next thermal shock. To save time one sample was shocked and was being

dried while the other was being heated to the preselected temperature in the furnace. After every shock each specimen was checked for fracture. Failure was determined by the occurrence of a visible crack of minimum length of 20 mm. At places where a crack would be hidden among surface defects use of magnifying glass of magnification x2 and a microscope of up to x6 magnification was made. Change of flexural strength ; a result of quenching was determined using four point loading in order to establish a more concrete criteria of failure.

Variation in the speed of propagation of ultrasonic waves was monitored to measure the degree of damage as the specimen was subjected to repeated thermal shocks from a preselected temperature below 'the critical temperature difference'.

5.5 RESULTS AND DISCUSSION

5.5.1 Results

5.5.1.1 Thermal shock resistance

ji

Figures 5.1 and 5.2 present the thermal shock severity, AT .versus flexural strength and thermal shock

severity versus velocity of ultrasonic pressure waves respectively for the case of Nyeri clay. The modulus of rupture curve (Figure 5.1) suggests that decline in strength from 8.05 MN/m^2 to 3.85 MN/m^2 occurred between quenching temperatures, AT, of 480°C and 580°C whereas the velocity-temperature curve (Figure 5.2) gave a wider range of 480°C to 640°C . Scatter diagram for velocity of ultrasonic waves versus modulus of rupture for Nyeri clay is presented in Figure 5.3.

The modulus of rupture against thermal shock severity for the Maragua clay is shown in Figure 5.4. The modulus of rupture decreased gradually with thermal shock severity after a critical quench temperature of approximately 450°C . This value of critical temperature difference was obtained by fitting a least-square quadratic polynomial to the strength data at quench temperatures beyond 430°C . Figure 5.5 shows the velocity of ultrasonic waves against thermal shock severity. It can be seen that there was a gradual decrease in velocity of sound waves after the same critical quench temperature of 480°C . Figure 5.6 presents the scatter diagram of velocity of sound versus modulus of rupture. The decrease in strength for the Maragua clay was from 6.40 MN/m^2 to 4.75 MN/m^2 .

5.5.1.2 Thermal fatigue

Thermal fatigue life survival probability (T-SPT diagrams) for Nyeri and Maragua clays are presented in Figures 5.7 and 5.8 respectively. Both diagrams are composed of straight lines that run parallel. The values of the material constant, n , obtained by the equation {33}:

$$\frac{M}{M'} = \left(\frac{AT'}{AT} \right)^n \quad \dots(2.50)$$

were 9 and 7 for the Nyeri and Maragua clay respectively (M and M' are number of thermal cycles at thermal shock severity of AT and AT' respectively).

The population mean (or data mean) is predicted with the aid of median ranks {47}; for 90 percent confidence, the respective data (Nyeri and Maragua) are plotted against 5 and 95 percent ranks (see Tables A.3.2 and A.3.3 in Appendix A.3). Figures A.3.1 and A.3.2 present the Weibull slope error and the percent failed at the mean respectively. The confidence intervals and range of values discussed in Section 5.5.2.2 are based on the median ranking described above.

Figures 5.9 and 5.10 shew fracture stress distribution at two different crosshead speeds of 2.26 rcm/min and 3.76 nm/min for the Nyeri and Maragua clay respectively.

Tables 5.6 and 5.7 present the variation of the average speeds of ultrasonic waves with repeated thermal shock for Nyeri and Maragua samples respectively.

5.5.2 DISCUSSION

5.5.2.1 Thermal shock resistance

Ziegler and Hasselmm {4f>} h^ve shcuvn that the interpretation of results concerning thermal shock resistance is a delicate matter and should be analysed carefully. They have shown that the relative strength behaviour in stable crack propagation can be described by:

$$a_2 \quad AT_i \wedge^3 \\ koT = \wedge \quad \dots (5_6)$$

where σ_j and a_2 are strength of specimens subjected to thermal shock severity of AT_j and AT_2 respectively.

For the Nyeri data crack propagation occurred over the range of $480^{\circ}\text{C} < \Delta T < 580^{\circ}\text{C}$. The value of $(\Delta T_j/A)^{1/3}$ which represents the predicted value of strength was 0.93 and the corresponding stress ratio σ_2/σ^{\wedge} was 0.48, which is much smaller than the predicted value. Following Ziegler and ffasselm&En*s {48} rrrriments it can be said that the strength loss was rather high over the temperature difference 480°C to 580°C for crack propagation to have occurred in a stable manner. Thus most of the specimens must have failed by unstable crack propagation, and so Figure 5.1 presents a precipitous decline in strength at a critical temperature difference of $\Delta T = 480^{\circ}\text{C}$. There is a probable bi-modal strength distribution in the temperature range $480^{\circ}\text{C} < \Delta T < 580^{\circ}\text{C}$ for this sample.

In the Maragua data crack propagation occurred over a wider range of $450^{\circ}\text{C} < \Delta T < 680^{\circ}\text{C}$. The value of $(\Delta T_j/\Delta T_2)^{1/3}$ was 0.87 while the stress ratio σ_2/a^{\wedge} was 0.73 which is comparable to the predicted value, thus suggesting a crack propagation of a stable nature.

Figures 5.2 and 5.5, showing the variation of speed of propagation of ultrasonic waves for Nyeri and Maragua clays respectively, indicate change in speed of propagation of waves at about the same critical temperature . indicated by the fracture strength temperature data of Figures 5.1 and 5.4.

Decline in the speed of propagation of ultrasonic waves was observed in the specimens that were shocked at thermal severity beyond the critical temperature difference. Thus this study has shown that low frequency (40 kHz) ultrasonic waves propagation speed can be used to investigate the thermal shock resistance of the ceramics under consideration.

The scatter diagrams of Figures 5.3 and 5.6 show the correlation between the fracture strength and the speed of propagation of ultrasonic waves for Nyeri and Maragua clays respectively. The correlation coefficients for the Nyeri and Maragua data were 0.824 and 0.889 respectively. Some of the scatter could be attributed to the fact that fracture strength is greatly influenced by surface conditions of the specimens. However, this claim should be verified by the testing of polished specimens in the future. The values of correlation coefficients are compared with the values from Table A.3.1 (in the Appendix) to test their significances [47]. From Table A.3.1, with degrees of freedom = 28, number of variables 2 (velocity of sound and strength), and 99 percent confidence, the value of correlation coefficient $r_{\text{corr}} = 0.463$. Since in both the Nyeri and Maragua data the values of the correlation coefficients are greater than 0.463 it can be concluded with 99 percent confidence that variations in strength and variation in the velocity of

propagation of ultrasonic waves are interdependent in both samples: and 68 percent, in the case of Nyeri clay, and 79 percent, in the case of Maragua clay, of the variation of velocity of propagation of ultrasonic waves can be accounted for by the variations of the strength of the specimen or vice-versa.

The fracture strength-velocity relationships suggest that measurement of variation in the speed of ultrasonic waves can be used to study the cumulative effect of repeated thermal shock (thermal fatigue) as reported by Newman, D.R. (personal communication).

The thermal shock resistance factors, R , obtained from the properties of the materials listed in Tables 5.2 and 5.3 were 95°C and 58°C for the Nyeri and the Maragua clays respectively. No conclusion can be drawn on the relationship between the thermal shock resistance factor and the critical temperature difference before the values of the rupture strength (a_R)» Young's modulus (E), Poisson's ratio (ν) and coefficient of thermal expansion (α) are determined accurately. The principal source of error introduced by the rupture stress (a_R) is due to the probabilistic characteristic of strength in brittle materials as shown in Figure 5.9. However, the thermal shock resistance factor is usually lower than the critical temperature difference for most ceramics and

rises with increasing critical temperature difference {49}.

5.5.2.2 Thermal fatigue

From the Nyeri test data it can be concluded that the mean lives, M , are 8 shocks at a thermal shock severity of $AT = 530^{\circ}\text{C}$ and 26 shocks at $AT = 470^{\circ}\text{C}$. However, the true mean lives at 90 percent confidence, can be as low as 6 shocks and as high as 10 shocks at a shock severity of $AT = 470^{\circ}\text{C}$ it can be as low as 19 shocks and as* high as 32 shocks.

From the Maragua test sample the mean lives, M , at thermal shock severities of 530°C and 470°C are 25 and 59 shocks respectively. The true mean lives at 90 percent confidence can be as low as 16 and as high as 34 shocks at $AT = 530^{\circ}\text{C}$ thermal shock severity and as low as 37 shocks and as high as 80 shocks at a shock severity of $AT = 470^{\circ}\text{C}$.

The parallel lines obtained in the 'thermal shock severity - probability-time' (T-SPT) diagrams of Figures 5.7 and 5.8 suggest that the method proposed by Kamiya and Kamigaito {32, 33} is valid for the specimen tested. It was reported by Kamiya and Kamigaito {50} that there were variations in the inclinations of the lines for some heterogeneous systems. However, in the present samples of Nyeri and Maragua clays the

T-SPT diagram lines were parallel, suggesting the existence of a major phase that controls the crack growth. More values (T-SPT lines) at temperature difference between the ones considered in this study should be obtained before the above statement can be established unequivocally.

Values of the parameters, m and n , found from the thermal shock (T-SPT) data and flexure strength data are summarized in Table 5.5. Most values determined from the T-SPT diagrams seem to agree with those determined from the strength data with the exception of the T-SPT value of m for Nyeri clay which was very large compared to the flexural data. These discrepancies were observed by Kamiya and Kamif^aito {3c} in other specimens and were attributed to the different statistical nature involved when considering the Weibull distribution for the two types of loading.

The variation of the speed of propagation of ultrasonic waves with the number of shocks is presented in Tables 5.6 and 5.7 for the Nyeri and Maragua samples respectively. The Nyeri clay was shocked at a temperature difference, ΔT , of 280°C while the Maragua was at 380°C . These values were selected from the performance of the two types of clays exhibited in the previous experiments.

Analysis of variance is a powerful method for analyzing experimental data involving quantitative measurement. It can be used to compare the contribution of the number of thermal shocks on the speed of propagation of ultrasonic waves in specimens. This requires normally distributed sets of data, which these are not. So the analysis was carried out on the logarithms of the data {3}.

A single factor experiment (1-way) analysis of variance {51} was carried out on the logarithms of the data for both Nyeri and Maragua samples, the results of which are shown in Tables 5.8 and 5.9 respectively. Considering the Nyeri data, on the basis of the results in Table 5.8, it can be concluded with 99.9 percent confidence that the number of shocks at the thermal shock severity of 280°C significantly affected the speed of propagation of ultrasonic waves in the samples. However, the effect of thermal shock at 380°C on the Maragua clay is insignificant when the variation in the speed of ultrasonic waves is considered.

5.6 CONCLUSIONS

It is essential to relate the experimental results to the materials of construction of stoves. The three basic factors that were investigated are:

- i) crack resistance (ΔT_c - the minimum temperature difference to initiate cracking) ,
- ii) damage resistance (loss of strength suffered by the specimen during cracking), and
- iii) fatigue resistance.

However, the main weakness of the results obtained is that the experiments were carried out under severe conditions of cooling. In cooking stoves these conditions are caused when water or any other fluid spills on the ceramic lining.

The major deduction that can be derived are as follows:

- i) The crack resistance (ΔT_c)

Nyeri clay had a critical temperature difference (ΔT_c) of 480 C for crack initiation, while the Maragua clay had a slightly less critical temperature difference of 450°C.

- ii) The damage resistance

Nyeri clay suffered more damage than the Maragua

clay. The ratio of the strength before and after cracking, a_2/a_1 , was 0.48 for the Nyeri sample compared to the value of =0.73 for the case of the Maragua sample.

iii) Fatigue resistance

- a) The method proposed by Kamiya and Kanigaito (32, 33, 50) for the prediction of thermal fatigue life was found applicable. Maragua clay was found to have longer fatigue life than the Nyeri clay. Quantitative values of thermal fatigue life are shown in Figures 5.7 and 5.8, for each clay.
- b) For the case of Nyeri clay, significant differences were found between the speeds of propagation of ultrasonic waves passing through specimens thermally shocked different number of times (4, 11 and 19) at a shock severity of 280°C.
- c) For the case of Maragua clay, no significant difference were found between the speeds of propagation of ultrasonic waves passing through specimens thermally shocked

different number of times (4, 11 and 19) at a shock severity of 380°C. This could be due to insufficient number of thermal shocks.

Overall implications of this experimental study are presented further in the next chapter.

Major Compounds	Nyeri Clay %	Maragua Clay %
SiO ₂	64.70	66.92
Al ₂ O ₃	22.57	26.42
Fe ₂ O ₃	4.79	3.99
K ₂ O	2.29	1.26
MgO	0.46	0.21
CaO	0.06	0.02
Losses (ignition)	0.29	0.48

Table 5.1: Chemical Composition of Specimens

	Weibull Modulus	Strength (MN/m ²)	
		Flexural	Tensile
Nyeri Clay	11	8.17	5.89
Maragua Clay	13	6.92	5.18

Table 5.2: Strength of Specimens

Physical Properties	Nyeri clay	Maragua clay
Modulus of elasticity (GN/m ²)	10.74	14.86
Poisson's ratio (1)	0.25*	0.25*
Specific heat capacity (J/kg K)	931±(10)	880±(8)
Coefficient of expansion (1/ K)	6.0x10 ⁻⁶ *	6.0x10 ⁻⁶ *
Density (kg/m ³)	2580	2700

Table 5.3: Physical properties of specimens

((*) Assumed values,

values in brackets are standard deviation).

Temperature range °C	Thermal Conductivity W/mK
74 - 129	0.45
107 - 218	0.52
203 - 469	0.56

Table 5.4(a): Values of thermal conductivity for
Nyeri clay ;

Temperature range °C	Thermal Conductivity W/mK
90 - 230	0.46
145 - 440	0.49
220 - 640	0.53

Table 5.4(b): Values of thermal conductivity for
Maragua clay. (Obtained from University
of Nairobi, 3rd year project (1986))

Material	From T-SPT				From strength data	
	AT(20°C base temp.)		AT(100°C base temp.)		n	m
	n	m	n*	m'		
Nyeri Clay	9	29	8	25	6	11
Maragua Clay	7	15	6	14	5	13

Table 5.5: Values of n and m determined from T-SPT data and strength data.

	Number of shocks on 5 samples			
	0	4	11	19
Mean speed of ultrasonic waves (m/s)	2193.4	2178.2	2164.2	2158.0
Standard error (m/s)	±30.3	±29.0	±26.9	±27.0

Table 5.6: Speed of propagation of ultrasonic waves through Nyeri clay before and after thermal shocks

	Number of shocks on 4 samples			
	0	4	11	19
Mean speed of ultrasonic waves (m/s)	2585.3	2467.8	2434.5	2411.8
Standard error (m/s)	±74.3	±57.4	±49.9	±47.9

Table 5.7: Speed of propagation of ultrasonic waves through Maragua clay before and after thermal shocks

Source of variance	Sum of squares	Degree of freedom	Mean Square	Mean square ratio
Treatment	0.3747	2	0.1874	13.98
Residual	0.1611	12	0.0134	
Total	0.5358	14		
Minimum mean square ratio for factors to be significant at 99.9 percent confidence is 13.0 {47}.				

Table 5.8: Analysis of variance for the Nyeri clay.

Source of variance	Sun of squares	Degree of freedom	Mean square	Mean square ratio
Treatment	0.0631	2	0.0316	0.417
Residual	0.6807	9	0.0756	
Total	0.7438	11		
Minimum mean square ratio for factors to be significant at 90 percent confidence is 3.01 {47}.				

Table 5.9: Analysis of variance for the Maragua clay.

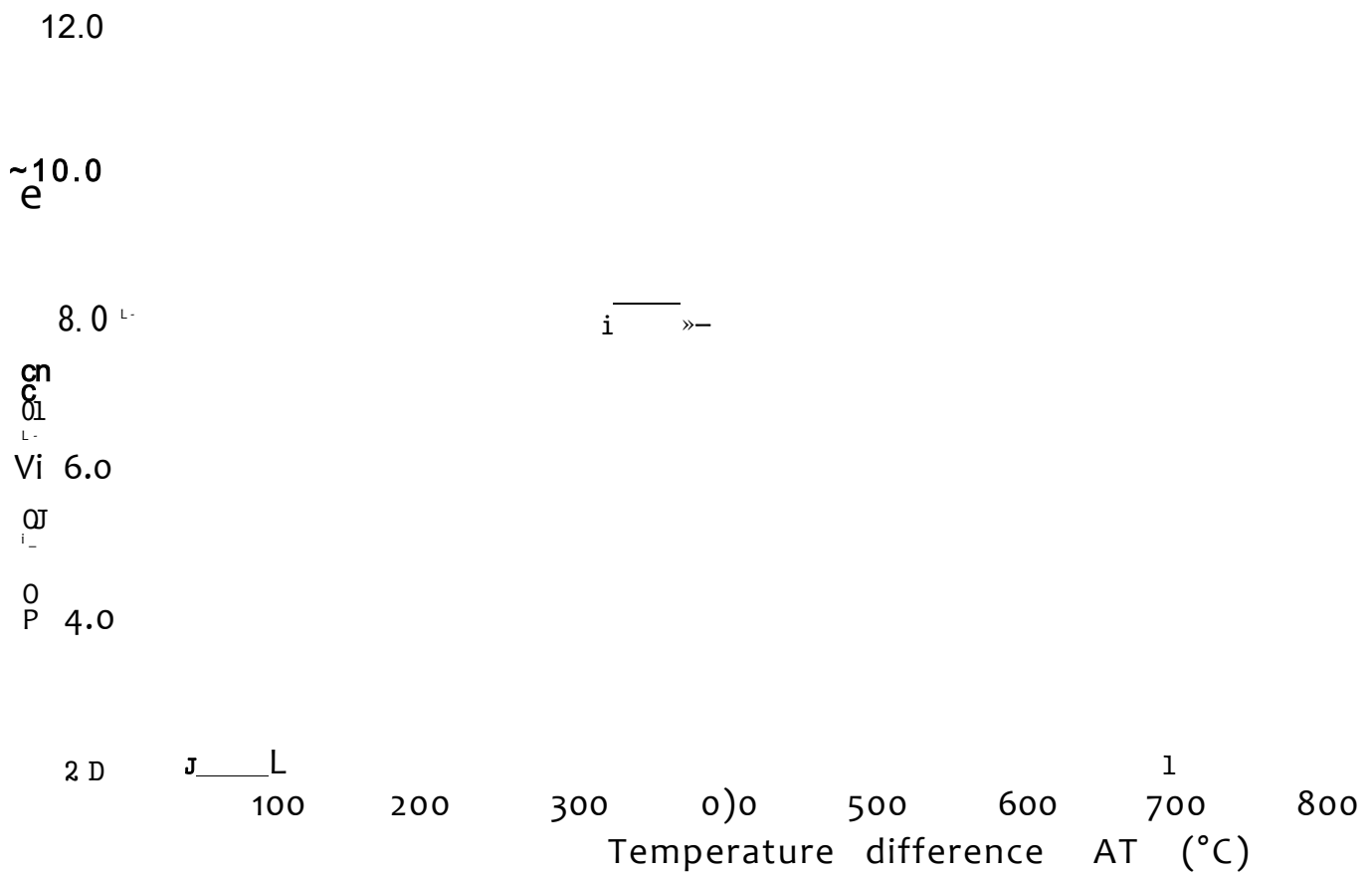


Figure 5.1: Fracture strength of the Nyeri specimen after water quenching at different thermal shock severities

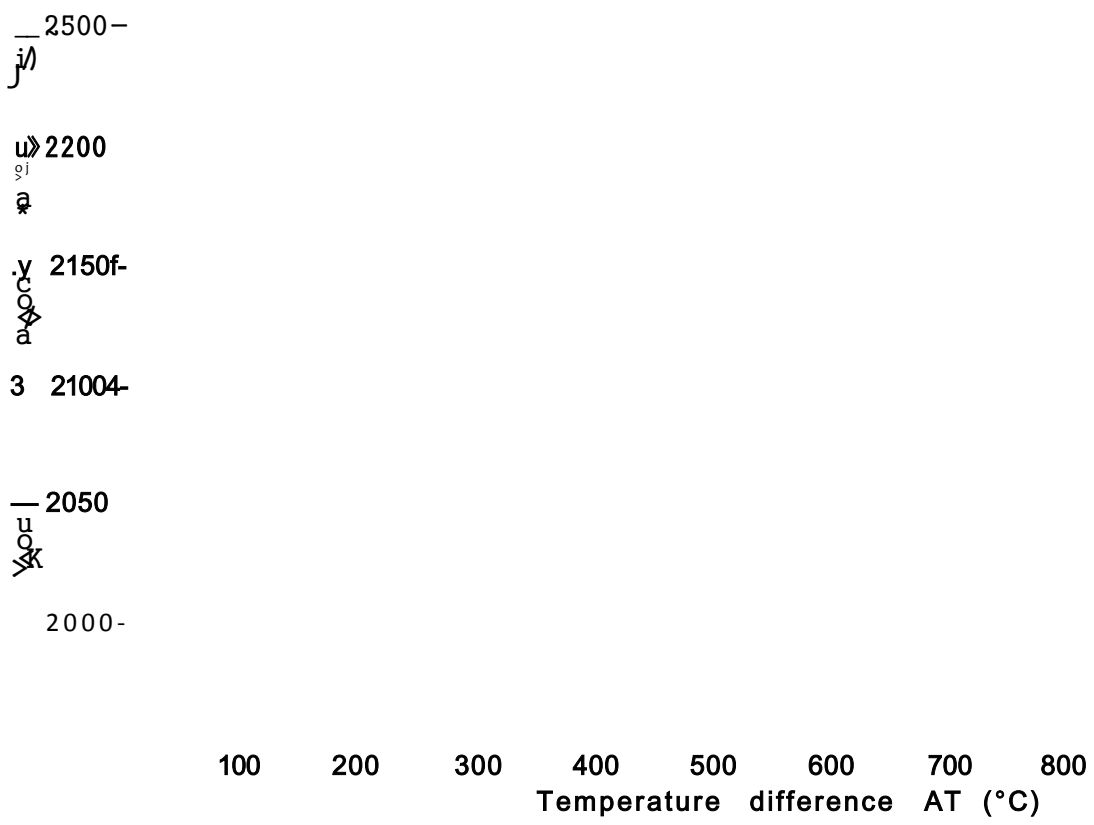


Figure 5.2: Speed of ultrasonic pressure waves (40 kHz) versus thermal shock severity for the Nyeri specimen

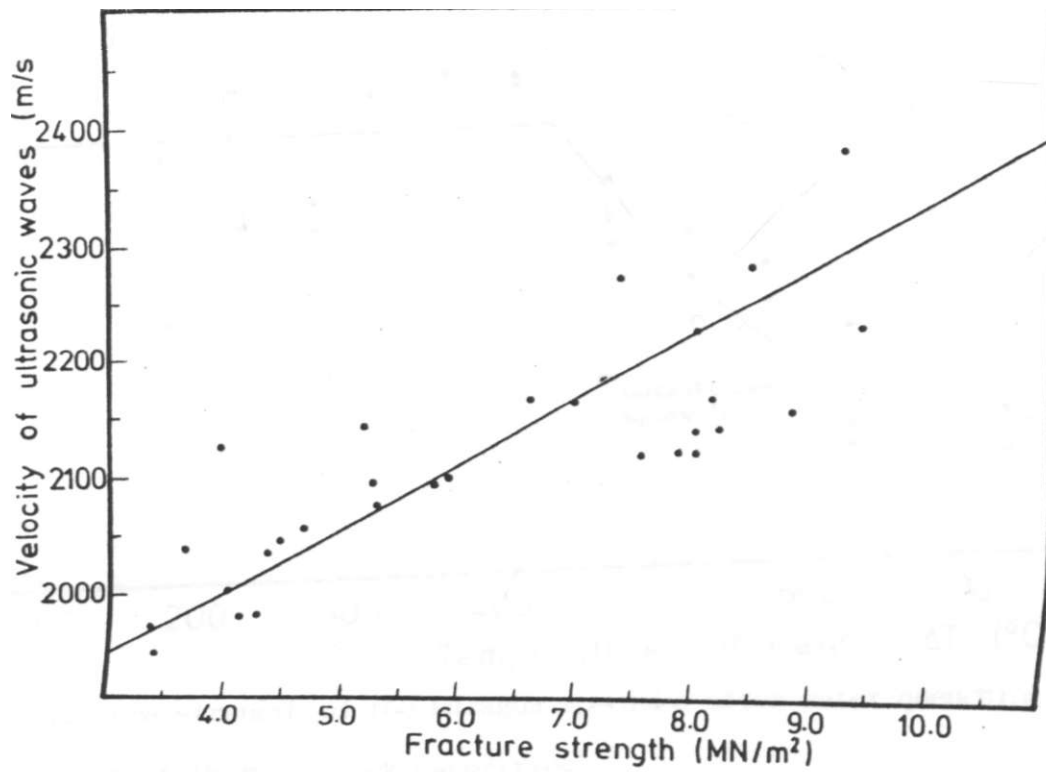


Figure 5.3: Speed of ultrasonic pressure waves versus fracture strength for the Nyeri specimen

E 7.0

6.0
5.0
4.0
3.0
2.0
1.0
0.0

Quadratic least-square fit

0 100 200 300 400 500 600 700 800
Temperature difference AT (°C)

Figure 5.4: Fracture strength of the Maragua specimen after water quenching at different thermal shock severities

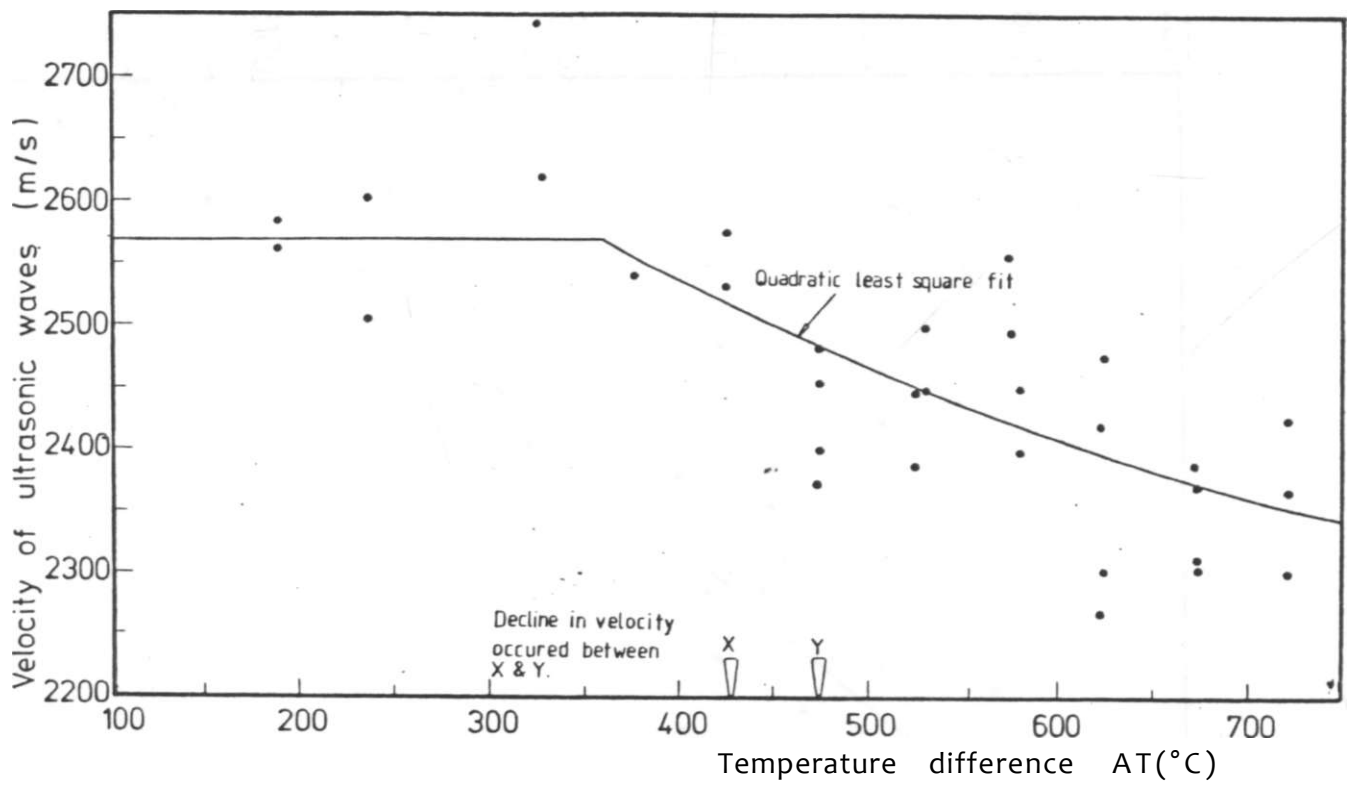


Figure 5.5: Speed of ultrasonic pressure waves (40 kHz) versus thermal shock severity for the Maragua specimen

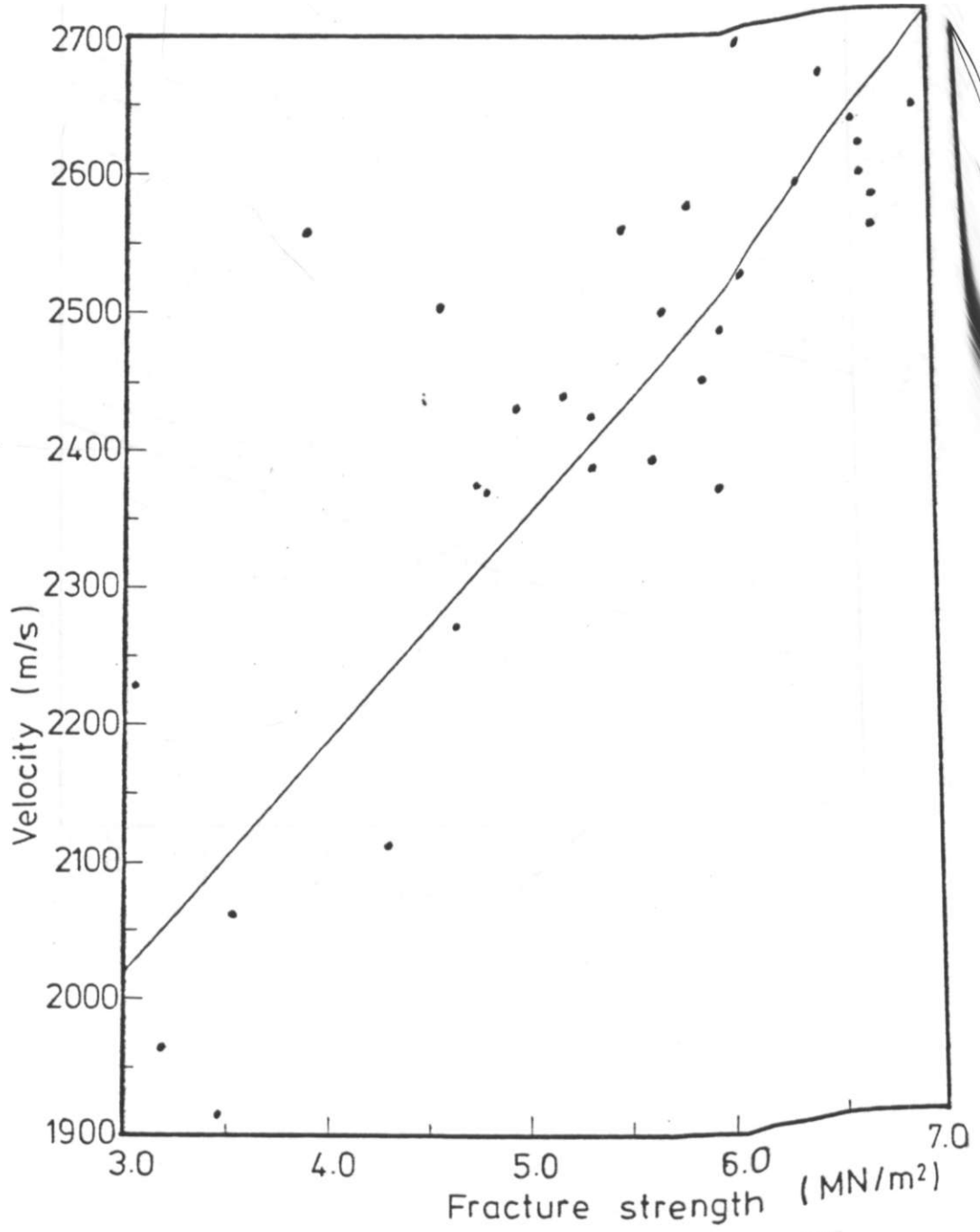


Figure 5.6: Speed of ultrasonic pressure waves versus fracture strength for Maragua sample

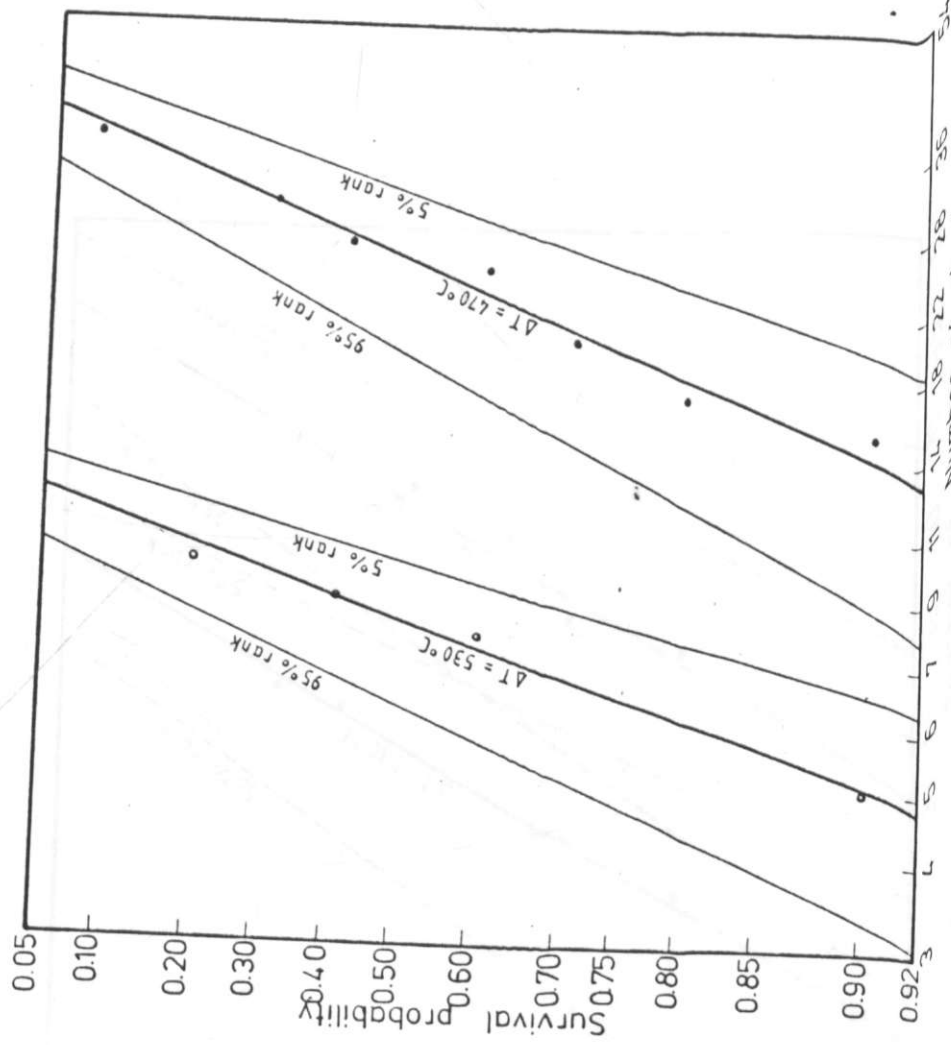
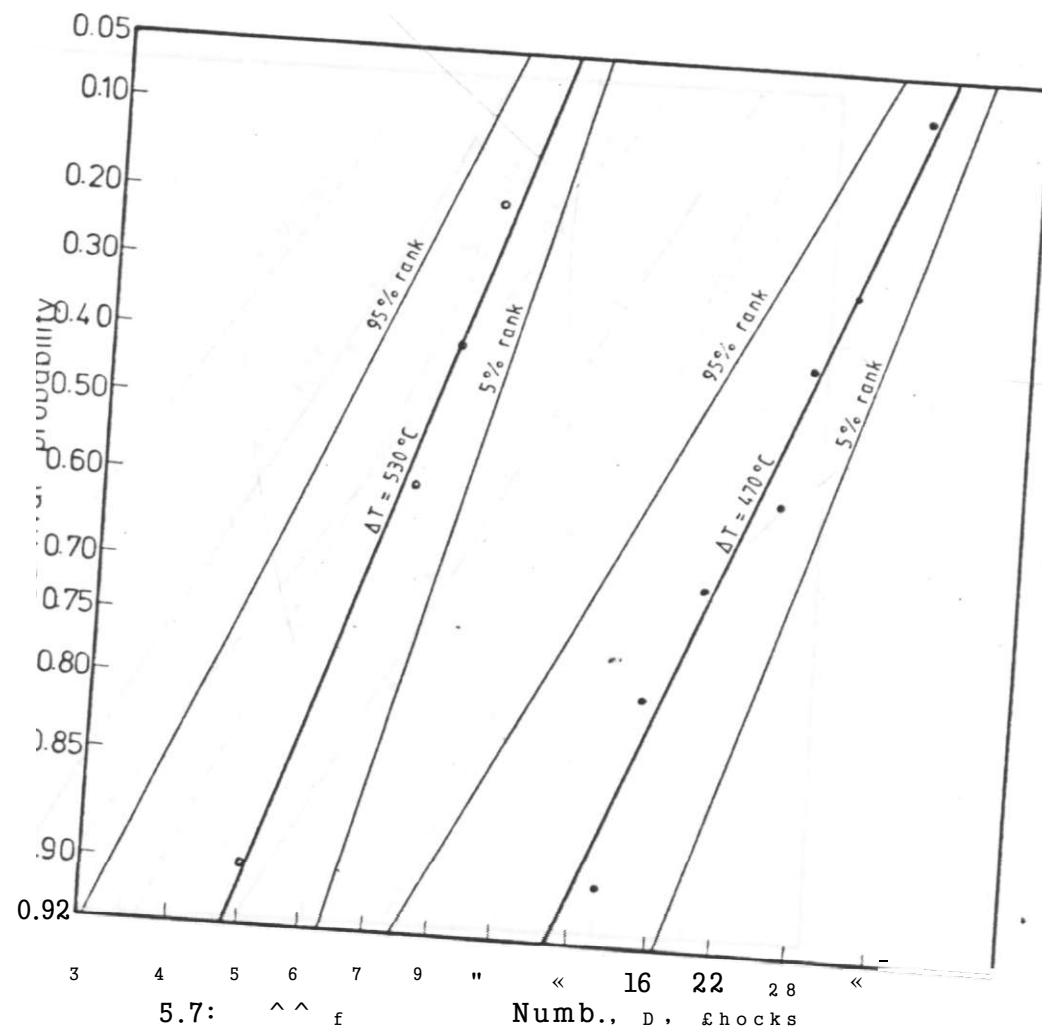


Figure 5.7: Thermal fatigue life versus survival probability (T-SPT diagram) for the Nyeri clay



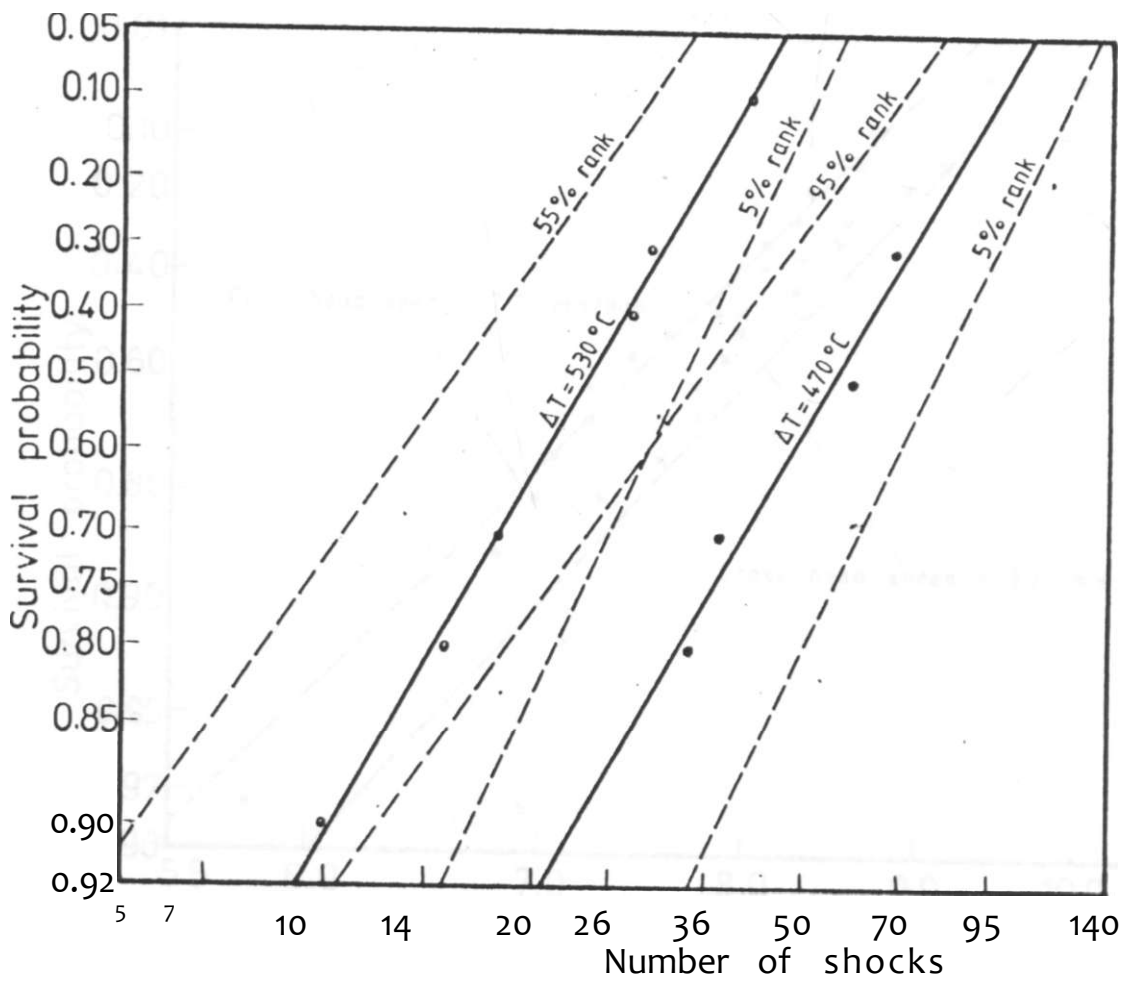


Figure 5.8: Thennal fatigue life, versus survival probability (T-SFT diagram) for the Maragua specimen

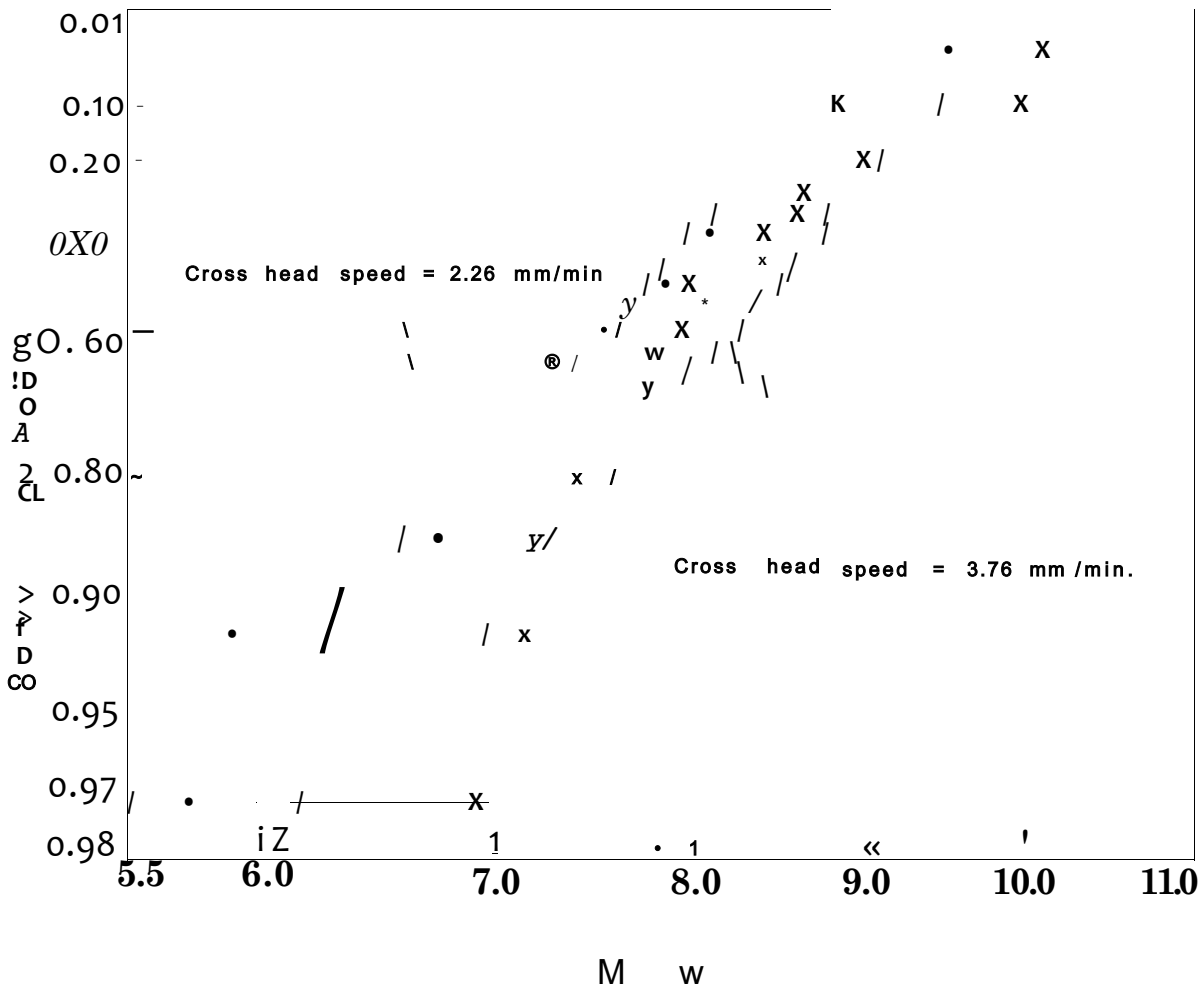


Figure 5.9: Fracture stress distribution of the Nyeri specimen for different cross head speeds

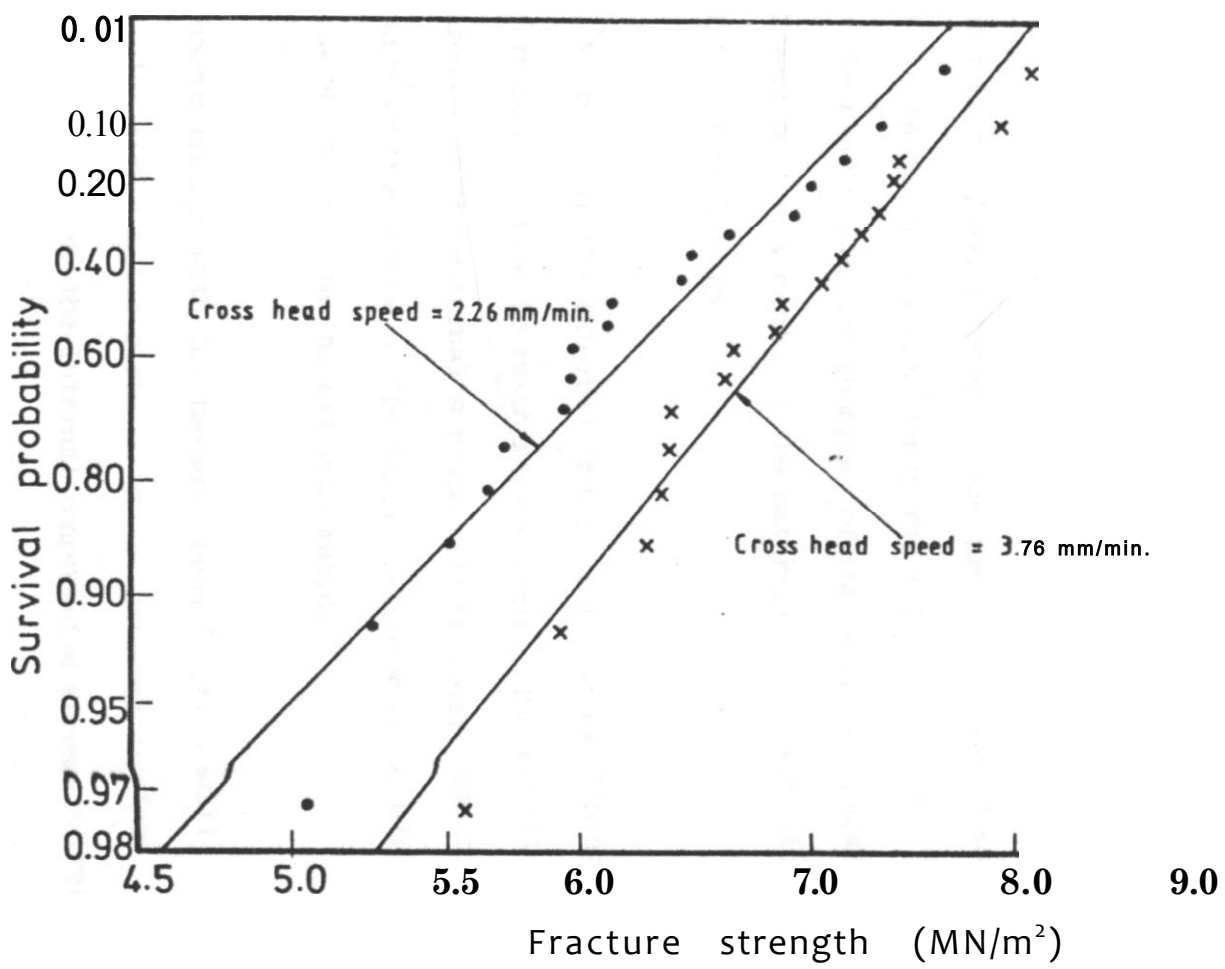


Figure 5.10: Fracture stress distribution of the Maragua specimen for different cross head speeds

CHAPTER SIX

6. OVERALL CONCLUSIONS AND RECOMMENDATIONS

6.1 CONCLUSIONS

The following conclusions may be drawn from the present work:

1. The numerical model presented has proved its usefulness by providing quickly and simply the relative changes that can be expected by the changing of the geometric parameters as well as the changing of the material of construction of the stove linings.
2. An increase in the external radius of the stove lining increases the time to reach steady state. The tensile stresses at the external surface will be lower and the compressive stresses at the inner surface will be higher with an increase in the external radius.
3. Ceramic linings with low thermal conductivities will develop high tensile stresses at the external surface without affecting the internal compressive stress a great deal.
4. Ceramic linings with lower heat capacities per unit volume have a slightly higher inner surface temperatures

and outer surface tensile stresses during the transient state. However, the difference is narrow during the steady state. The time to reach steady state is also shorter for such linings.

High heat transfer coefficient (within the limits of heat transfer conditions in stoves) at the outer surface introduces a slight increase in the tensile stresses at the external surface during the transient state without affecting the compressive stresses at the inner surface. " In the real stove situation these conditions may occur during a cold windy day.

The Nyeri clay had a critical temperature difference of 480°C for crack initiation while the Maragua clay had a slightly less critical temperature difference of approximately 450 C.

It was found that measurement of the variation of the speed of low frequency (40 kHz) ultrasonic pressure waves passing through test specimens could be used to monitor thermal shock resistance (the critical temperature difference) in cylinders with lengths that are about 5 times their diameters. However, there is more scatter when using this technique and it might require the testing of a higher number of specimens than would

the measurement of bending strength.

8. The Nyeri clay suffered more damage after thermal shocking than the Maragua clay. The ratio of strength before and after cradling, σ_2/σ_1 , for the case of the Nyeri clay was 0.48 while the value of σ_2/σ_1 was 0.73 for the case of the Maragua sample. The decrease in strength for the Nyeri clay was from 8.05 (MN/m²) to 3.85 (MN/m²) compared to the decrease in strength for the Maragua sample which was from 6.40 (MN/m²) to 4.75 (MN/m²).
9. The method proposed by Kamiya and Kamigaito [33] was found to be applicable to the 'non-engineering' ceramics tested. The Maragua clay was found to have a better fatigue resistance than the Nyeri clay. The Nyeri test samples had mean lives of 8 and 26 cycles at thermal shock severities, ΔT , of 530°C and 470°C respectively. The Maragua test sample had mean lives of 25 and 59 cycles at thermal shock severities of 530°C and 470°C respectively.
10. For the case of the Nyeri clay significant differences were found between the speeds of ultrasonic pressure waves passing through specimens shocked different

number of times (4, 11, and 19) at a shock severity, AT, of 280°C.

11. For the case of the Maragua clay no significant difference was found between the speeds of ultrasonic waves passing through specimens thermally shocked different number of times (4, 11, 19) at a shock severity, AT, of 380°C. This could have been due to insufficient number of shocks.

From the current studies it can be concluded that the Maragua clays are more suited for the general stove usage than the Nyeri clay. However, it would be uneconomical for a local stove producer from Nyeri to use the Maragua clay transported all the way from Maragua. Thus producers should strive for 'good' ceramics (good thermal shock resistance, good damage resistance and good fatigue resistance) for stove applications by the use of additives. Some recommendations for the producers are given in Section 6.2.

6.2 RECOMMENDATIONS

1. Any ceramic lining (insert) should be produced from a material that has a reasonably good strength and

relatively low Young's modulus and coefficients of thermal expansion in an effort to lower thermal stresses generated due to temperature gradient and to increase the thermal shock resistance.

2. Since the measurement of the parameters like Young's modulus, coefficient of thermal expansion, thermal conductivity and elastic surface energy require sophisticated laboratory facilities, testing of specimens for thermal shock resistance, damage resistance and fatigue resistance is required before deciding on what material to use for the production of linings.
3. The bending test should be used during thermal shock testing as it shows two features: the critical temperature for crack initiation and the loss of strength after cracking. Simple construction of flexure testing machines has been shown by van der Valden (52).
4. Ceramic linings should be made of clays with a suitable additive. Before production of these inserts further tests to determine the type and quantity of additive to be used should be carried out. The tests could comprise of thermal shock tests and thermal fatigue tests. Additives like grog or sand are believed to improve the thermal shock resistance of these linings.

5. Before a material is used in production its resistance to thermal fatigue should be tested. Actual simulation of stove conditions takes very long and it is important to be able to predict results in actual stores from accelerated experiments. To relate the accelerated fatigue test and the actual conditions a sample of insert that had been produced say, 2 years ago, and is still in use can be traced and if the composition used (clay and additives) can be determined from past experience, then an accelerated thermal fatigue test can be conducted on test specimens produced from the same material. The fatigue life obtained can be taken as a requirement that should be fulfilled by other materials from which inserts are to be produced. It is difficult to make prediction of the actual fatigue life of the ceramic tested but can be used as a relative test to aid materials selection. This test is more suited to materials with the same material constants, n , as that of the material to be compared with.

6.3 SUGGESTIONS FOR FUTURE WORK

1. Development and intensive mathematical treatment of the stove model is required in an effort to study the thermal

and stress conditions. Presently coroutine facilities at the Mechanical Engineering Department in the University of Nairobi can allow such studies. The studies should lock into areas such as:

- i) the simulation of heat supply in stoves,
- ii) the treating of the problem as that of an anisotropic material ~~when~~ the case arises, and
- iii) the treating of the gecmetry of the ceramic lining as in the real situation (for instance: not assuming a long cylinde'r condition, not neglecting the slight taper, etc.)

2. More work needs to be done on the thermal and physical properties of the ceramic linings used in stoves. Values of thermal conductivity, specific heat capacity, Young's modulus and, coefficient of thermal expansion should be investigated as a function of temperature. If functions of the type $f(T) = a+bT+cT^2+_____$ can be obtained it would be convenient to incorporate them in the numerical model.

I

3. As most of the fracture aspect of this work was done under severe thermal conditions, a method of predicting or working out of performance under less severe conditions which are actually prevalent in stoves should be investigated.

More materials from different parts of Kenya should be tested to investigate thermal shock resistance, damage resistance as well as fatigue resistance. These materials should be tested by mixing them with additives like grog or sand, etc. The effect of the type and amount of additive to be mixed with clay should be studied properly.

The effect of firing temperature limits should be investigated for different samples (and additives).

More work on the thermal fatigue aspect of these ceramics is essential. More fatigue data should be obtained at thermal shock temperatures below and between the ones considered in this work. Moreover, fatigue in the actual stove conditions should be simulated and the fatigue life of the ceramics investigated. It may be possible to get a relationship between these results (fatigue in actual conditions) and the accelerated results (thermal shocking).

Use of strain gauges can be made to investigate the fracture of the linings by the use of special strain gauges and an X-Y recorder as was done by Mai and Jacob [41].

APPENDICES

Appendix A1

A1.1: Finite difference equations for the cylindrical model

The physical situation of the stove model was mathematically described by Equation (2.4) as:

$$\frac{C_p}{k} \frac{\partial T}{\partial t} = \frac{\partial^2 T}{\partial r^2} + \frac{1}{r} \frac{\partial T}{\partial r} \quad (2.4)$$

The boundary conditions were given by:

$$Q = -kA \left. \frac{\partial T}{\partial r} \right|_i \quad (3.2)$$

at the inner surface, and

$$h(T(r_o, t) - T_j) = -k \left. \frac{\partial T}{\partial r} \right|_{r_o} \quad (3.3)$$

at the outer surface.

- Where
- T = temperature (K)
 - r = radius (m)
 - Q = heat load (W)
 - k = thermal conductivity (W/nK)
 - Cp = specific heat capacity (J/kgK)

- ρ = density (kg/m³)
 h = combined natural convective and radiative heat transfer coefficients (W/m²K)
 r^i = inner radius (m)
 r_o = outer radius (m)
 t = time (sec)

Solving Equation (2.4) using Forward Difference

Approximation on the left side and Central Difference

*

Approximation on the right side the following Finite Difference

Equation can be obtained:

$$\frac{T_{n+1,i} - T_{n,i}}{\Delta t} = \frac{T_{n,i+1} - 2T_{n,i} + T_{n,i-1}}{(\Delta r)^2}$$

$$1 + \frac{K}{r} \left(\frac{T_{n,i-K\Delta r} - T_{n,i-1}}{2\Delta r} \right) \quad (A1.1)$$

where T^i is the temperature of the i th node at the n th time step, Δt the time increment, Δr the radius increment, K is thermal diffusivity ($k/C_F \rho$), and r the radius at any point.

The temperature at the next time step, $n+1$, will be given by:

$$\begin{aligned}
 T &= T \frac{r^{-KAt}}{(Ar)^2} \frac{<At}{2(r_{\pm} + (i-1)Ar)Ar} \dots \\
 &+ T \frac{J^{KAt}}{(Ar)^2} \frac{<At}{2(r_{\pm} + (i-1)Ar)Ar} \dots \\
 &+ T \frac{n - \frac{2KAt}{(Ar)}}{n, i} \dots \dots (A1.2)
 \end{aligned}$$

The stability of the above equation is determined by the inequality given by {38}:

$$(Ar)^2 \dots (M.3)$$

Equation (A1.2) can be simplified by introducing the following coefficients:

$$A(i) = \frac{[1 + \frac{\dots}{2(v(i-1)Ar)^J}]}{(Ar)^{2i}} \dots (A1.4)$$

$$B(i) = \frac{i^i}{(Ar)^2} - \frac{Ar}{2(r_{\pm} + (i-1)Ar)} \dots (A1.5)$$

$$e = i \frac{jfAt}{(Ar)^i} \dots (A1.6)$$

to read as:

$$T_{n+1,i} = T_{n,i+1} A^{(i)} + T_{n,i-1} B^{(i)} + T_{n,i} C \dots (A1-7)$$

Equation (A1.7) applies to all internal nodes of the cylinder wall.

At the inner surface during heating, the boundary condition is given by Equation (3.2). Using Central Difference Approximation on Equation (3.2) and employing Equation (A1.7), the temperature of the inner surface for the next time step (during heating-up) is given by:

$$T_{n+1,1} = T_{n,2} A^{(1)} + \left(T_{n,2} - \frac{q}{k} \right) B^{(1)} + T_{n,1} C \dots (A1-8)$$

where q is the heat load per unit area.

At the outer surface the boundary condition is given by Equation (3.3). Applying Central Difference Approximation and substituting in Equation (A1.7) will give the following expression for the temperature at the next time step:

$$T_{n+1,N+1} = T_{n,N+1} A^{(N+1)} + T_{n,N} B^{(N+1)} + T_{n,N+1} C + T_{n,N} B^{(N+1)} \dots (A1.9)$$

For the case of laminar flow at the outer surface the convective heat transfer coefficient, h , at any time, t , is given by:

$$h_n = 1.16 \left(\frac{V}{L} \right)^{0.25} + \left[\frac{0.865}{(T_{n+1} - T_J)^{0.33}} \right] \quad \text{..(A1.11)}$$

and for the case of turbulent flow the first term on the right hand side of Equation (A1.11) will change to $0.95X(T_{n+1} - T_J)^{0.33}$.

At the inner surface the convective heat transfer coefficient, $h_{n,i}$ is given by {39}:

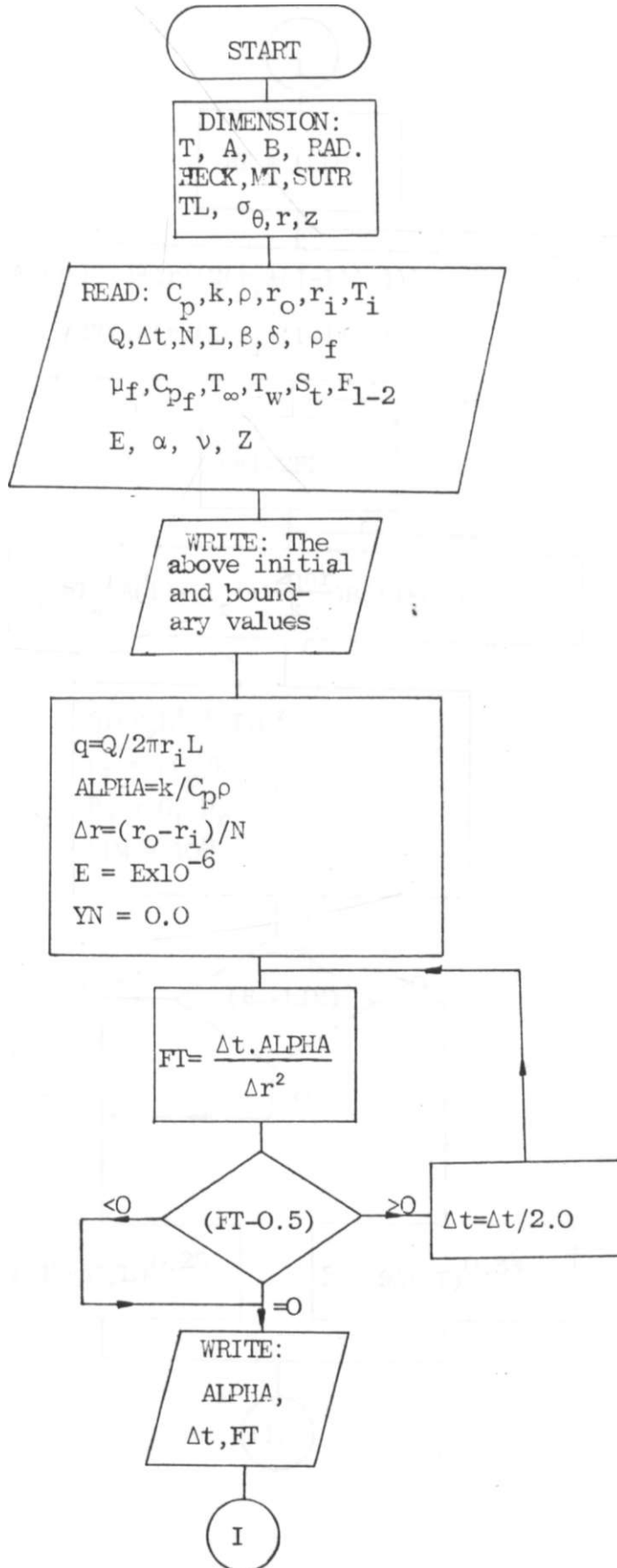
$$h_{n,i} = 1.42 \left\{ (T_{n+1} - T_J/L) \right\}^{0.25} \quad \text{..(A1.12)}$$

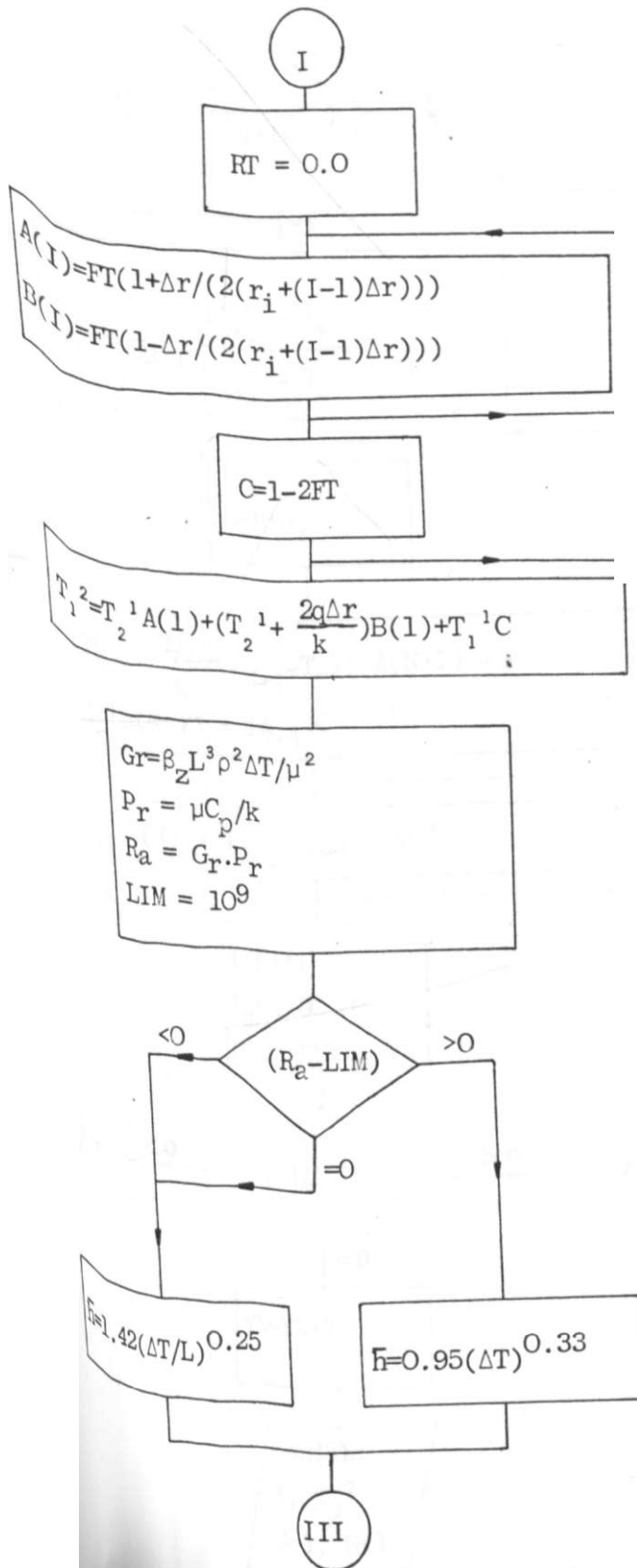
for the case of laminar flow, and:

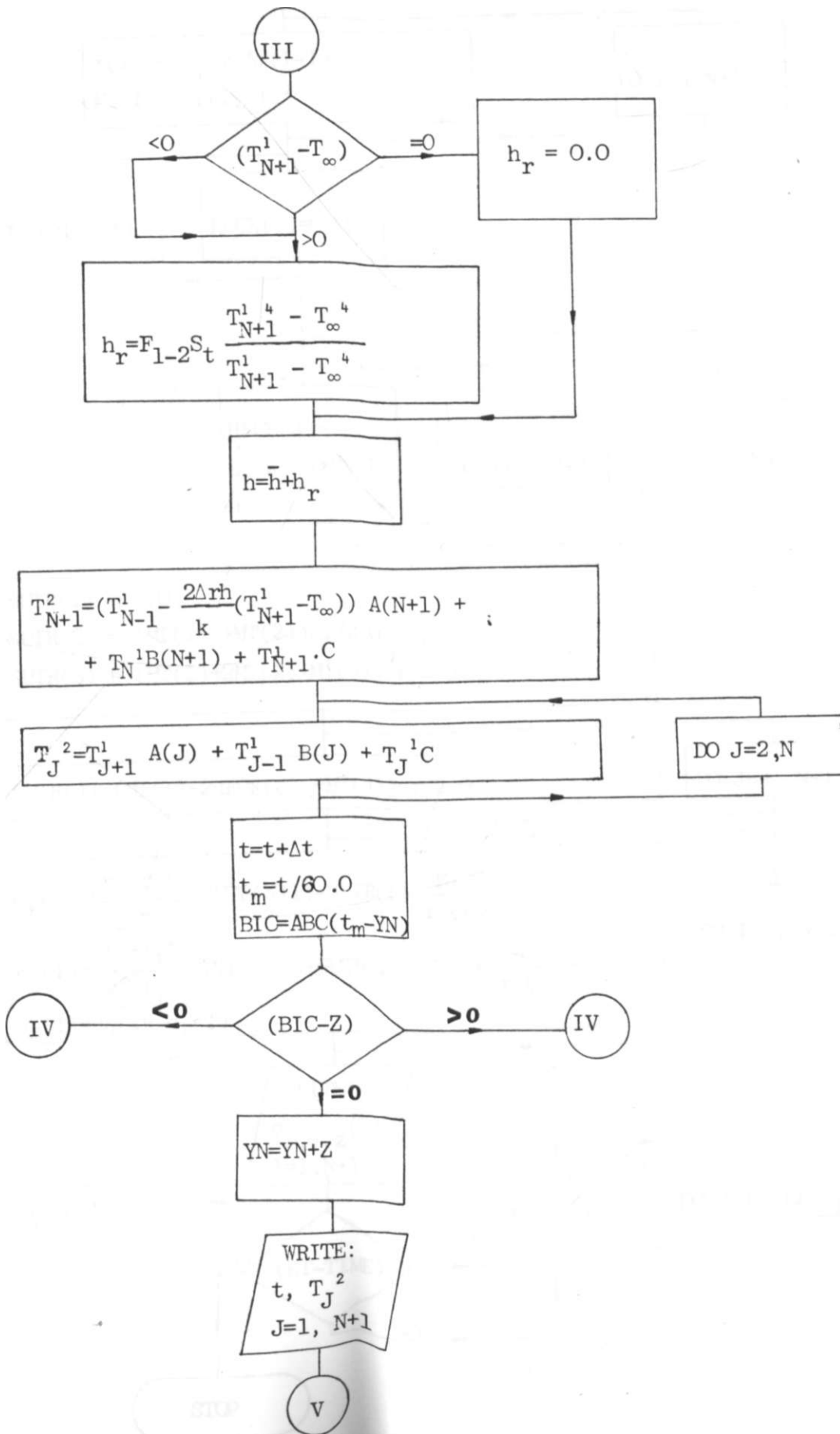
$$h_{n,r} = 0.95 (T_{n,i} - T_{CO})^{0.33} \quad \text{..(A1.13)}$$

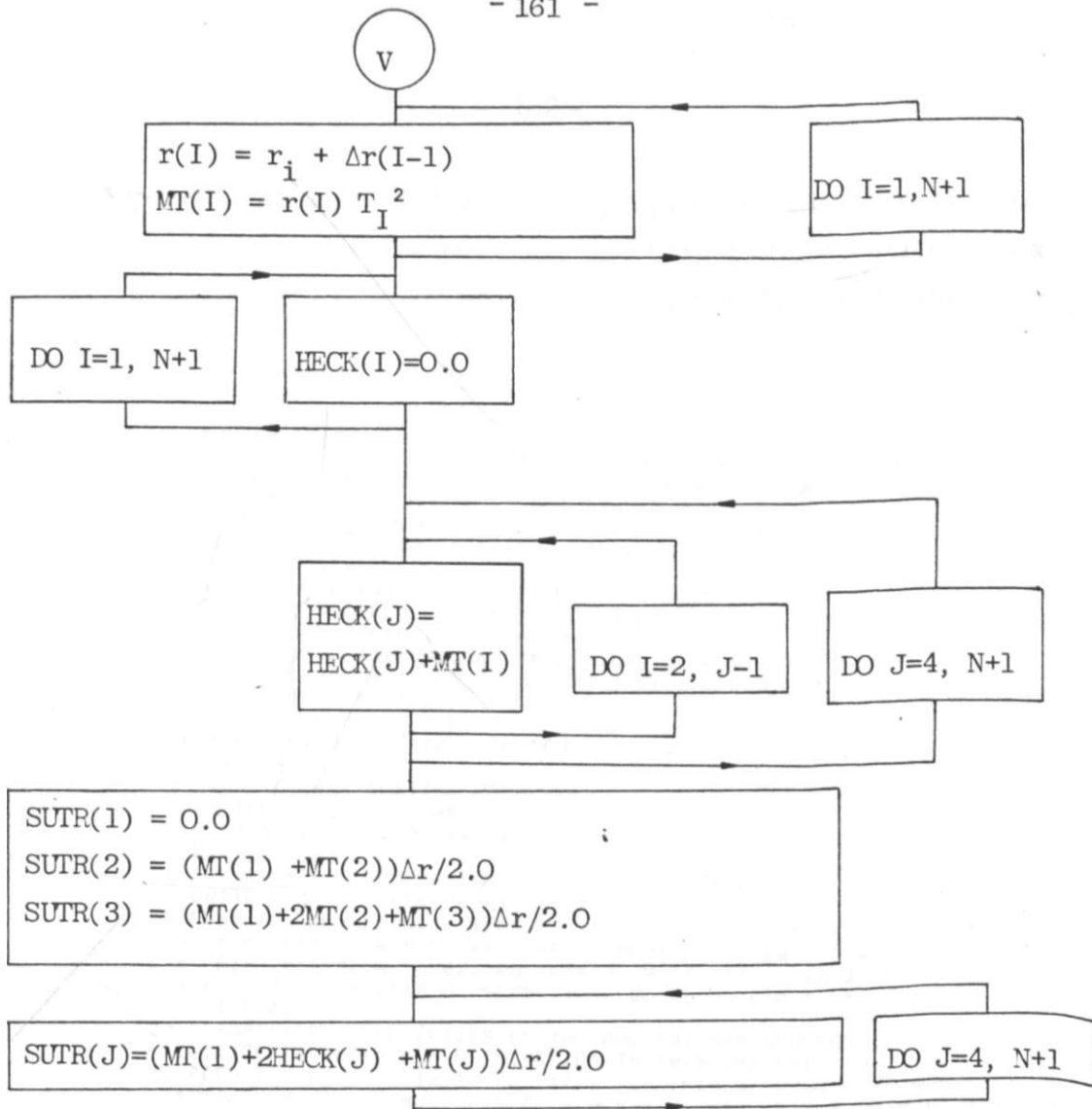
for the case of turbulent flow

Appendix A1.2: A program to calculate transient temperature and stress distributions across the wall of a hollow circular cylinder







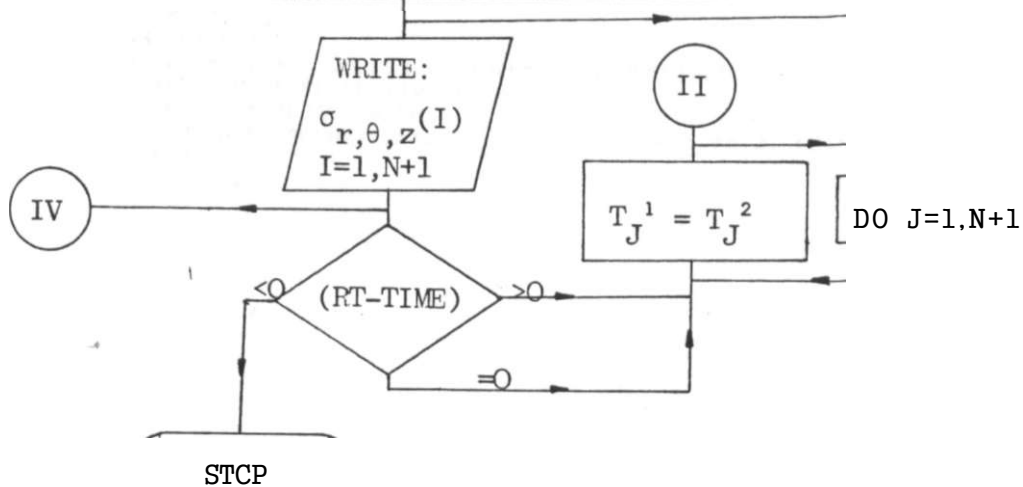


$$a_{(1)} = \frac{r^2 - r_0^2}{r(1-v)} \left(-SUTR(N+1) - SUTR(I) \right) \quad \text{Ea}$$

$$a_{(1)} = \frac{r^2 + r_0^2}{r(1-v)} \left(SUTR(N+1) + SUTR(I) + MT(I) \right) \quad \text{Ea}$$

$$a_2(I) = a_r(I) - a_r(I)$$

DO I=1, N+1



Appendix A1.2.1: A Fortran IV program to calculate transient temperature and stress distributions across the wall of a hollow cylinder during heating

```

MASTER CERAMIC
C  A PROGRAMME TO DETERMINE TRANSIENT TEMPERATURE AND STRESS
C  DISTRIBUTION ACROSS THE WALL OF A HOLLOW CIRCULAR CYLINDER-
REAL MK5H)
DIMENSION T< 50 >, A< 50 >, B* 50 >, C< 50 >, RAD( 50 >), HECK< 50 >
DIMENSION SUT R( 50 >), SIGR< 50 >, SI6T< 50 >), SIGA< 50 >, IL* 50 >
REAL KC,KA,NU
C  READING IN OF INITIAL AND BOUNDARY VALUES
READ< 5, 10 >CP, KC, CR, RI, RO, TI, GT, N, DT
10  FORMA r< 6F8. 3, F 10. 2, 13, K10. 8 >
READ< 5, 15 >BETA, G, SL, RHO, TMU, KA, CA, TA, TW, SIGMA, FOI
15  FORMAT( F 6. 4. F 4. 2. 2F 5. 3, F 8. 6, F 5. 3, F<6. 1, 2F 7. 3, E10. 5, F 5. 3 >
READ< 5, 18 >E, AL, TNU
1B  FORMAT(E10.5,F10.8,F5.3 )
C  WRITING OUT OF INITIAL AND BOUNDARY VALUES
WRITE( 6, 20 >
20  FORMAT* 10X,'INITIAL VALUES' >
C  HEAT INPUT PER UNIT AREA
G=GT/(3.141593**2,0*RI)#SL> :
WRITE* 6, 28 >
28  FORMAT<18X,' PROPERTIES OF CFRAMIC MODEL'/)
WRITE* 6, 30 >CP, CR, KC, G, RI, RO, TI, N, DT, SL
30  FORMAT* ' CF=' , F10. 3, ' J/KG. C' , 16X, ' CR * RHO )=' , F 10. 3, ' KG/CU. M' /
* ' KC=' , F10. 3, ' W/M.K' , 17X, 'HEAT INPUT G =' , F10. 3, ' W/SG.M' /
> ' RI=' , F10. 3, ' M. ' , 20X, ' RO' , F10. 3, ' M, ' / ' TI=' , F10. 3, ' K. ' , 20X,
> ' N=' , 13 / ' D1=' , F10. 8, ' SECS' , 18X, ' SL < L )=' , F10. 5, ' M. ' >
WRITE* 6, 33 >
33  FORMAT*18X,' PROPERTIES OF THE AMBIENT ATMOSPHERE'/)
WRITE* 6, 35 >BETA, G, RHO, TMU, KA, CA, TA, TW, SIGMA, FOI
35  FORMAT* ' BET A=' , F10. 7, ' /L" , 17X, ' G=' , F10. 5, ' M/SG, S' / ' RHO=' , F10. 3,
* ' KG/CU. M' , 14X, ' TMU=' , F10. 7, ' N/S. SGM' / ' KA=' , F10. 4, ' W/M. K' , 17X, ' CA=
< ' , F10. 3, ' J/KG. C' / ' TA=' , F10. 6, ' K, ' , 20X, ' TW=' , F10. 6, ' .K' / ' SIGMA=' , E
* 10. 5, 19X, ' FOI* ' , F 5. 3 >
YN=0.0
E=E/1000000.0
ALF=HA-KC/* CP*CR )
DR=* RO-RI)/N
DR2=DR#*2
C  LOOP FOR THE FULFILMENT OF STABILITY CRITERIA * FT<=0.5 >
11  FT=DT#ALFHA/DR2
IF* FT.GT.0.5 > GO TO 42
GO TO 43
12  DT=DT/2.0
GO TO 41
43  WRITE* 6, 38 >
38  FORMAT*2X,' VALUES OF THERMAL DIFFUSSIVITY,DISTANCE-STEP AND FOURI
JER NUMBER RESPECTIVELY'/)
WRITE* 6, 40 >ALPHA, DR, FT
40  FORMAT* ' ALPHA=' , F15. 9, ' SGM/S' , 2X, ' DR"' , F 5. 3, ' * M' )' , 2X, ' FT=' , F10. 7.
* / )
N1=N+1

```

```

RT=0.0
C WRITING OUT OF INITIAL TIME AND TEMPERATURE VALUES
WRITE( 6, 90 )RT
DO 50 J=1, N1
50 T( J )=T1-273. 0
WRITE( 6, 60 X T( J ), J=1, N1 )
60 FORMAT( 15( 1X, F8.4 > >
DO 70 N1
T( J )=T( J )+273. 0
A( J )=FT* < 1.0+DR/ < 2. 0*< RI+( J-1 >*DR ) ) )
E< J >=FT# < 1, 0- DR/( 2. 0*( RI+ < J-1 )*DR ) ) )
C < J )=1. 0-2. 0*FT
70 CONTINUE
C CALCULATION OF TEMPERATURE AT THE INNER SURFACE
TL( 1 )=T( 2 )*M I )+( T( 2 H 2. 0#Q*DKVKC )#E:( 1 )+T( 1 )>>C( 1 )
C CALCULATION OF HEAT TRANSFER COEFFICIENT FOR THE OUTER SURFACE
C
GR=fcETA*G* < SL ** 3.0 >* < RHO#*2. 0 >* < T( N1 )-TA )/< TMU**2. 0 )
FR=TMU#CA/KA
RA =GR*FR
LIM=1000000000. 0
IF < RA.GT.LIM ) GO TO 71
HC=1. 42* < ( T( N1 )-TA )/SL >* < 0. 25
GO TO 72
71 HC=0. 95* < T( N1 )-TA >* < 0. 3333
72 IF( T( N1 ).NE. TW ) BO TO 73
HR=0.0
GO TO 74
73 HR=F01#SIGMA* < T( N1 )**4-TW**4 )/( T( N1 )-TUI)
74 H=HC+HR
C
C CALCULATION OF TEMPERATURE OF THE OUTER SURFACE
TL( N1 )=< T( N-1 )-< 2. 0#DR#H* < T( N1 )-TA >/KC ) >*A< HI >
<< +T( N >*EK N1 ) * T( N1 )#C( N1 )
C CALCULATION OF TEMPERATURE FOR THE INNER NODES
DO 80 J=2, N
TL( J )=T( J+1 >*A< J )+T( J-1 )*E< J )+T< J >#C< J )
80 CONTINUE
• Rr*RT+DT
TM=RT/60.0
E'IC-ABS( TM-YN )
IF( BIC.NE. 5. 0000 > GO TO 111
YN=YN+5.00
C WRITING OUT OF TIME AND TEMPERATURE VALUES
WRITE( 6, 90 )TM
90 FoRMAt( ' ACTUAL TIME T=' , F6. 1, ' MINS. ' )
WRITE( 6, 101 )
101 FoRMAt( ' TEMP. < C ' ) )
DO 105 J' 1. N1
105 TL( J )=TL( J >-273. 0
WRITE( 6, 100 X TL( J ). J=1, N1 )

```

```

00 130 1=1,N1
C
C   DETERMINATION OF STRESSES USING TRAPEZOIDAL INTEGRATION
C
      RAD<I )=RI+DR*t1-1 )
      MT<I )=TL<I )*RAD<I >
130  CONTINUE
      DO 140 J=4,KII
      HECK<J )=0.0
140  CONTINUE
      DO 150 J=4,N1
      DO 150 1=2,<J-1 >
      HECK<J )=HECK<J )+MT<I )
150  CONTINUE
      SUTR<1 )=0.0
      SUTR<2 )=( MT<1 )/2.0+MT<2 )/2.0 >*DR
      SUTR<3 )=< MT<1 >»2.6*0<2 >»m<3 ) )#DR/2.0
      DO 140 J=4,N1
      SUTR<J )=( M<11 )+2.0*IE:CK<J >+Mt<J ) >*DR/2.0
160  CONTINUE
      RR=R0#*2.0-RI* *2.0
      DO 165 1=1,N1
C   CALCULATION OF STRESSES
      SIGR<I >=t ( S AD<I >**2.6-R1*#2.0 >*SUTR<N1 VRR-SUTR<I ) >#AL*E
      £/< ( RAD<I )**2.0 )*( 1.0- INU > )
      SIGT<I )=( ( RrtDt I >**2.0 RI**2,0 >#SUTR<N1 )/RR+SUTR<I )-MT<I >*RAD<I )
      £*AL#E/t ( RAD<I )**2.0 )*< 1.0-TNU > )
      SIGA<I >=SIGT<I )+SI BK<I )
165  CONTINUE
C   WRITING OUT OF STRESS VALUES
      WRIT<6,170 X SIG<1 >, 1=1,N1 )
      WRITE<6,175 )< SIGT<I >, 1=1,N1 >
      URIT<6,180 )< SIGA<I >, 1=1,N1 )
180  FORMAT<' A',50<1X,F7.2 >
170  FORMAT<' R',50<1X,F7.2 > )
175  FORMAT<' H',50<1X,F7.2 > )
100  FORMAT<t15t1X,F8.4 >>
      DO 110 J>1*N1
110  TL<J )=TL<J 1+273.0
111  CONTINUE
      IF<tRT.BE.126B0.0 > GO TO 120
      DO 200 J=1,N1
      Tt J)<TLt J)
200  CONTINUE
      GO TO 70
120  CONTINUE
      STOP
      END
      FINISH

```

Appendix A1.2.2: A Fortran IV program to calculate transient temperature distribution across the wall of a hollow cylinder during cooling

```
MASTER CERAM7EMP
C A PROGRAMME TO DETERMINE TRANSIENT TEMF', DISTRIBUTION ACROSS
C CYLINDER WALLS DURING COOLING
  DIMENSION T< 50 >, A< 50 >, B* 50 ), C( 50 )
  REAL KC,KA,NU
C READING IN OF INITIAL AND BOUNDARY VALUES
  READ( 5, 10 )CF< KC, CR, RI, RO, TI, G, N, DT
10  FORMAT* 6F8.3,F10.2,13.F10.8 )
  READ< 5, 15 >BETA, G, SL,RHO, TMU, KA, CA, TA, TU, SIGMA, FOI
15  FORMAt( F6. 4, F4. 2, 2F5. 3, FB. 6. F5. 3, F6. 1,2F7. 3, E10. 5, F5. 3 >
C WRITING OUT OF INITIAL AND BOUNDARY VALUES
  WRITE* 6,20)
20  FORMAT* 10X,'INITIAL VALUES' )
  WRITE* 6,28 )
28  FORMAT*18X, ' PROPERTIES OF CERAMIC MODEL'/)
  WRITE* 6, 30 )CP, CR, KC, R, RI, RO, JI, N, DT, St.
30  FORMAT* ' CF-',F10.3,' J/KG,C'?16X, ' CR * RHO )=',F10. 3, ' KG/CU. M' /
  *' KC=',F10. 3, ' W/M. K', 17X, ' HEAT INPUT G =',F10.3, ' W/SG.M' /
  %' RI=',F10. 3, ' M.', 20X, ' RO', F10. 3. ' M. ' /' TI=', FIB. 3, ' K. ', 20X,
  *' N=',13/' DT=', F10. 8, ' SECS', 18X, ' SL ( L)=' , FIB. 5, ' M. ' )
  WRITE* 6,33 )
33  FORMAT* 1tIX, ' PROPERTIES OF THE AMBIENT ATMOSFHtRE'/)
  WRITE* 6,35)BETA,G-RHO,TMU,KA,CA,TA,TW,SIGMA,FOI
35  FORMAtC BETA=',F10.7,' /C',17X, ' G=',F10.5,' M/SG.S'/' RHO=',F10.3,
  KG/CU. M', 14X, ' TMU=',F10.7, ' N/S.SGM'/' KA=',F10. 4, ' W/M.K',17X-' CA=
  *', F10. 3, ' J/KG. C'/' TA=', F10.6, ' K, ', 20X, ' TW=', F10. 6, ' K'/' SIGMA=', E
  $10,5,19X, ' F01=',F5.3 )
  YN=0.0
  ALPHA=KC/< CF*CR )
  DR=(RO-RI)/N
  DR2«DR**2
C LOOP FOR THE FULFILMENT OF STABILITY CRITERIA * FT<=0.5 )
41  FT=DT*fVLPHA/0R2
  IF < FT.GT.0. 5 ) GD TO 42
  GO TO 43
42  DT=DT/2.0
  GO TO 41
43  WRITE* 6, 38 )
38  FORMAT*2X,' VALUES OF THERMAL DIFFUSSIVITY,DISTANCE-STEP AND FOURI
  *ER NUMBER RESPECTIVELY'/)
  WRITE* 6, 40 JftLPHA,DR, D7
40  FORMAT* ' ALFHA=',F15.9,2X, 'DR=',F5.3,2X, ' DT=',F10.7)
  N1=N+1
  RT=0.0
C WRITING OUT OF INITIAL TIME
  WRITE* 6, 90 >RT
C READING IN OF INITIAL TEMPERATURE VALUES
  READ* 5, 50 X T* J ), J=1, N1 )
50  FORMAT*15F8. 4)
C WRITING OUT OF INITIAL TEMPERATURE VALUES
  WRITE* 6. 60 >1 T* J ), Jb1.N1 )
60  FORMAT*15*IX. F6. 4 ))
```

```

DO 70 J=1,N1
T< J )=T< J >+273. 0
A< J )=FT*< 1. 0-DR/< 2. 0*RI+( J-I)*DR > >
E< J )=FT*< 1. 0+DR/< 2. 0#< RI+< J-I >#DR > >)
C< J >=1. 0-2. 0*f T
70 CONTINUE
C CALCULATION OF HEAT TRANSFER COEFFICIENT FOR THE INNER WALL
GRI=E:ETA*G*< SL**3.0 >*< RHO**2. 0 >#( T< 1 )-TA )/< TMU**2. 0 )
PR=TMU*CA/KA
LIM=1000080000. 0
RAI=GRI*fr
IF(RAI.GT.LIM > GO TO 61
HCI=1. 42*< < T< 1 )-TA >/SL >**0. 25
GO TO 62
61 HCI=0.95*<T( 1>-TA>**0.3333
C CALCULATION OF HEAT TRANSFER COEFFICIENT FOR THE OUTER WALL
62 GR=E:ETA*G*< SL**3. 0 >*< RHO**2. 0 >*< T( N1 )-TA )/< TNU**2. 0 )
RA=GR*PR
IF<RA.GT.LIM> SO 10 71
HCI=1. 42*< < T< N1 )-TA )/SL >**0. 25
GO TO 72
71 HCI=0. 95*< T< N1 >-TA >#0. 3333
72 IF< T( N1 ).NE. TW > GO TO 73
HR=0.0
GO TO 74
73 HR=F01*SII NA*< T< N1 >**4-TU##4 )/( T< N1 )-TW >
74 H=HC+HR
C CALCULATION OF TEMPERATURE AT THE INNER SURFACE
T< 1 >=< 1(2 )-2.0*HCI*DR*< T< 1 )-TA )/KC )*( 1 >+T< 2 >1A< 1 )+T< 1 )*( 1 )
C CALCULATION OF TEMPERATURE AT THE OUTER SURFACE
T< N1 )=< T( N-I )-( 2. 0X:DR*H*< T< N1 >-TA >/KC ) >*A< N1 I
+T( N >*E< N1 )*< N1 )*C< N1 )
C CALCULATION OF TEMPERATURES FOR THE INNER NODES
DO 80 J=2< N
T( J )=T( J+I )iA( J )+T( J-I >*E< J >+T< J >#C< J )
60 CONTINUE
RT=RT+DT
TM=RT/60.0
C CALCULATED VALUES OF TEMPERATURE DISTRIBUTIONS ARE PRINTED
C OUT AT AN INTERVAL OF ONE MINUTE
E!IC=AE!S( TM-YN )
IF<BIC.NE.1.0000 ) GO TO 111
YN=YN+1.0
C WRITING OUT OF TIME AND TEMPERATURE VALUES
WRITE( 6, 90 )TM
90 FOKMATC ACTUAL TIME T , F7.3. '<MINS. V >
DO 105 J=1,HI
105 T< J )=T( J >-273. 0
WRITE< 6. 108 )< T( J )i J "1< N1 )
100 FORMAT( 151 1X. FB. 1 ) >
DO 110 J< 1i N1
110 T( J )=T< J )• 273. 0
111 CONTINUE
IF(RT.GE.72GB, B ) GO TO 120
L=L+1
L1=L+1
GO TO 70
120 CONTINUE
STOP
END
FINISH

```

Appendix A2

A2.1: The trapezoidal method for approximating an integral

Any definite integral may be thought of as an area or an algebraic sum of areas. One can often obtain good accuracy by using numerical methods for approximating integrals. One of the simplest methods is the trapezoidal rule which shall be derived now.

»

Supposing the definite integral $\int_{b_1}^{b_2} f(x)dx$ is to be evaluated. The interval $b_1 < x < b_2$ can be divided into n subintervals each of length $\Delta x = (b_2 - b_1)/n$ by inserting the following points:

$$x_1 = b_1 + \Delta x$$

$$x_2 = b_1 + 2\Delta x$$

$$x_{n-1} = b_1 + (n-1)\Delta x$$

between $x_0 = b_1$ and $x_n = b_2$

The integral from b_1 to b_2 is just the sum of the integrals from b_1 to x_1 , from x_1 to x_2 , and so on, and finally, the integral from x_{n-1} to b_2 as given by:

$$\int_{b_1}^{b_2} f(x)dx = \int_{b_i}^{x_1} f(x)dx + \int_{x_1}^{x_2} f(x)dx + \dots + \int_{x_{n-1}}^b f(x)dx$$

..(A2.1)

The integral over the first subinterval is now approximated by the area $\frac{1}{2}(f(b_1)+f(x_1))\Delta x$; over the second subinterval by the area of the trapezoid $\frac{1}{2}(f(x_1)+f(x_2))\Delta x$; and so on. Thus the integral can be approximated as follows:

$$\int_{b_1}^b f(x)dx \approx \left[\frac{1}{2}(f(b_1)+f(x_1)) + \frac{1}{2}(f(x_1)+f(x_2)) + \dots + \frac{1}{2}(f(x_{n-1})+f(b_2)) \right] \Delta x$$

..(A2.2)

Now considering the determination of the circumferential stresses by the use of Equation (2.15) given by:

$$\sigma_{\theta} = \frac{F}{A} \left[\frac{r+r_1^2}{r_2^2-r_1^2} \int_{r_1}^{r_2} \frac{Tr}{r} dr + \int_{r_1}^r \frac{Tr}{r} dr - Tr^2 \right] \quad \text{..(2.15)}$$

the stresses at each node where the temperatures were numerically solved will be determined independently. Thus the equation will have the form:

$$\sigma_{\theta\theta} = \frac{1}{1-\nu} \left[\frac{r}{r^2} \frac{d}{dr} \left(\frac{r}{r^2} \frac{d}{dr} \left(\frac{p}{r} \right) \right) + \frac{1}{r} \frac{d}{dr} \left(\frac{p}{r} \right) - \frac{p}{r^2} \right] \quad \text{..(A2.3)}$$

New since T is a function of r only, T_r will also be a function of r ($f(r)$). The equation is now a definite integral equation with two integrals, $\int_{r_i}^{r_{i+1}} f(r) dr$ and $\int_{r_n}^{r_{n+1}} f(r) dr$ and can be solved by the use of Trapezoidal Integration Technique at each node r_{ij} . The same technique is used to determine the radial and axial stresses by solving Equation (2.14) and (2.16) numerically.

A2.2: Solution for the general axisymmetrical problem

Hoyle's method for the solution of the general axis-symmetrical problem [15] involves the finding of a set of X and ϵ stress functions from the equations given by:

$$\frac{d^2 X}{dr^2} + \frac{1}{r} \frac{dX}{dr} + \frac{H_i}{3r^2} = \frac{9l}{1-\nu} \quad \text{..(2.10)}$$

$$3r^2 \frac{d^2 \epsilon}{dr^2} + r \frac{d\epsilon}{dr} - 9\epsilon = 0 \quad \text{..(2.ii)}$$

and then substituting these values in the stress equations given by Equations (2.6), (2.7), (2.8) and (2.9).

The above equations can be solved by Finite Difference Approximation techniques. However, the problem lies in the equations being dependent on the values of x as well as ϵ .

To determine the distribution of x and ϵ an iterative procedure can be used. An account of the method in the form of a procedure is given below:

- (i) A sub-routine which will work through internal nodes is written improving x values at internal nodes according to the Finite Difference Equation derived from the governing Equation (2.11), and improving x values at the boundary nodes according to equations derived from relevant boundary conditions. A similar sub-routine for working through the nodes at which ϵ can vary (derived from Equation (2.10)) is written.

- (ii) Keeping the nodal values of x fixed at a certain initial value (usually taken as zero) the ϵ sub-routine is repeatedly applied on the variable thus changing them from the initially assumed values (usually taken as zero again) until a specified convergence criterion is satisfied. The values of K obtained will be taken as .

- (iii) At this point since there is a set of x -values to which no change has yet been made, the next step, then, is to improve the position as regards x by repeated application of the x sub-routine until another convergence criterion is satisfied. In doing so the convergence of the x -values is very slow and exponential extrapolation will be necessary in which the extrapolation coefficients are chosen mainly by human observation of how slow the convergence takes place. Thus obtaining an improved set of x -values, which will be called X_j .
- (iv) The value of x must be held temporarily at x_j at this point, for the purpose of producing a second improvement in the values of y which can be called y_2 . This process of iterating one set of variable while holding the other constant causes oscillating divergence. This trouble can be avoided by taking the arithmetic mean, node by node, of the variables in y_1 and y_2 and obtaining the resulting \hat{y} -values as \hat{y} .
- (v) Using the \hat{y}_3 in the formulae and starting from the X_j results, the x variables are iterated to convergence (in this case no averaging technique is necessary), thus obtaining the values of x .

(vi) The process from this point is repeating the whole procedure by producing further sets of variables $(\mathfrak{L}_5, X_5) > (\mathfrak{L}_7, X_7) >$ etc., until two consecutive sets are identical. The production of identical consecutive sets constitutes the overall termination condition.

At the time of study the computing facilities did not have features that allow intermediate program monitoring for iteration studying and this method could not be used. However, now this method of computing stresses can be studied as a further research.

A2.3: Transient thermal stresses in solid circular cylinders

The stresses developed in brittle circular cylinders initially at a uniform temperature and suddenly immersed in a fluid medium at a different temperature have been extensively studied before [18, 31]. It was assumed that the structure of the material is perfectly elastic, homogeneous and therefore isotropic in properties, and that the heat-transfer rates are uniform at all temperatures. The cylinders were assumed to be infinitely long and temperature variations occur only in the radial direction.

In such cases the stresses can be expressed in terms of the following dimensionless parameters:

$$\frac{t}{r_0^2} \quad - \quad \text{non-dimensional time}$$

$$\frac{r_0 h}{k} \quad - \quad \text{non-dimensional heat transfer}$$

$$\frac{(1-\nu)\alpha_0}{E\alpha AT} \quad - \quad \text{non-dimensional stress}$$

where k , E , α , ν , AT and α_0 are thermal diffusivity, Young's modulus, coefficient of thermal expansion, Poisson's

ratio

difference of medium temperature and the initial

temperature of the cylinder, and circumferential stress
actively (see Appendix A1.1 for the rest of the symbols).

The variation of non-dimensional surface circumferential
stress σ_s in an infinite circular cylinder with non-dimensional
for varying Biot Numbers is shown in Figure A2.1.

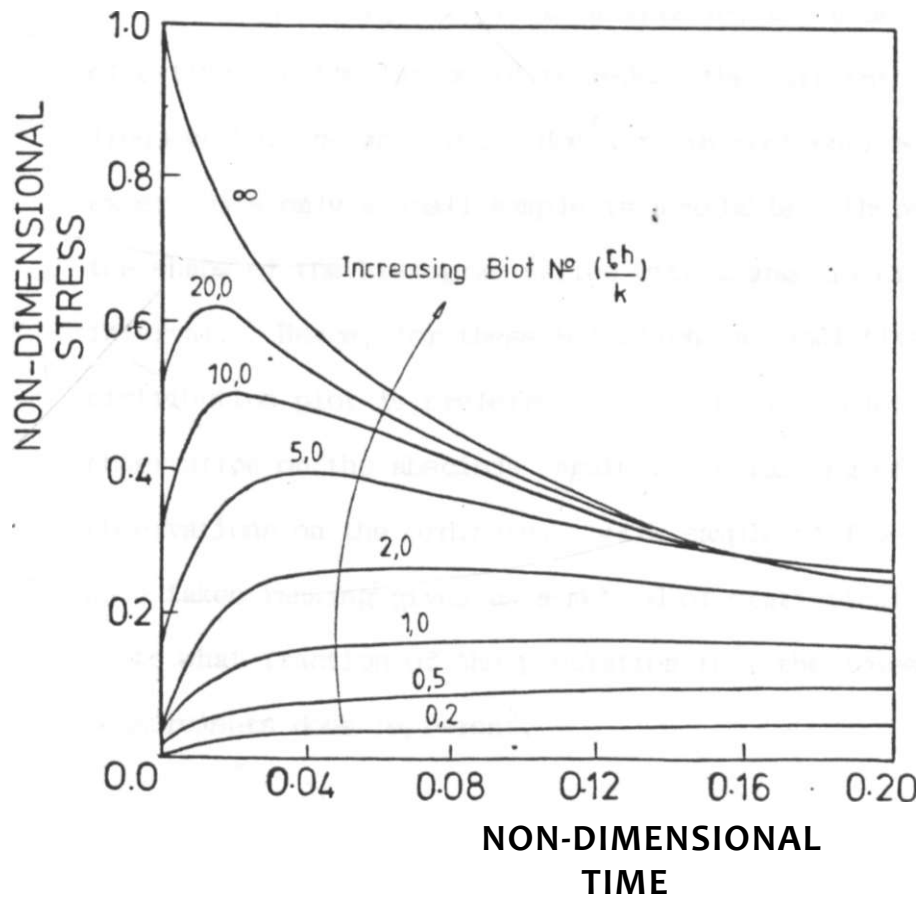


Figure A2.1: The variation of non-dimensional surface circumferential stress in an infinite circular cylinder with non-dimensional time for varying Biot Numbers

Appendix A3.

Concepts of statistical analyses

A3.1: Concept of ranking

When a large sample is available, the usual method of estimating population is to reduce the data into frequency-histogram form. However, in most engineering experiments only a small sample is available; therefore, the shape of the histogram varies with change in class interval. Hence, for these situations a cumulative distribution plot is preferred. This involves plotting the observation on the abscissa against the ranking of these observations on the ordinate. If a sample of five measurements were taken ranking gives us a method of statistical estimate as to what fraction of the population that the lowest of five measurements does represent.

In the sample of five items the first failure may have occurred at A where, say, 15 percent of the population has values less than A. If another sample of five were taken the lowest life B might represent only, say, 9 percent of the population. When this is repeated several times, the data represents a series of such percentage numbers randomly distributed. In median ranking, the median of these numbers is

then used as a true rank of the first failure out of the group tested. In the same manner, median ranks for the second, third, etc., failure out of five can be estimated. These values are given in Tables A3.2.

The concept of ranking can be extended to any other rank such as 5, 16, 90 or 95 percent. Thus for example, the 5 percent rank of the lowest of 9 measurements is 0.57 percent (Table A3.3). This means only 5 percent of the cases the least of 9 measurements would represent less than 0.57 percent of the population.

A3.2: Concept of correlation analysis

Correlation analysis is a method of determining a degree of association between variables. The correlation coefficient, r_{corr} , is defined as the quantitative measure of association between variables. When r_{corr} is 1.0, this indicates the perfect correlation between the variables; and when r_{corr} is zero, there is no correlation. Table A3.1 can be used to determine the degree of significance of the correlation coefficient computed from a sample at a certain confidence level. This table provides the maximum value of the correlation coefficient which can be expected

by chance alone when actually no correlation exists. The 95 percent confidence indicate that there is only a 5 percent chance of having r_{corr} as large as those on the table when no correlation exists. In order to conclude at a given confidence level that the correlation does exist the calculated correlation coefficient should exceed the tabulated value.

A3.3: The Weibull distribution

Since Weibull distribution is generally not a symmetrical distribution, the mean and the median values will not be the same, as is the case in the normal distribution. In order to determine mean life one can make use of Figure A3.2 by locating the Weibull slope on the abscissa and reading off percentage failed at the mean on the ordinate. The life on the Weibull plot corresponding to this percentage will be the mean life. Figure A3.1 presents Weibull slope errors at 90 percent confidence interval.

	<i>M^{III}, Confidence level</i>				<i>99% Confidence level</i>				
	<i>Total number of variables</i>				<i>Total number of variables</i>				
	2	3	4	5	2	3	4	5	
1	.997	.999	.999	.999	1.000	1.000	1.000	1.000	1
2	.950	.975	.983	.987	.990	.995	.997	.998	2
3	.878	.930	.950	.961	.959	.976	.983	.987	3
4	.811	.881	.912	.930	.917	.949	.962	.970	4
5	.754	.836	.874	.898	.874	.917	.937	.949	5
6	.707	.795	.839	.867	.834	.886	.911	.927	6
7	.606	.758	.807	.838	.798	.855	.885	.904	7
8	.632	.726	.777	.811	.765	.827	.860	.882	8
9	.602	.697	.750	.786	.735	.800	.836	.861	9
10	.576	.671	.726	.763	.708	.776	.814	.840	10
11	.553	.648	.703	.741	.684	.753	.793	.821	11
12	.532	.627	.683	.722	.661	.732	.773	.802	12
13	.514	.608	.664	.703	.641	.712	.755	.785	13
14	.497	.590	.646	.686	.623	.694	.737	.768	14
15	.482	.574	.630	.670	.606	.677	.721	.752	15
16	.468	.559	.615	.655	.590	.662	.706	.738	16
17	.456	.545	.601	.641	.575	.647	.691	.724	17
18	.444	.532	.587	.628	.561	.633	.678	.710	18
19	.433	.520	.575	.615	.549	.620	.665	.698	19
20	.423	.509	.563	.604	.537	.608	.652	.685	20
21	.413	.498	.552	.592	.526	.596	.641	.674	21
22	.404	.488	.542	.582	.515	.585	.630	.663	22
23	.396	.479	.532	.572	.505	.574	.619	.652	23
24	.388	.470	.523	.562	.496	.565	.609	.642	24
25	.381	.462	.514	.553	.487	.555	.600	.633	25
26	.374	.454	.506	.545	.478	.546	.590	.624	26
27	.367	.446	.498	.536	.470	.538	.582	.615	27
28	.361	.439	.490	.529	.463	.530	.573	.606	28
29	.355	.432	.482	.521	.456	.522	.565	.598	29
30	.349	.426	.476	.514	.449	.514	.558	.591	30
35	.325	.397	.445	.482	.418	.481	.523	.556	35
40	.304	.373	.419	.455	.393	.454	.494	.526	40
45	.288	.353	.397	.432	.372	.430	.470	.501	45
50	.273	.316	.379	.412	.354	.410	.449	.479	50
60	.250	.308	.348	.380	.325	.377	.414	.442	60
70	.232	.286	.324	.354	.302	.351	.386	.413	70
80	.217	.269	.304	.332	.283	.330	.362	.389	80
90	.205	.254	.288	.315	.267	.312	.343	.368	90
100	.195	.241	.274	.300	.254	.297	.327	.351	100
125	.174	.216	.246	.269	.228	.266	.294	.316	125
150	.159	.198	.225	.247	.208	.244	.270	.290	150
200	.138	.172	.196	.215	.181	.212	.234	.253	200
300	.113	.141	.160	.176	.148	.174	.192	.208	300
400	.098	.122	.139	.153	.128	.151	.167	.180	400
500	.088	.109	.124	.137	.115	.135	.150	.162	500
1,000	.062	.077	.088	.097	.081	.096	.106	.116	1,000

v - number of observations

Table A3.1: Values of correlation coefficient r_{corr} as per Lipsion and SHeth {47}

<i>r</i>	<i>Sample size n</i>									
	<i>J</i>	2	3	4	5	6	7	8	9	10
i	.5000	.2929	.2063	.1591	.1294	.1091	.0943	.0830	.0741	.0670
2		.7071	.5000	.3864	.3147	.2655	.2295	.2021	.1806	.1632
3			.7937	.6136	.5000	.4218	.3648	.3213	.2871	.2594
4				.8409	.6853	.5782	.5000	.4404	.3935	.3557
5					.3706	.7345	.6352	.5596	.5000	.4519
6						.8009	.7705	.6787	.6065	.5481
7							.9057	.7979	.7129	.6443
8								.9170	.8194	.7406
9									.9259	.8368
10										.9330

<i>J*</i>	<i>Sample size n</i>									
	11	12	13	14	15	16	17	18	19	20
1	.0611	.0561	.0519	.0483	.0452	.0424	.0400	.0378	.0358	.0341
2	.1489	.1368	.1266	.1178	.1101	.1034	.0975	.0922	.0874	.0831
3	.2366	.2175	.2013	.1873	.1751	.1644	.1550	.1465	.1390	.1322
4	.3244	.2982	.2760	.2568	.2401	.2254	.2125	.2009	.1905	.1812
5	.4122	.3789	.3506	.3263	.3051	.2865	.2700	.2553	.2421	.2302
6	.5000	.4596	.4253	.3958	.3700	.3475	.3275	.3097	.2937	.2793
7	.5878	.5404	.5000	.4653	.4350	.4085	.3850	.3641	.3453	.3283
8	.6756	.6211	.5747	.5347	.5000	.4695	.4425	.4184	.3968	.3774
9	.7634	.7018	.6494	.6042	.5650	.5305	.5000	.4728	.4484	.4164
10	.8511	.7825	.7240	.6737	.6300	.5915	.5575	.5272	.5000	.4755
11	.9389	.8632	.7987	.7432	.6949	.6525	.6150	.5816	.5516	.5245
12		.9439	.8734	.8127	.7599	.7135	.6725	.6359	.6032	.5736
13			.9481	.8822	.8249	.7746	.7300	.6903	.6547	.6226
14				.9517	.8899	.8356	.7875	.7447	.7063	.6717
15					.9548	.8966	.8450	.7991	.7579	.7207
16						.9576	.9025	.8535	.8095	.7698
17							.9600	.9078	.8610	.8188
18								.9622	.9126	.8678
19									.9642	.9169
20										.9659

Order number:

Table A3.2: Median ranks as per Lipson and Sheth {47}

Table of 5% ranks

<i>J*</i>	<i>Sample size n</i>									
	1	2	3	4	5	6	7	8	9	10
1	.0500	.0253	.0170	.0127	.0102	.0085	.0074	.0065	.0057	.0051
2		.2236	.1354	.0976	.0764	.0629	.0534	.0468	.0410	.0368
3			.3684	.2486	.1893	.1532	.1287	.1111	.0978	.0873
4				.4729	.3426	.2713	.2253	.1929	.1688	.1500
5					.5493	.4182	.3413	.2892	.2514	.2224
6						.6070	.4793	.4003	.3449	.3035
7							.6518	.5293	.4504	.3934
8								.6877	.5709	.4931
9									.7169	.6058
10										.7411

x

Table of 95% ranks

<i>J*</i>	<i>Sample size n</i>									
	1	2	3	4	5	6	7	8	9	10
1	.9500	.7764	.6316	.5271	.4507	.3930	.3482	.3123	.2831	.2589
2		.9747	.8646	.7514	.6574	.5818	.5207	.4707	.4291	.3942
3			.9830	.9024	.8107	.7287	.6587	.5997	.5496	.5069
4				.9873	.9236	.8468	.7747	.7108	.6551	.6076
5					.9898	.9371	.8713	.8071	.7436	.6965
6						.9915	.9466	.8889	.8312	.7776
7							.9926	.9532	.9032	.8500
8								.9935	.9590	.9127
9									.9943	.9632
10										.9949

Order number.

Table A3.3: 5 and 95 percent ranks as per
Lipson and Shetb: {47}

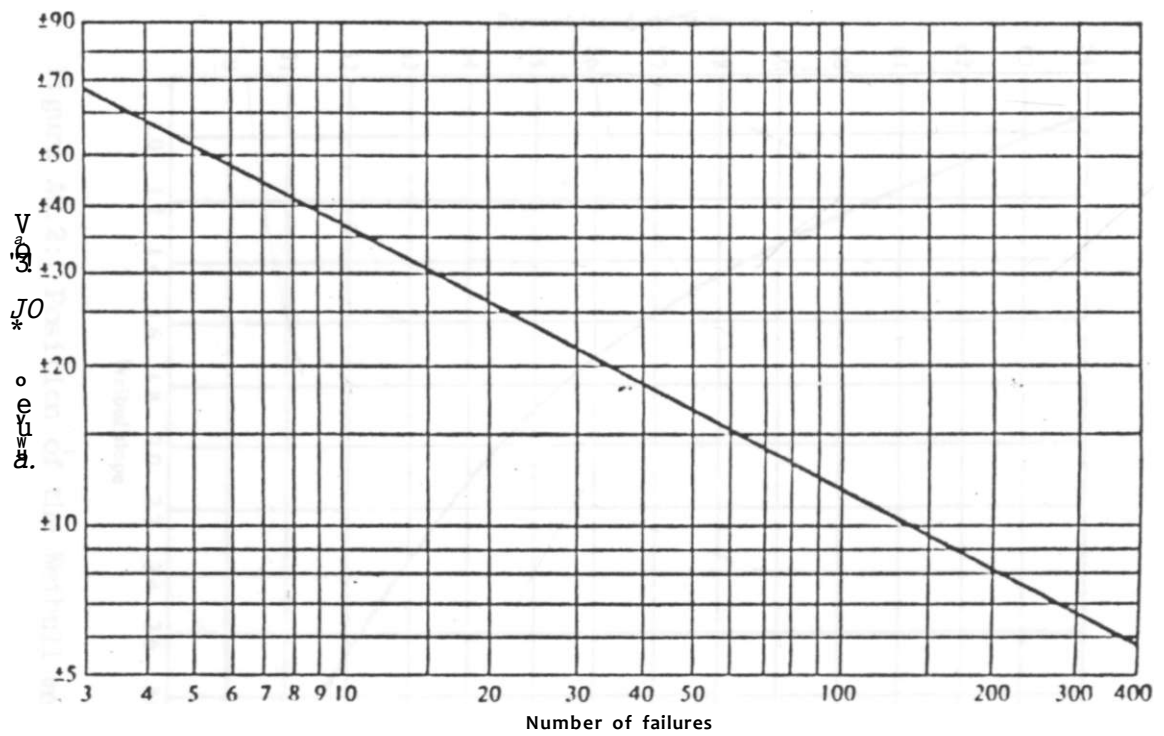


Figure A3.1: Weibull slope error at 90 percent confidence interval, as per Lipson and Sheth [47]

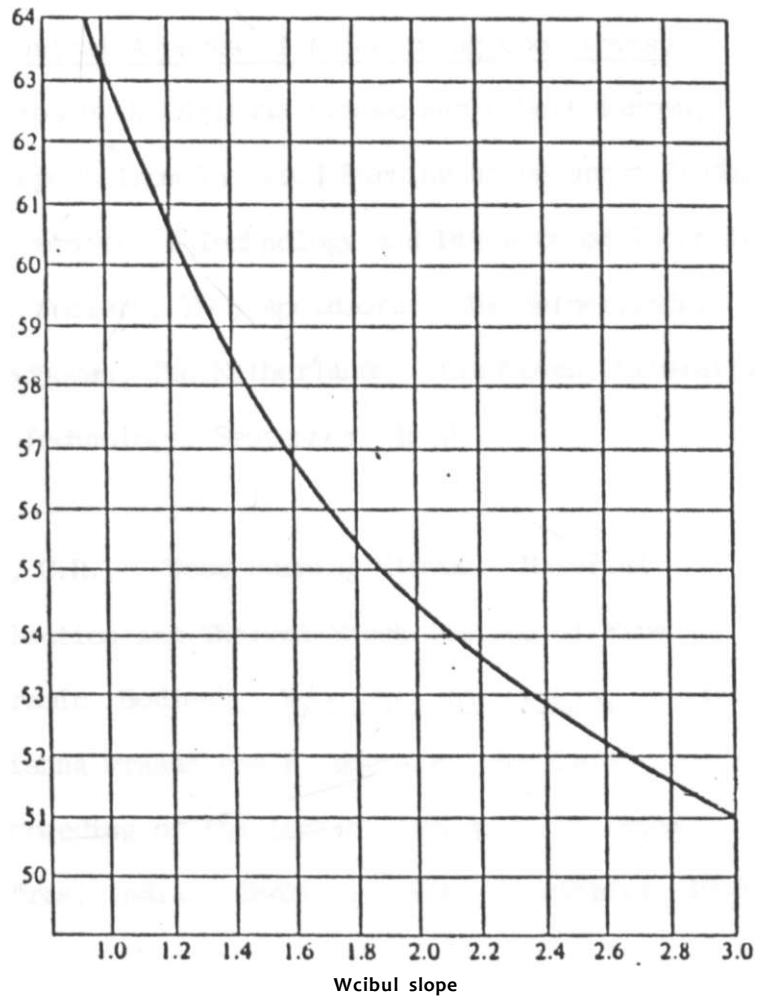


Figure A3.2: Position of the Weibull mean as per
Lipson and Sheth {47}

REFERENCES

1. Prasad, K.K. and P. Bussmann, "Heat Transfer Characteristics of Metal, Ceramic and Clay Stoves", Technical Aspects of Woodburning Cookstoves, edited by K. Krishna Prasad and Ernest Sangeu, A Report from The Wood Burning Stove Group Eindhoven University of Technology and Division of Technology for Society, TNO, Apeldoorn The Netherlands, Eindhoven, The Netherlands: Eindhoven University of Technology, September 1983 .

2. Chaplin, C.R., "Wood Burning Stoves: Material Selection and Thermal Shock Testing of Fired Ceramic Bodies", Wood Heat for Cooking, Edited by Krishna Prasad and P. Verhaart, Reprinted from the Proceeding of the Indian Acaderr^ of Sciences, Madras, India: Indian Academy of Sciences, 1983.

3. Newman, D.R., "Woodstoves Materials Testing at Kenyatta University College - Appropriate Technology Centre", A Report from Kenyatta University, Appropriate Technology Centre, Nairobi: Kenyatta University, 1983.

4. Timoshenko, S.P. and J.N. Goodier, Theory of Elasticity, Third Edn., Tokyo: McGraw-Hill Kogakusha, Ltd., 1970.
5. Kingery, W.D., Introduction to Ceramics, New York: John Wiley and Sons, Inc., 1967.
6. Ozisik, M.N., Heat Transfer, A Basic Approach, Singapore: McGraw-Hill Book Corrpany, 1985.
7. Carslaw, H.3. and J.C. Jaeger, Conduction of Heat in Solids, Second Edn., London: Oxford University Press, 1959.
8. Kaplan, W., Advanced Calculus, Second Edn., Massachusetts: Addison-Wesley Publishing Company, 1973.
9. Liebmann, G., "A New Electrical Analog Method for the Solution of Transient Heat Conduction Problem", Transactions of American Society of Mechanical Engineers, Vol. 78, 3, (1956).

10. Wrobel, L.C. and C.A. Brebbia, "Boundary Element in Heat Transfer", Numerical Methods in Heat Transfer, New York: John Wiley and Sons, Ltd. 1981.
11. Kantorovich, L.V. and V.I. Krylov, Approximate Method of Higher Analysis, Third Edn., New York: Interscience Publishers Inc., 1958.
12. Biot, M.A., "Thermoelasticity⁴ and Irreversible Thermodynamics", Journal of Applied Physics, Vol. 27, 3, 240-253, (1956).
13. Biot, M.A., "Variational Principles in Irreversible Thermodynamics and Applications to Viscoelasticity", Physics Review, Vol. 97, 6, 1463-1469, (1955).
14. Boley, B.A. and J.II. Weiner, Theory of Thermal Stresses, New York: John Wiley and Sons, Inc., 1960.
15. Hoyle, R.D., "Transient Temperature Stresses in Axially Symmetrical Systems with Special Application to a Solid Rotor of a Steam Turbine", Proceedings of the Institution of Mechanical Engineers, Vol. 169, 553-558, (1955).

16. Thomas, G.B., Calculus and Analytic Geometry,
Fourth Edn., Massachusetts: Addison-Wesley
Publishing Company, 1974.

17. Buist, W.S., "A Method of Determining Transient
Thermal Stresses in Spheres and Cylinders",
South African Mechanical Engineer, Vol. 31,
63-66, (1981).

18. Glenny, E. and M.G. Royston, "Transient Thermal
Stresses Promoted by The Itapid Heating and Cooling
of Brittle Ceramic Cylinders", Transactions of
British Ceramic Society, Vol. 57, 10, 645-676,
(1958).

19. Singh, J.P., J.R. Tbomas, and D.P.H. Hasselman,
"Analysis of Effect of Heat Transfer Variable on
Thermal Stress Resistance of Brittle Ceramics
Measured by Quenching Experiments", Journal of
American Ceramic Society, Vol. 63, 140-144, 1980.

20. Glandus, J.C., Thesis Un. Limoges, Limoges, France:
l'University de Limoges, 1981.

26. Lawn, B.R. and T.R. Wilshaw, Fracture of Brittle Solids, Cambridge: Cambridge University Press, 1975.
27. Jayatilaka, Ayal de S., Fracture of Engineering Brittle Materials, London: Applied Science Publishers Ltd., 1979.
28. Coble, R.L. and W.D. Kingery, "Effect of Porosity on Thermal Stress Fracture", Journal of American Ceramic Society, Vol. 38, 33-37, (1955).
29. Cardall, W.B. and J. Ging, "Thermal Shock Analysis of Spherical Shapes", ibid., Vol. 38, 44-54, (1955).
30. Hasselman, D.P.H., "Thermal Shock by Radiation Heating", Journal of American Ceramic Society, Vol. 46, 5, 229-234, (1963).
31. Hasselman, D.P.K., R. Badalian, K.R. McKinney and C.M. Kim, "Failure Prediction of the Thermal Fatigue Resistance of a Glass", Journal of Material Science, Vol. 11, 458-464, (1976).

32. Kamiya, N. and O. Kamigaito, "Prediction of Thermal Fatigue Life of Ceramics", ibid., Vol. 14, 573-582, (1979).
33. Kamiya, N. and O. Kamigaito, "Prediction of Thermal Fatigue Life of Ceramics", ibid., Vol. 13, 212-214, (1978).
34. Evans, A.G. and H. Johnson, "The Fracture Stress and Its Dependence on Slow Crack Growth", ibid.,
i
Vol. 10, 214-222, (1975).
35. Deiter, G.E. Mechanical Metallurgy, Second Edn.,
Tckyo: McGraw-Hill Kogakusha, Ltd., 1976, (p.286).
36. Manson, S.S. and R.W. Smith, "Theory of Thermal Shock Resistance of Brittle Materials Based on Weibull's Statistical Theory of Strength", Journal of American Ceramic Society, Vol. 38, 18-27, (1955).
37. Stanley, P. and J. Margensen, "Failure Probability Analysis of an Elastic Orthotropic Brittle Cylinder Subjected to Axisymmetric Thermal and Pressure Loading", International Journal of Fracture, Vol. 13, 6, 787-806, (1977).

38. Krieth, F., Heat Transfer, Third Edn., Madison:
Feffer and Simons International Edition, 1973.
39. Holman, J.P. Heat Transfer, Fourth Edn., U.S.A.:
McGraw-Hill Inc., 1976, (pp. 235-272).
40. ASHRAE Handbook, 1985 Fundamentals, Atlanta: American
Society of Heating, Refrigerating and Air-
conditioning Engineers, Inc., 1985.
41. Mai, Y.W. and L.J.S. Jacob, "Thermal Fracture of
Building Glass Subjected to Solar Radiation",
Third International Conference on Mechanical
Behaviour of Materials, Edited by K.J. Miller
and R.F. Smith, Cantoridge: Pergamon Press Ltd.
1980.
42. Benedict, R.P., Fundamentals of Temperature, Pressure
and Flow Measurement, New York: John Wiley and
Sons, Inc., 1966, (pp.53-125).
43. Szilard, J., ed., Ultrasonic Testing, New York:
John Wiley and Sons, Ltd., 1982.

44. Goldsmith, A., T.C. Waterman and H.J. Hirschhorn,
Handbook of Thermophysical Properties of Materials,
Poland: Pergamon Press, 1961.
45. Karniya, N. and C. Kamigaito, "Estimation of Weibull
Parameters by Omission of Some Data in Sample",
Journal of Material Science, Vol. 19, 4021-4025,
(1984).
46. Davidge, R.W., "The Mechanical Properties and Design
Data for Engineering Ceramics", Ceramics
International, Vol. 1, 2, 75-80, (1975).
47. Lipson, C. and N.J. Sheth, Statistical Design and
Analysis of Engineering Experiments, Tokyo:
McGraw-Hill Kogakusha, Ltd., 1973.
48. Ziegler, G. and D.P.H. Hasselman, "Effects of Data
Scatter on Apparent Thermal Stress Failure Mode of
Brittle Ceramics", Ceramics International, Vol. 5,
3, 126-128, (1979).
43. Anzai, K. and H. Hashimoto, "Thermal Shock Resistance
of Silicon Nitride", Journal of Material Science
Vol. 12, 2351-2353, (1977).

50. Kamiya, N. and O. Kamigaito, "Application of Fracture Mechanics to Heterogeneous Systems - Prediction of Fatigue life of Ceramics", Journal of Materials Science, Vol. 19, 159-166, (1984).

51. Yeamans, K.A., Statistics for the Social Scientist: 2, Applied Statistics, Middlesex, England: Penguin Books Ltd., 1968.

52. van der Valden, J.H. 'Evaluation and Adjustment of Raw Material Mixtures for the Manufacture of Wood Burning Clay Stoves", From Design to Cooking, edited by C.E. Krist-Spit and D.J. van der Heeden, A Report from The Wood Burning Stove Group Eindhoven University of Technology and Division of Technology for Society, TNO, Apeldoorn, The Netherlands, Eindhoven, The Netherlands: Eindhoven University of Technology, January 1985.